AD_____

AWARD NUMBER: W81XWH-05-1-0469

TITLE: Novel Molecular Interactions and Biological Functions of the Neurofibromatosis 2 Tumor Suppressor Protein, Merlin

PRINCIPAL INVESTIGATOR: Olli Carpen, M.D., Ph.D.

CONTRACTING ORGANIZATION: University of Helsinki
Helsinki 00014 Finland

REPORT DATE: August 2007

TYPE OF REPORT: Annual

PREPARED FOR: U.S. Army Medical Research and Materiel Command
Fort Detrick, Maryland 21702-5012

REPORT DOCUMENTATION PAGE

Form Approved
OMB No. 0704-0188

1. REPORT DATE *(DD-MM-YYYY)*	**2. REPORT TYPE**	**3. DATES COVERED** *(From - To)*
01-08-2007	Annual	29 Jul 2006 – 28 Jul 2007

4. TITLE AND SUBTITLE

Novel Molecular Interactions and Biological Functions of the Neurofibromatosis 2 Tumor Suppressor Protein, Merlin

5a. CONTRACT NUMBER

5b. GRANT NUMBER
W81XWH-05-1-0469

5c. PROGRAM ELEMENT NUMBER

6. AUTHOR(S)

Olli Carpen, M.D., Ph.D.

E-Mail: olli.carpen@helsinki.fi

5d. PROJECT NUMBER

5e. TASK NUMBER

5f. WORK UNIT NUMBER

7. PERFORMING ORGANIZATION NAME(S) AND ADDRESS(ES)

University of Helsinki
Helsinki 00014 Finland

8. PERFORMING ORGANIZATION REPORT NUMBER

9. SPONSORING / MONITORING AGENCY NAME(S) AND ADDRESS(ES)
U.S. Army Medical Research and Materiel Command
Fort Detrick, Maryland 21702-5012

10. SPONSOR/MONITOR'S ACRONYM(S)

11. SPONSOR/MONITOR'S REPORT NUMBER(S)

12. DISTRIBUTION / AVAILABILITY STATEMENT
Approved for Public Release; Distribution Unlimited

13. SUPPLEMENTARY NOTES

14. ABSTRACT
The project studies molecular functions of neurofibromatosis 2 tumor suppressor protein merlin and the ERM protein ezrin. Phosphorylation is an important mechanism in theregulation of both proteins. We have studied the interplay between protein kinase A (PKA) andmerlin. We identified an N-terminal phosphorylation site at merlin S10. Phosphorylation of S10 does not affect phosphorylation of S518 or ezrin binding. It affects, however, actin dynamics and cell morphology and migration in Nf2 -/- mouse embryonic fibroblasts (MEF) and Schwann cells. This suggests a role for merlin in mediating PKA induced changes of the actin cytoskeleton. We also show a link between PKA and calpain in the regulation of merlin cleavage and subcellular localization. We previously showed that oncogenic tyronsine kinase Src phosphorylates ezrin at Y477. Using reconstituted MEF cells from ezrin -/- mice we studied the biological importance of Y477 phosphorylation. Our results show that ezrin is a key regulator of Src induced malignant behavior in three dimentional culture conditions.

15. SUBJECT TERMS

Neurofibromatosis 2, merlin, ezrin, phosphorylation, PKA, Src, microtubule, cytoskeleton

16. SECURITY CLASSIFICATION OF:			**17. LIMITATION OF ABSTRACT**	**18. NUMBER OF PAGES**	**19a. NAME OF RESPONSIBLE PERSON**
a. REPORT	**b. ABSTRACT**	**c. THIS PAGE**			USAMRMC
U	U	U	UU	81	**19b. TELEPHONE NUMBER** *(include area code)*

Table of Contents

Page

Introduction..... 4

Body..... 4

Key Research Accomplishments..... 9

Reportable Outcomes..... 10

Conclusion..... 11

References..... 12

Appendices..... 13

Introduction

The neurofibromatosis 2 (NF2) gene product merlin and the ezrin-radixin-moesin (ERM) family protein ezrin are structurally related proteins that demonstrate some functional similarities and interact with each other, but possess opposite effects on cell growth. The experiments of this proposal aim to explore the poorly understood molecular and cell biological basis of the tumor suppressor function of merlin. Specific emphasis has been given to cell cycle stage-dependent targeting of merlin (task 1), analysis of molecular interactions of merlin previously identified by us (tasks 2 and 3), and comparative analysis of phosphorylation-dependent regulation of merlin and ezrin (task 4). All four tasks proposed in the research plan have been pursued and the goals in most tasks have been accomplished. Results from this project and other groups have opened some new avenues that will be followed.

Body

The progress of the project is described in accordance with the tasks outlined in the proposal.

Task 1. *To analyze the mechanisms, regulation and functional consequences of the cell cycle dependent nucleocytoplasmic regulation of merlin.*

a) Phosphorylation may be one potential way of regulating the nucleocytoplasmic shuttling of merlin. We reported previously that phosphorylation of serine 518 does not affect the nuclear localization of merlin. In this report we show that also serine 10 is phosphorylated by PKA (see Task 4), and have therefore generated mutants replacing S10 with alanine (A) or aspartate (D). The S10A mutant cannot be phoshorylated, whereas S10D is thought to mimic a constitutively phosphorylated protein. We also generated double mutants of both PKA phosphorylation sites. Wild type and mutant merlin constructs have been transfected into Nf2-/- mouse embryonic firoblasts (MEFs).

Nuclear localization of reattaching and cell cycle synchronized cells will be compared to wild-type merlin and quantified. This work is still ungoing.

It has previously been shown that oxidative stress can induce the transfer of merlin into the nucleus after cleavage by activated μ-calpain (Kaneko, 2001). We have set up the methods to study calpain regulation of merlin and can now activate μ-calpain mediated cleavage of merlin in transfected COS-7 and 293HEK cells. Calpain was activated in cells expressing wild type merlin, and cells stained with an N- or C-terminal antibody to identify the subcellular localization of the cleavage products. Calpain activation resulted in the relocalization of merlin from the membrane to the perinuclear region, which was not seen in cells treated with a specific calpain inhibitor, Z-Llal. Nuclear localization was not, however, as evident, but further characterization is needed. It has previously been shown that PKA regulates calpain function (Shiraha et al., 2002). Therefore, the PKA pathway was also activated or inactivated in merlin wild type expressing cells, or cells transfected with S10A or S10D, but no difference was detected. All experiments resulted in the relocalization of merlin (Fig. 1).

Kressel et al. (2002) showed that a cytoplasmic retention signal is present in exon 2 and a nuclear export signal in exon 15 of merlin, and that merlin constructs with exon2 deleted and the export signal mutated localize to the nucleus. Within the export signal motif, two amino acids are highly conserved in merlin from different species, glutamic acid at positions 545 and 547. We converted the charge of the residues from negative to positive (lysine). We created constructs with the E545K and E547K mutations and/or exon 2 deletions, to study their nuclear localization. COS-7 and 293HEK cells transfected with E545K+E547K still localized to the membrane, most likely because they still contained the cytoplasmic retention signal in exon 2. When exon 2 was deleted in isoform I, the protein relocated to the perinuclear region but no nuclear merlin could be seen. Interestingly, the exon 2 deletion in isoform II still localized to the membrane. When exon 2 was deleted and 545 and 547 mutated, no merlin could be detected at the membrane, instead nuclear and perinuclear staining could be seen (Fig. 2).

b, c) In order to find merlin interaction partners in the nucleus we immunoprecipitated merlin from nuclear extracts or whole cell lysates. Precipitates were run on SDS-PAGE, silver stained, and bands enriched in the nuclear fraction were cut out for mass spectrometry analysis. The resulting protein sequences obtained did not, however, include specific components and this approach was not pursued further.

Bimolecular fluorescence complementation analysis, BiFC, allows the direct visualization of protein interactions in living cells. This approach is based on complementation between two nonfluorescent fragments of the yellow fluorescent protein (YFP) when they are brought together by interactions between proteins fused to each fragment (Hu et al., 2002). Thus, fluorescence is seen only in regions were tested proteins interact *in vivo*, and these interactions can be directly visualized in cells. This method has been used in many studies for interaction analysis of nuclear proteins. We decided to set up this system, in order to test whether known merlin interactions take place also in the nucleus. So far, we have introduced merlin, ezrin and control constructs to the BiFC-vectors, and shown that the system is applicable to merlin-ezrin interaction studies. Merlin wild type and ezrin including the T567D mutation to mimic an open conformation, exhibited fluorescence complementation at the plasma membrane. The mutation of serine 518 to alanine (S518A), previously reported to decrease merlin-ezrin binding *in vitro* (Alfthan et al., 2004), affected dimer interaction showing mainly cytoplasmic localization and reduced fluorescence complementation (Fig. 3).

Task 2. *To characterize the association between merlin and microtubules and its functional relevance.*

A report on the biochemical and functional aspects of the interplay between merlin and microtubules was finalized and published (Muranen et al. 2007).

We have previously shown that PKA phosphorylation of serine 518 affects tubulin binding and that tubulin is affected by merlin expression. To further analyze the effect PKA phosphorylation of merlin has on tubulin binding, we transfected Nf2-/- Schwann

cells and MEFs with S10A and S10D constructs. The tubulin cytoskeleton of these cells did not show any difference compared to wild type expressing cells. Pull down experiments are being made with tubulin and PKA phosphorylated wild type merlin or S10A, but results are still inconclusive.

Task 3. *To study the role of merlin -- HEI10 interaction and its role in regulation of cell growth.*

As explained in the previous report, we have not been able to produce functional HEI10 antibodies, despite of several attempts by different methods in different species. This makes further studies of HEI10 function *in vivo* difficult. As one means of overcoming this problem we are introducing HEI10 to BiFC constructs (see Task 1). Using this method we can study the subcellular localization of HEI10 and merlin binding in different cell types without the need of specific antibodies.

Task 4. *To understand how kinase activity differentially regulates the functional activity of merlin and ezrin.*

Subtasks a (Characterization of the PKA induced phosphorylation of the FERM-domain of merlin) and b (Functional consequences of PKA-induced phosphorylation of merlin) have been carried out and a report of these studies has been submitted for publication (Laulajainen et al. submitted, see appendix).

a) We have mapped merlin's N-terminal PKA phosphorylation site to serine 10 (Laulajainen et al., Fig. 1). We showed that mutations S10A and S10D (see Task 1) do not affect the electrophoretic mobility of the protein, which still run as three bands in SDS-PAGE. The phosphorylation status of serine 10 did not affect serine 518 phosphorylation, as judged by electrophoretic mobility and staining of cells with the phosphospecific antibody p518 (Laulajainen et al., Fig. 2). We attempted to produce a phosphospecific serine 10 antibody by immunizing rabbits with a synthetic ten residue phosphopeptide and affinity purifying the antiserum with an immobilized phosphopeptide

and with a non-phosphorylated peptide. The serum contained antibodies that recognize the N-terminus of merlin, however, specificity for the phosphorylated serine 10 was not yielded.

b) Tubulin binding to S10A and S10D is being tested (see Task 2). We did not detect a difference on cell proliferation in cells expressing S10A and S10D mutants compared to wild type merlin. S10A and S10D localized to cortical membrane structures and to cell extensions, like the wild type protein (Laulajainen et al., Fig. 2). The first 18 amino acids of merlin, which precede the FERM domain, are not present in the ERM proteins, and have been indicated in merlin binding to actin (Brault et al., 2001). Since serine 10 is part of this domain, we looked at the effect of merlin serine 10 mutants on the actin cytoskeleton. Regulation of this site affected actin cytoskeleton organization and dynamics *in vivo*. We showed that S10A affects cellular morphology by inducing long extensions and reduces the amount of cellular F-actin (Laulajainen et al., Figs 3 and 4), while merlin S10D stabilized F-actin filaments (Laulajainen et al., Figs 4 and 5). By using a wound-healing assay and live cell imaging we demonstrate that dephosphorylation of serine 10 lead to defects in migration, possibly through altered ability of the cells to form lamellipodia (Laulajainen et al., Fig. 6). This suggests a role for merlin in mediating PKA induced changes of the actin cytoskeleton.

As described in Task 1, PKA regulates calpain function (Shiraha et al., 2002). We have tested whether mutations of merlin's N-terminal PKA phosphorylation site, serine 10, affect the calpain mediated cleavage of merlin. The PKA phosphorylated N-terminal GST-construct was cleaved to a lesser extent than the unphosphorylated protein *in vitro*. Interestingly, in μ-calpain-activated COS-7 cells expressing merlin the hyperphosphorylated form of merlin was not present while the hypophosphorylated form increases. This indicates and interplay between merlin phosphorylation status and calpain, and that μ-calpain may regulate the phosphorylation of serine 518 (Fig. 4).

c) Subtask c (Characterization of the Src induced tyrosine phosphorylation of ezrin) has resulted in a manuscript (Heiska et al. 2007, see appendix).

We previously identified tyrosine 477 as a novel substrate in ezrin phosphorylated by the oncogenic tyrosine kinase Src (Heiska and Carpen 2005). To study, whether Src and ezrin act in concert in tumorigenesis, we reconstituted genetically ezrin-deficient cell lines (MEF cells from ezrin -/- mice) with wild-type (WT) or phosphorylation deficient ezrin (Y477F subctitution) together with constitutively active Src. In two-dimensional cultures, Src induced malignant features independent of whether the cells expressed WT or mutant ezrin or were ezrin deficient (Heiska et al. 2007, Figs. 2 and 3). The features included alterations in actin cytoskeleton, increased proliferation rate and changes in cell adhesion. However, marked differences were seen in experiments, in which cells were cultured in three dimensional environment or without possibility for matrix attachment. Whereas WT and mutant ezrin expressing cells had identical morphology on culture plates (Heiska et al. 2007, Fig. 2) they showed marked differences in three dimensional matrix, where only wild-type ezrin was targeted to specific regions on the plasma membrane (Heiska et al. 2007, Fig. 4). Only cells expressing WT ezrin and active Src grew efficiently in soft agar (Heiska et al. 2007, Fig. 5). WT but not Y477F ezrin promoted Src-induced growth in suspension (Heiska et al. 2007, Fig. 6A). Furthermore, expression of ezrin significantly promoted Src-induced growth and invasion in Matrigel, a three-dimensional extracellular matrix from mouse tumor (Heiska et al. 2007, Fig. 6B and C). These results lead us to conclude that the pathways activated by Src depend on the type of environment and that ezrin is a crucial element of Src-induced malignant features of cells growing in three dimensional matrices.

Key Research Accomplishments

-mapping of the N-terminal PKA phosphorylation site to serine 10
-demonstration that serine 10 does not affect serine 518 phosphorylation, the electrophoretic mobility of merlin, or ezrin binding
-demonstration that the expression of S10D stabilizes actin filaments
-demonstration that the expression of S10A causes long extensions in cells, reduces the amount of F-actin and affects lamellipodia formation

-demonstration that cells expressing S10A show reduced mobility
-demonstration that PKA regulates calpain cleavage of merlin
-demonstration that activation of calpain affects the subcellular localization of merlin
-demonstration that Src induced phosphorylation of ezrin at Y477 regulates cytoskeletal organization in three dimensional environment
-demonstration that Src induced phosphorylation of ezrin at Y477 is required for colony formation of MEF cells in soft agar
-demonstration that Src induced phosphorylation of ezrin at Y477 is required for anchorage independent growth of MEF cells
-demonstration that Src induced phosphorylation of ezrin at Y477 is required for growth of MEF cells in Matrigel
-demonstration that Src induced phosphorylation of ezrin at Y477 is controls invasive capacity of MEF cells in Matrigel

Reportable Outcomes

Publications:

Muranen T, Grönholm M, Lampin A, Lallemand D, Zhao F, Giovannini M, Carpén O. The tumor suppressor merlin interacts with microtubules and modulates Schwann cell microtubule cytoskeleton. Hum Mol Gen (2007) 16:1742-51

Presentations:

Poster presentation: 09-13.12.2006. Leena Heiska, Fang Zhao, Itsiko Saotome, Andrea I. McClatchey, Olli Carpén, Ezrin Promotes Src-dependent Functions Associated with Malignancy. 46th Annual Meeting of the American Society of Cell Biology, San Diego, CA

Poster presentation: 10-12.6.2007. Minja Laulajainen and Taru Muranen, Regulation of Merlin by Protein Kinase A. 2007 Children's Tumor Foundation International Neurofibromatosis Consortium. Park City, Utah.

Poster presentation: 27-30.6.2007. Taru Muranen, Regulation of Merlin by Protein Kinase A. 2007 European Cytoskeletal Forum. Dijon, France.

Scientific talk: 11.5.2007 Taru Muranen, The tumor suppressor merlin interacts with microtubules and modulates Schwann cell microtubule cytoskeleton. The Cell Biology Club. Lammi, Finland.

Novel research tools:

Bimolecular fluorescence complementation, BiFC
Mutation constructs including exon 2 deletions and E545K and E547K mutations
and single and double mutants of S10 and S518
Merlin retroviral constructs
An antibody against the amino-terminus of merlin

Conclusions

The research project has advanced well in three of the four main tasks. The progress in studies on the merlin – HEI10 interaction has been hampered by inability to obtain a suitable HEI10 antibody. The project has resulted in several interesting observations on the biology of the NF2 tumor suppressor protein, merlin and the related protein ezrin, and in one publication and two manuscripts. Posttranslational modification via phosphorylation is an important mechanism in the regulation of both merlin and ezrin. We have focused on the kinase PKA, how it phosphorylates and regulates merlin. We have now identified a novel N-terminal PKA phosphorylation site to serine 10. We show that although the phosphorylation status of this residue does not affect serine 518

phosphorylation or ezrin binding it affects actin dynamics and cell morphology and migration in Nf2 -/- MEFs and Schwann cells. Nf2 deficient schwannoma cells exhibit cytoskeletal anormalities manifested by morphological changes and F-actin instability (Pelton et al., 1998). As Schwann cells are susceptible to tumor formation in NF2 disease, our findings may provide clues on the molecular pathways involved in this tumorigenetic events. Our studies on the interplay between ezrin and Src have identified ezrin as a key regulator of Src induced malignant phenotype in three dimensional environment. In fact, ezrin is the first identified molecule that controls the three most important phenotypic characteristics of malignant behavior: anchorage independent growth, proliferation and invasion in three dimensional matrix. The results may have implications in development of novel therapeutic approaches for inhibition of invasive/metastatic growth.

References

Alfthan K., Heiska L., Grönholm M., Renkema G.H. and Carpen O. (2004) Cyclic AMP dependent protein kinase phosphorylates merlin at serine 518 independently of P21-activated kinase and promotes merlin-ezrin heterodimerization. *J. Biol. Chem.*, 279, 18559-18566.

Brault E, Gautreau A, Lamarine M, Callebaut I, Thomas G and Goutebroze L. (2001) Normal membrane localization and actin association of the NF2 tumor suppressor protein are dependent on folding of its N-terminal domain. *J. Cell Sci.* 114, 1901-12.

Heiska, L., O. Carpén. (2005) Src phosphorylates ezrin at tyrosine 477 and induces a phosphospecific interaction between ezrin and a kelch-repeat protein family member. *J. Biol. Chem***.** 280, 10244-52.

Hu CD, Chinenov Y and Kerppola TK.(2002) Visualization of interactions among bZIP and Rel family proteins in living cells using bimolecular fluorescence complementation. *Mol. Cell.* 9(4), 789-98.

Kaneko T, Yamashima T, Tohma Y, Nomura M, Imajoh-Ohmi S, Saido TC, Nakao M, Saya H, Yamamoto H, and Yamashita J. (2001) Calpain-dependent proteolysis of merlin occurs by oxidative stress in meningiomas: a novel hypothesis of tumorigenesis. *Cancer.* 92(10), 2662-72

Kim HA, DeClue JE and Ratner N. (1997) cAMP-dependent protein kinase A is required for Schwann cell growth: interactions between the cAMP and neuregulin/tyrosine kinase pathways. *J. Neurosci. Res.* 49(2), 236-47.

Kressel M and Schmucker B. (2002) Nucleocytoplasmic transfer of the NF2 tumor suppressor protein merlin is regulated by exon 2 and a CRM1-dependent nuclear export signal in exon 15. *Hum. Mol. Gen.* 11(19), 2269-78.

Pelton PD, Sherman LS, Rizvi TA, Marchionni MA, Wood P, Friedman RA and Ratner N. (1998) Ruffling membrane, stress fiber, cell spreading and proliferation abnormalities in human Schwannoma cells. *Oncogene.* 17(17), 2195-209.

Shiraha H, Glading A, Chou J, Jia Z, and Wells A. (2002) Activation of m-Calpain (Calpain II) by Epidermal Growth Factor Is Limited by Protein Kinase A Phosphorylation of m-Calpain. *Mol. Cell Biol.*, 22 (8), 2716–2727

Appendices

Figure legends

Figures 1-4

Articles and manuscripts

Muranen T, Grönholm M, Lampin A, Lallemand D, Zhao F, Giovannini M, Carpén O. The tumor suppressor merlin interacts with microtubules and modulates Schwann cell microtubule cytoskeleton. Hum Mol Gen (2007) Jul 15;16(14):1742-51.

Laulajainen M, Muranen T, Carpén O, Grönholm, M. Protein kinase A mediated phosphorylation of the NF2 tumor suppressor protein merlin at serine 10 affects the actin cytoskeleton organization. *Submitted*

Heiska L, Zhao F, Saotome I, McClatchley AI, Carpén O Ezrin is key regulator of Src-induced malignant phenotype in three-dimensional environment. *Manuscript in preparation*

Figure legends:

Figure 1. Calpain activation results in perinuclear localization of merlin

COS-7 cells were transfected with wild type merlin. Calpain was activated and cells treated with either a calpain inhibitor Z-Llal or PKA activators Forskolin and IBMX. Cells were stained with an N- (A-19) or C-terminal (KF10) antibody to identify merlin. Calpain activation resulted in the relocalization of merlin from the membrane to the perinuclear region except for in cells treated with the calpain inhibitor, Z-Llal.

Figure 2. **Merlin mutant constructs relocalize to the perinuclear and nuclear region**

COS-7 (upper two rows) and 293HEK (lower two rows) cells were transfected with full length merlin which contained mutations E545K+E547K and/or exon 2 deletions and stained with the merlin antibody A-19. Merlin with the E545K+E547K mutation still localizes to the membrane. Merlin relocalizes to the perinuclear region in cells with the exon 2 deletion in isoform I but not in isoform II. When exon 2 is deleted and 545 and 547 mutated, no merlin can be detected at the membrane, instead nuclear and perinuclear staining can be seen.

Figure 3. Visualization of merlin-ezrin interactions using bimolecular fluorescence complementation (BiFC) analysis.

COS-7 cells were transfected with merlin wt and mutant constructs in BiFC vectors. Fluorescence is seen only in regions, where tested proteins interact. Wild-type merlin (WT)-ezrin T567D heterodimer fluorescence was associated preferentially with the plasma membrane. S10D and S518A reduced the efficiency of fluorescence complementation and resulted in unspecific localization mainly in the cytoplasm. However, the double alanine mutant (S10A+S518A) had no effect on fluorescence complementation with ezrin T567D.

Figure 4. Interplay between merlin phosporylation and calpain

A) GST-merlin N-terminus 1-314 (N) or the same construct phosphorylated by PKA (pN) were incubated with activated μ–calpain. Proteins were run on SDS-PAGE and

immunoblotted with merlin A-19 antibody (left) or silver stained (right) for loading control. The PKA phosphorylated N-terminus was cleaved to a lesser extent than the unphosphorylated protein. B) COS-7 cells were transfected with merlin wt or mutation constructs and calpain activated. WT cells were also treated with the PKA activators Forskolin and IBMX. Cells were lysed, run on SDS-PAGE and immunblotted with A-19. Upper panel shows longer exposure time than lower panel, to detect all phosphorylation variants. Calpain activation causes the hyperphosphorylated form to disappear while the hypophosphorylated form increases, except for in cells with activated PKA.

Figure 1.

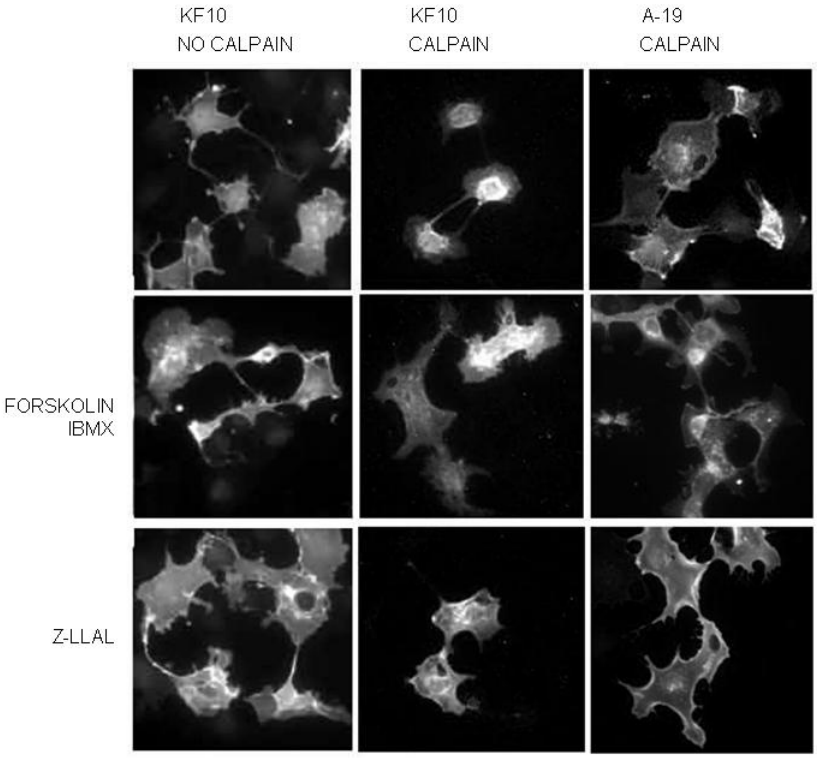
KF10
NO CALPAIN
KF10
CALPAIN
A-19
CALPAIN
FORSKOLIN
IBMX
Z-LLAL

Figure 2.

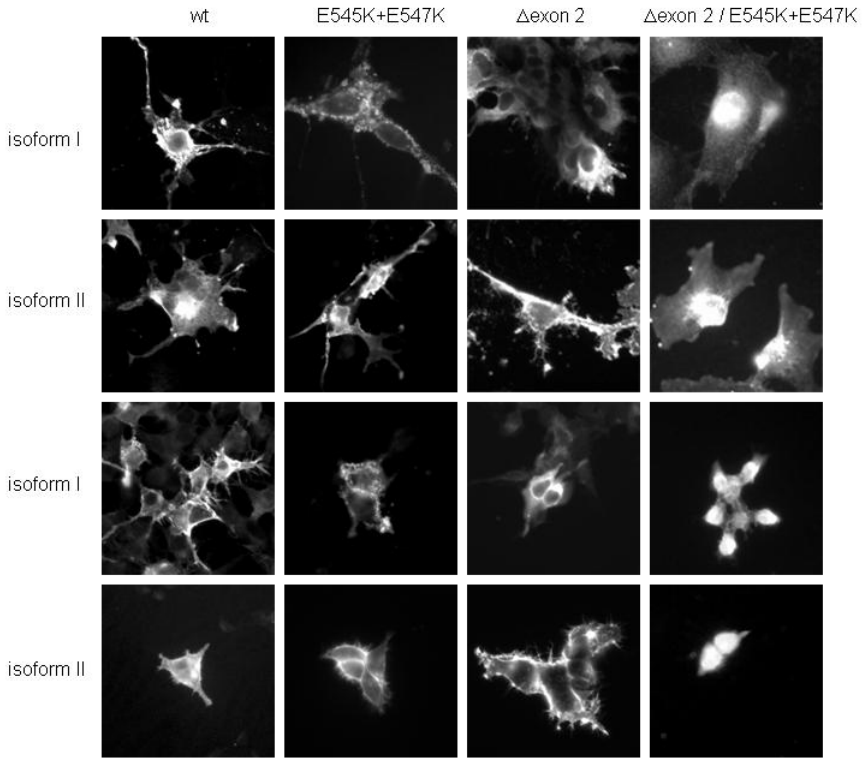
wt
E545K+E547K
Δexon 2
Δexon 2 / E545K+E547K
isoform I
isoform II
isoform I
isoform II

Figure 3.

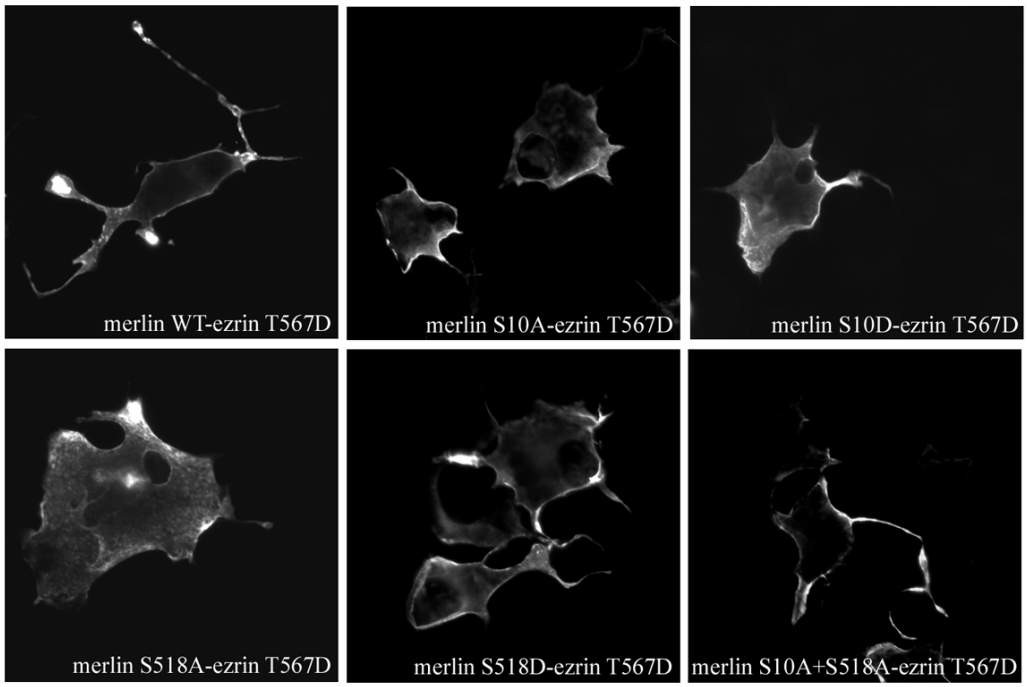
merlin WT-ezrin T567D
merlin S10A-ezrin T567D
merlin S10D-ezrin T567D
merlin S518A-ezrin T567D
merlin S518D-ezrin T567D
merlin S10A+S518A-ezrin T567D

Figure 4.

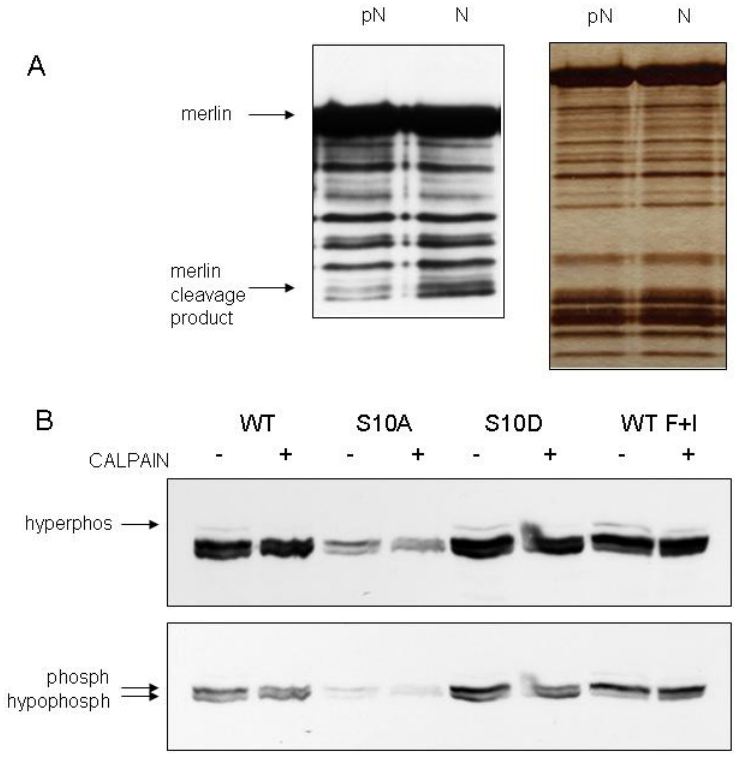
A
pN
N
pN
N
merlin
merlin
cleavage
product
B
WT
S10A
S10D
WT F+I
CALPAIN
- + - + - + - +
hyperphos
phosph
hypophosph

Human Molecular Genetics, 2007, Vol. 16, No. 14 **1742–1751**
doi:10.1093/hmg/ddm122
Advance Access published on June 12, 2007

The tumor suppressor merlin interacts with microtubules and modulates Schwann cell microtubule cytoskeleton

Taru Muranen[1,*], Mikaela Grönholm[1], Aurelie Lampin[2], Dominique Lallemand[2], Fang Zhao[1], Marco Giovannini[2] and Olli Carpén[1,3]

[1]Program of Neuroscience, Department of Pathology, University of Helsinki, Biomedicum Helsinki C511, PL 63, 0014 Finland, [2]Inserm U674, Fondation Jean Dausset-CEPH et Institut Universitaire d'Hématologie, 75010 Paris, France and [3]Department of Pathology, University of Turku and Turku University Central Hospital, 20520 Turku, Finland

Received March 09, 2007; Revised and Accepted April 30, 2007

The lack of neurofibromatosis 2 tumor suppressor protein merlin leads to the formation of nervous system tumors, specifically schwannomas and meningiomas. Merlin is considered to act as a tumor suppressor at the cell membrane, where it links transmembrane receptors to the actin cytoskeleton. Several tumor suppressors interact with another component of the cytoskeleton, the microtubules, in a regulated manner and control their dynamics. In this work, we identify merlin as a novel microtubule-organizing protein. We identify two tubulin-binding sites in merlin, one residing at the N-terminal FERM-domain and another at the C-terminal domain. Merlin's intramolecular association and phosphorylation of serine 518 regulate the interaction between merlin and tubulin. Analysis of cultured glioma cells indicates colocalization between merlin and microtubules especially during cell division. In primary mouse Schwann cells only minor colocalization at the cell periphery of interphase cells is seen. However, these cells drastically change their microtubule organization upon loss of merlin indicating a functional association of the proteins. Both *in vitro* assays and *in vivo* studies in Schwann cells indicate that merlin promotes tubulin polymerization. The results show that merlin plays a key role in the regulation of the Schwann cell microtubule cytoskeleton and suggest a mechanism by which loss of merlin leads to cytoskeletal defects observed in human schwannomas.

INTRODUCTION

Inactivation of the neurofibromatosis 2 (*NF2*) tumor suppressor gene leads to the development of multiple benign tumors of the nervous system, particularly meningiomas and schwannomas (1). The *NF2* gene encodes a 595-amino acid protein merlin (schwannomin), which is related to the ezrin–radixin–moesin (ERM) protein family. Merlin and ERM proteins are located primarily underneath the cell membrane where they anchor transmembrane proteins to the actin cytoskeleton (2,3). They form homo- and heterotypic interactions (4) which in turn regulate their binding to other proteins (5–7). Head-to-tail binding leads to a closed conformation of the ERM proteins (4); for merlin, the closed form is thought to act as a tumor suppressor, whereas the open protein is unable to regulate growth. Phosphorylation of a C-terminal serine (S518) by p21-activated kinase (PAK) or cAMP-dependent protein kinase A (PKA) weakens merlin's self-association and is believed to inactivate the growth-suppressing activity of merlin (8,9). However, the functional regulation of merlin is still not completely understood.

Merlin is also involved in receptor recycling and endocytosis. It inhibits platelet-derived growth factor receptor degradation (10) and binds hepatocyte growth factor-regulated tyrosine kinase substrate (HRS) (11), which is known to regulate receptor tyrosine kinase trafficking to the degradation pathway (12). Recently, merlin was shown to regulate EGF receptor recycling and turnover in *Drosophila* (13). Thus, increasing evidence positions merlin at the membrane where it can bind membrane receptors and regulate their expression and localization.

A common feature of many tumor suppressors is their ability to interact with microtubules and regulate microtubule

*To whom correspondence should be addressed. Tel: +358 9 19125651; Fax: +358 9 4717194; Email: taru.muranen@helsinki.fi

stability (14,15). Microtubules, themselves, are also known to regulate cell growth. They, for instance, control cell division and regulate endocytosis and recycling of growth factor receptors (16). We set out to study merlin–tubulin interaction when we noticed that endogenous merlin colocalizes with tubulin in mitotic structures of U251 glioma cells (17). Although merlin has previously been suggested to bind tubulin *in vitro* (3,18), no further evidence has been provided to support the binding. Here, we have studied the association between merlin and tubulin, the regulation of the interaction, the effects of merlin on microtubule dynamics and the consequences of loss of merlin on microtubules in Schwann cells. Our results show that merlin plays an important role in regulating microtubule cytoskeleton of mouse primary Schwann cells.

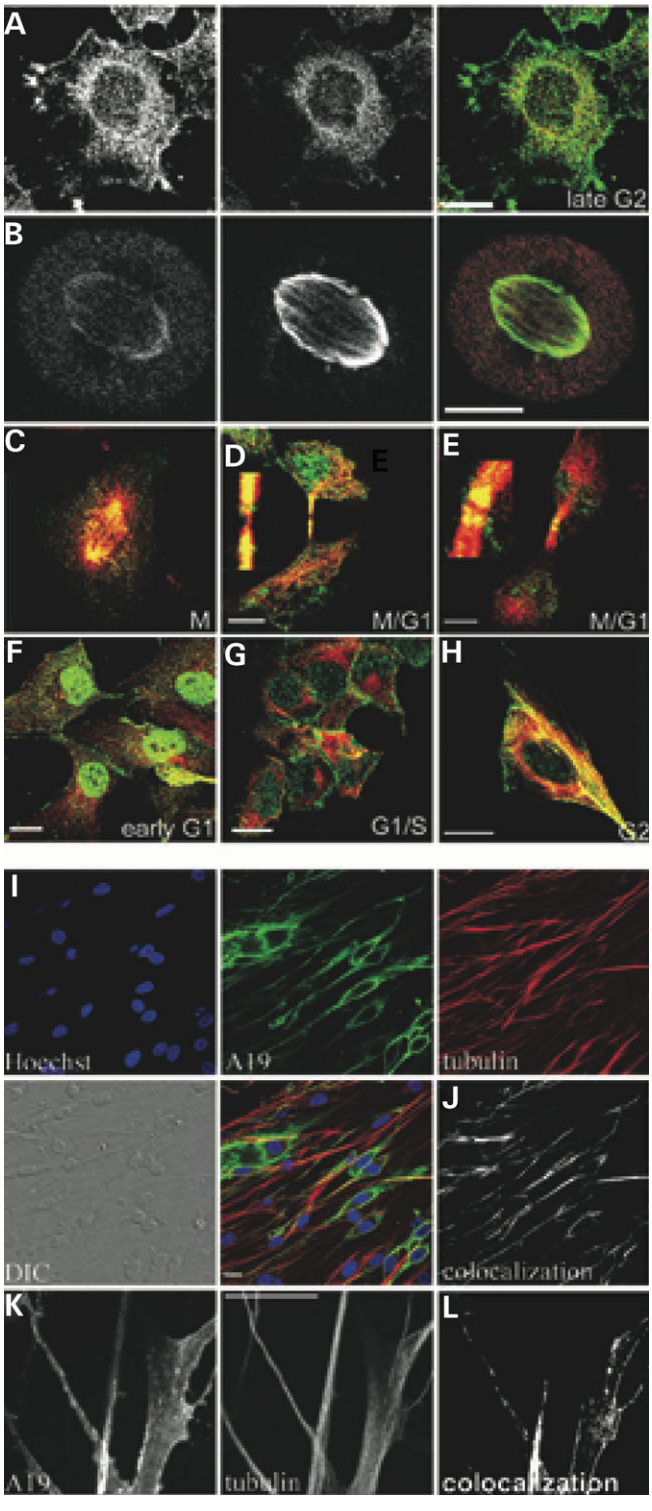

RESULTS

Merlin associates with microtubules

We have previously shown that in synchronized U251 glioma cells merlin localizes to mitotic structures (17,19). This led us to analyze the distribution of endogenous merlin and tubulin at various cell cycle stages in U251 glioma cells (Fig. 1A–H). We noticed parallel accumulation of merlin and tubulin around the nucleus in interphase cells before mitosis (A). During mitosis, merlin colocalized with microtubules at the mitotic spindles, although some diffuse merlin staining was also noticed in the cytoplasm (B and C). During cytokinesis especially the midbody demonstrated high degree of colocalization between merlin and tubulin (D and E). The colocalization was lost at early G1, when merlin accumulated in the nucleus (F). The staining patterns remained separate during the entire G1 and S phase (G). At G2, a partial colocalization was seen (H). We also studied cultured primary mouse Schwann cells, whose purity was verified by a Schwann cell-specific marker p75 (Supplementary Material, Fig. S1). In interphase cells merlin had a predominantly submembraneous localization, whereas tubulin was localized at the cytoplasm. Areas of potential colocalization were identified from confocal sections using image analysis software. The analysis revealed occasional sub-plasmalemmal regions and (I and J) and cell extensions (K and L) (colocalized points shown in white in Fig. 1J, L), in which codistribution was seen. In mitotic Schwann cells staining was mostly diffuse.

Merlin binds polymerized microtubules *in vitro*

We then wanted to identify the tubulin-binding regions in merlin. We mapped the interaction sites with a tubulin pull-down assay using various purified glutathione *S*-transferase

Figure 1. Distribution of merlin and microtubules in U251 glioma and primary mouse Schwann cells. (**A–H**) U251 glioma cells were synchronized and stained for merlin (green, A19) and tubulin (red, α-tubulin). The cells were fixed at different points of the cell cycle, the cell cycle phase was verified by FACS analysis and the localization of the two proteins was analyzed by confocal microscopy. Merlin and tubulin start to colocalize already in interphase cells when cells are approaching mitosis (**A**). During mitosis merlin localizes to mitotic spindles (**B, C**) and during cytokinesis at the midbody (**D, E** and insets). After mitosis the two proteins have separate staining patterns (**F, G**). At late G2, some colocalization can be seen again (**H**). (**I–L**) In the primary mouse Schwann cells merlin (green, A19) shows a predominantly submembraneous distribution, whereas microtubules (red, β-tubulin) are distributed within the cells body. Analysis of confocal sections with Image J analysis software demonstrates occasional submembraneous regions, where the two proteins colocalize (white areas in J and L). Scale bar 10 μm.

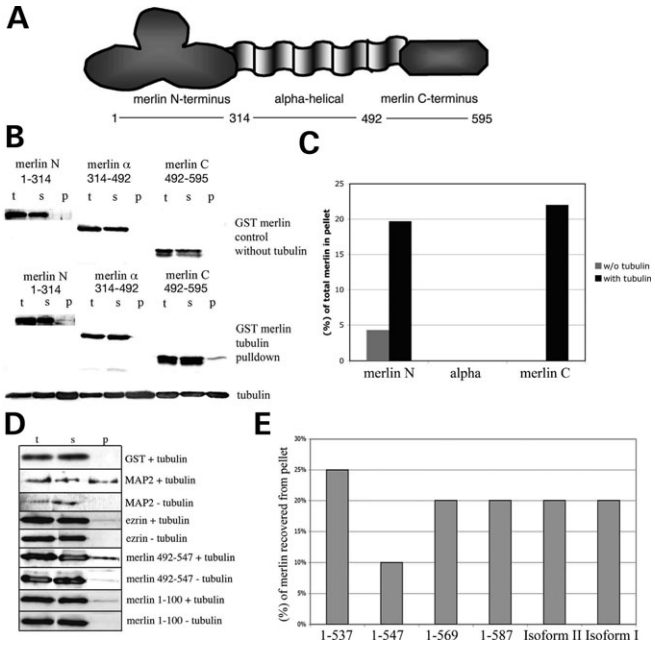

Figure 2. Merlin binds polymerized tubulin *in vitro*. (**A**) A schematic drawing on merlin's domains. (**B**) Tubulin binding sites in merlin were mapped by a tubulin pull-down assay, in which recombinant GST-merlin was pulled down with polymerized microtubules by ultracentrifugation. Merlin N (amino acids 1–314), α-helical merlin (amino acids 314–492) and merlin C (amino acids 492–595) constructs were used in the assay. Total (t), supernatant (s) and pellet (p) fractions with or without tubulin were run into SDS–PAGE, blotted either with merlin (A19 or C18) or GST-antibody and analyzed. (**C**) The amount of merlin in the pellet fraction was quantified by western blots by Typhoon Imager and compared to the total amount of merlin. (**D**) The binding sites in merlin were further mapped with merlin constructs 1–100 and 492–547. GST alone, MAP2 and ezrin N (1–309) were used as controls in the pull-down assay. The tubulin blots can be found from Supplementary Material, Figure S2. (**E**) *In vitro* translated ^{35}S methionine labeled merlin was produced and used for *in vitro* tubulin pull-down experiments. Merlin was pulled down with polymerized microtubules and the amount of merlin in the pellet was analyzed and compared with total amount of merlin (%). Merlin isoforms 1 and 2 and C-terminally deleted merlin constructs associated with microtubules. A patient mutation construct, merlin 1–547, did not associate with microtubules equally well. The graph represents the average of five experiments.

(GST)-merlin constructs. Tubulin was incubated with different GST-constructs after which polymerized tubulin was pulled down by centrifugation and quantified. Both the N-terminal FERM- (amino acids 1–314) and the C-terminal (amino acids 492–595) domain were recovered from the tubulin pellet, whereas the α-helical region (amino acids 314–492) of merlin or GST alone (quantification not shown) did not bind tubulin (Fig. 2B, C). We further mapped the N-terminal binding site to amino acids 1–100 and the C-terminal binding site to residues 492–547 (Fig. 2D). As a positive control we used microtubule-associated protein 2 (MAP2), a well-characterized tubulin interacting protein. As an additional control, we tested the N-terminus of ezrin, a FERM-domain protein homologous to merlin. Similar to merlin, the N-terminus of ezrin could be found in the tubulin pellet (Fig. 2D).

In addition, we produced *in vitro*-translated methionine-labeled merlin constructs and pulled them down with polymerized tubulin. With this assay we could see an interaction between tubulin and merlin isoforms I and II (Fig. 2E). C-terminal deletion constructs 1–569 and 1–587 bound tubulin similar to isoform I. As truncating mutations around amino acid 547 cause NF2 (http://neurosurgery.mgh.harvard.edu/NFclinic/NFresearch.htm), we tested whether merlin 1–547 would show altered binding to tubulin. Indeed, this construct demonstrated reduced binding in comparison with isoform I. However, a further truncation of 10 residues returned the binding activity (Fig. 2E) showing the complexity of the binding interphase.

Intramolecular association and phosphorylation of merlin regulate its binding to microtubules

Merlin undergoes conformational regulation and can form intramolecular association with its N- and C-terminal domains (6). This intramolecular association can mask many of the binding sites in merlin. Therefore, we studied whether intramolecular binding affects merlin–tubulin binding. Purified C-terminal GST-merlin was incubated together with increasing amounts of N-terminal merlin in order to saturate the C-terminal binding site. When C-terminus was saturated with the N-terminus it could no longer bind tubulin (Fig. 3A). GST alone incubated with the C-terminus was used as a negative control.

The C-terminal S518 of merlin can be phosphorylated by PAKs and cAMP-dependent PKA (8,9,20). This phosphorylation is thought to affect merlin's growth-regulating activity (21–23). We studied whether the phosphorylation plays a role in merlin–tubulin binding. We treated the C-terminus (492–595) of wild-type merlin or non-phosphorylatable merlin S518A mutant *in vitro* with PKA and performed the tubulin pull-down assay (Fig. 3B). Phosphorylation was verified by ^{32}P ATP labeling (not shown). Significantly lower amount of merlin was pulled down after PKA treatment indicating that the phosphorylation of the serine 518 decreases the *in vitro* binding of merlin to tubulin.

Merlin enhances microtubule polymerization *in vitro*

Many tumor suppressor proteins have been reported to affect tubulin polymerization (14) and therefore we studied whether merlin has an effect on tubulin polymerization. Purified tubulin was polymerized *in vitro* and the polymerization was monitored at OD_{350}. Microtubule-associated proteins (MAPs) and Taxol were used as positive controls and GST alone as a zero control. Nocodazole was used to control tubulin depolymerization (not shown). When recombinant merlin was added to the polymerization reaction, the rate of tubulin polymerization was increased (Fig. 4). Merlin N-, α- or C alone were not able to induce tubulin polymerization (not shown) and merlin 1–547, which has reduced affinity for tubulin, was also unable to induce tubulin polymerization.

Merlin affects the structure of Schwann cell microtubule cytoskeleton

As schwannomas, the hallmark of Neurofibromatosis 2, originate from Schwann cells, we studied merlin's effect on microtubule cytoskeleton in this cell type. We used primary mouse Schwann cells lacking merlin ($Nf2^{flox2/flox2}$, after addition of

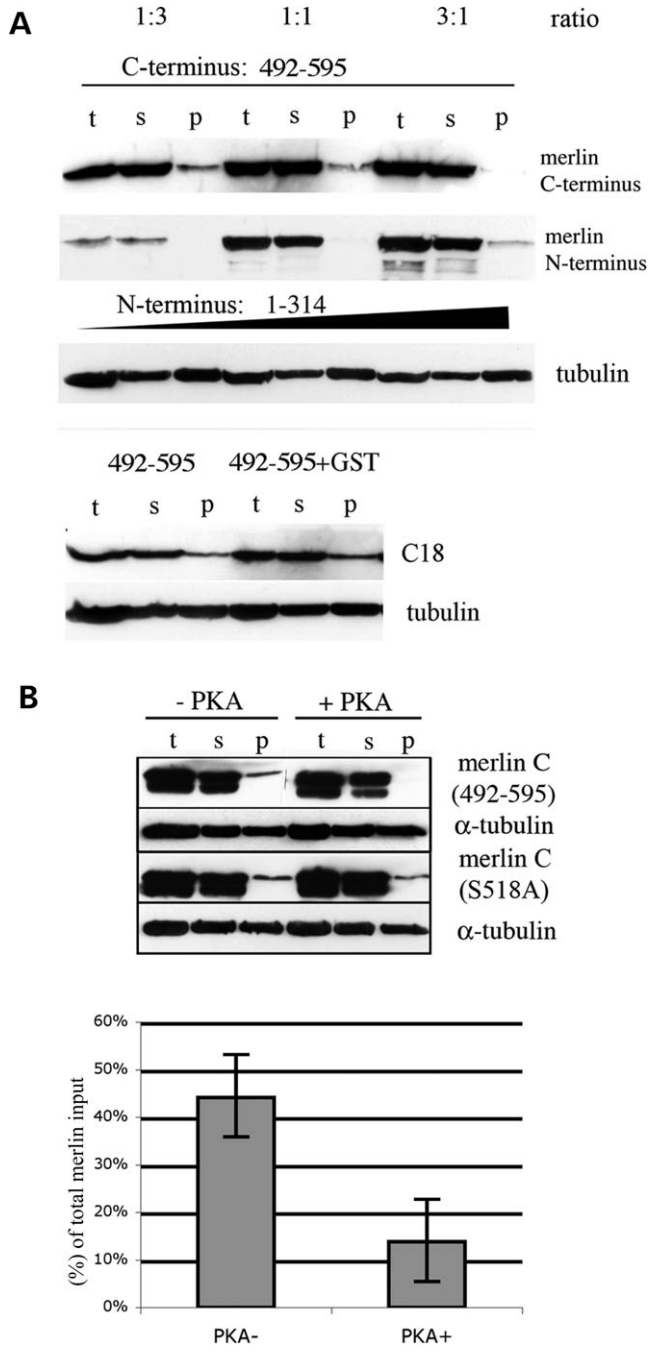

Figure 3. Intramolecular association and phosphorylation of S518 in merlin inhibits its binding to tubulin. (**A**) *In vitro* tubulin pull-down assay was performed with purified GST-merlin constructs. C-terminal merlin (amino acids 492–595) was incubated with increasing amounts of N-terminal merlin (1–314). Total (t), supernatant (s) and pellet (p) samples were analyzed by western blot with an antibody recognizing N- or C-terminal merlin (A19 or C18). When the C-terminus was saturated with the N-terminus, it could no longer bind tubulin. As a control, the C-terminus was incubated with plain GST. (**B**) The C-terminus of GST-merlin (wild-type or with S518A mutant) was phosphorylated *in vitro* with PKA and tubulin pull-down assay was performed. The amount of merlin in pellet was analyzed and compared with the total amount of merlin (%). PKA activity decreased markedly ($P = 0.006$) the binding of wild-type merlin to tubulin, but did not affect binding of the S518A mutant. The graph shows average $\pm$SD of six experiments.

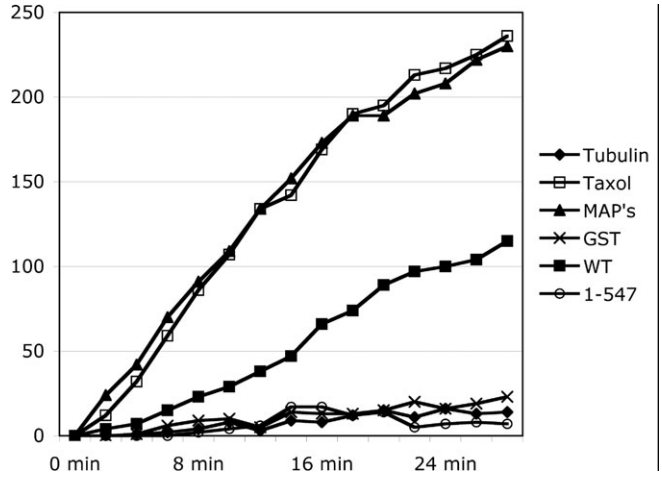

Figure 4. Merlin enhances tubulin polymerization *in vitro*. Purified tubulin from bovine brain was polymerized *in vitro* at +37°C and the polymerization was monitored at OD_{350}. Merlin GST-fusion proteins were incubated together with tubulin. Taxol and MAP2 were used as positive controls for tubulin polymerization, tubulin alone and tubulin together with GST were used as zero controls. When full-length merlin (WT) was added to the polymerization reaction, tubulin polymerized more rapidly. Merlin 1–547 was not able to induce tubulin polymerization. The graph shows an average of three experiments.

Cre-recombinase leading to genotype $Nf2^{\Delta 2/\Delta 2}$, from now on marked as Nf2 −/−, see also discussion) (24) and re-introduced wild-type merlin via adenovirus infection (Nf2 add-back). The microtubule cytoskeleton of the Nf2 −/− mouse Schwann cells differed markedly from cells re-expressing merlin via adeno-infection (Nf2 add-back). In the Nf2 add-back cells, microtubules were assembled as dense cables reaching from one end of the cell to the other and the cells displayed a normal spindle-like structure (Fig. 5A, D). Instead, the microtubules of the Nf2 −/− cells were disorganized, and the overall cell shape was more spread (Fig. 5B, D). Similar morphological differences have also been described in cultured human Schwann cells versus schwannoma cells (25).

The amount of polymerized versus unpolymerized (i.e. soluble) tubulin was analyzed from Schwann cells extracted with Triton X-100. More soluble α- and β-tubulin were present in Nf2 −/− cells than in wild-type ($Nf2^{flox2/flox2}$, marked as Nf2 +/+) or add-back cells (MWT) (Fig. 5C). The amount of soluble tubulin was associated with the expression level of merlin; increasing merlin expression resulting in reduced soluble tubulin. The total amount of tubulin in Nf2 −/− and the add-back Schwann cells were evaluated after solubilization in 6 M urea buffer. When the urea-lysates were analyzed in SDS–PAGE the add-back (MWT) and the Nf2 +/+ cells appeared to contain at least equal amount of tubulin as the Nf2 −/− cells. From this data we concluded that the ratio of polymerized/unpolymerized tubulin differs between Nf2 −/− and add-back cells; i.e. in Nf2 −/− Schwann cells the proportion of free tubulin (α/β) is higher than in the wild-type cells.

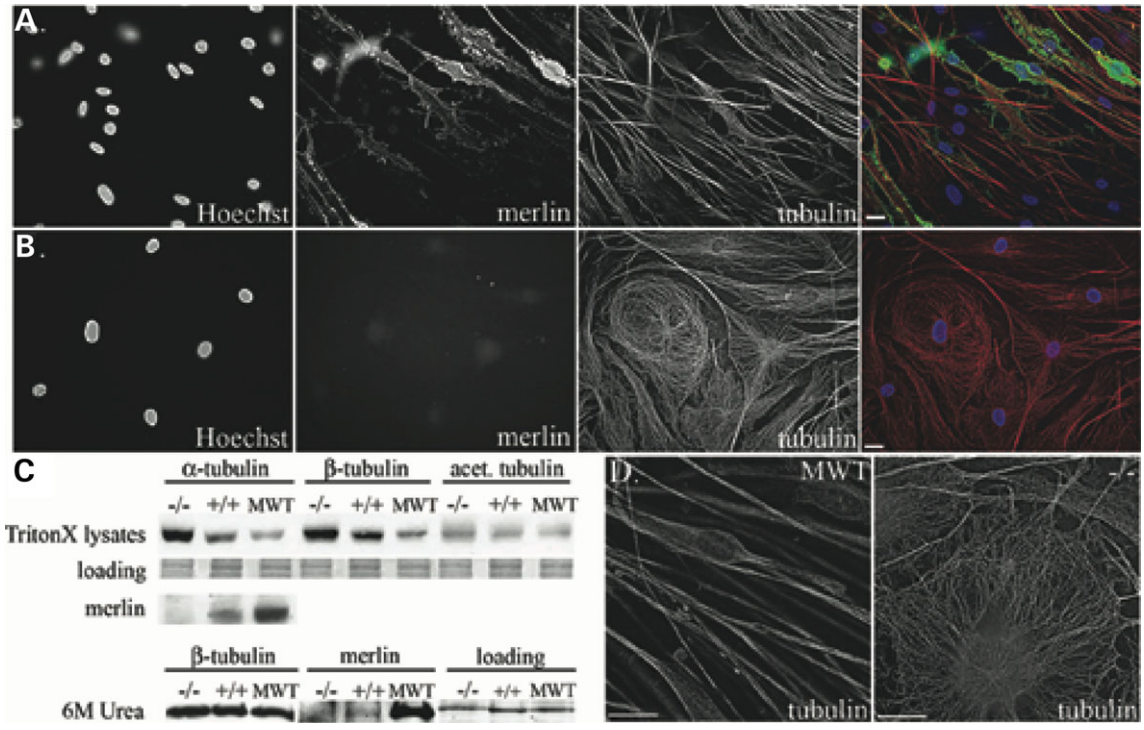

Figure 5. Microtubule cytoskeleton is altered in NF2 −/− Schwann cells. Primary mouse Schwann cells with merlin null background (NF2Δexon2, here marked as −/− (**B**) and the same cells with adeno-infected wild-type merlin (MWT) (**A**) were stained for merlin (green, A19) and β-tubulin (red) and imaged by fluorescence microscope and the images were deconvoluted. Microtubule organization is different in merlin −/− cells and in cells expressing merlin. Magnification ×630. (**C**) Triton X-100 lysates made from the −/−, +/+ and add-back (MWT) cells. Protein amounts were analyzed by Bradford assay and equal protein amounts used. As an additional loading control, the membranes were stained with Ponceau red. The lysates were probed for merlin (A-19), α-, β- and acetylated-tubulin by western blot. Total lysates of the −/−, +/+ and merlin add-back cells (MWT) were solubilized in 6 M Urea buffer and probed for β-tubulin and merlin (A-19). (**D**) A high-magnification image of tubulin in MWT and −/− cells. Scale bar 10 μm.

Tubulin polymerization dynamics differ in −/− and Nf2 add-back Schwann cells

The difference in the integrity of the tubulin cytoskeleton in −/− and add-back Schwann cells led us to test whether a difference in the polymerization rates of tubulin is also seen *in vivo*. We treated the Schwann cells with Nocodazole, which sequesters tubulin monomers and thereby depolymerizes microtubules. Incubation with Nocodazole reversed the normal morphology of Schwann cells and the cells obtained more fibroblast-like morphology (Fig. 6A, B; Supplementary video 1 and 2, for add-back and −/− cells, respectively). After 5 min of Nocodazole block release both cell types began to regain their normal shape by loosing the flattened morphology. The add-back Schwann cells began to obtain their normal morphology (i.e. long extensions) 2 h after the block release, whereas the −/− cells had only unorganized microtubules at this time-point (Fig. 6C, D; 120 min). After 4 h of block release both cell types had their microtubules re-grown. In addition, the add-back cells had regained their spindle-like shape (Fig. 6C, D; 240 min). This implies that the normal Schwann cell morphology is dependent on intact microtubule cytoskeleton and that merlin enhances microtubule organization in Schwann cells.

In addition, we used fluorescence recovery after photobleaching (FRAP) technology to study, whether tubulin dynamics were altered in primary Schwann cells lacking merlin. Schwann cells were transfected with EGFP-tubulin and 24 h after transfection the cells were analyzed by FRAP. Cells expressing merlin had a 25% faster tubulin recovery rate than the Nf2 −/− cells (Fig. 6E) ($P < 0.001$). The data suggest that merlin is able to enhance microtubule dynamics of Schwann cells *in vivo*.

DISCUSSION

In this study we describe a novel function for merlin in the regulation of microtubule organization and dynamics. We show that merlin directly binds tubulin and regulates microtubule dynamics *in vitro* and *in vivo*. Our results show that merlin contains two tubulin-binding sites, one in the FERM-domain and another in the C-terminal domain. The existence of two separate binding sites in merlin indicates that merlin could bind either laterally to the sides of the microtubules or cross-link individual microtubules to each other, this way bundling the microtubules to thicker entities. In addition, the entire protein is needed to induce tubulin polymerization, as shorter merlin fragments were not able to induce polymerization. Interestingly, the truncating patient mutation 1–547 showed reduced tubulin binding and did not induce polymerization, although it harbors the two identified tubulin binding sites. A further 10 residue deletion returned the binding activity indicating that mere loss of the binding site does not

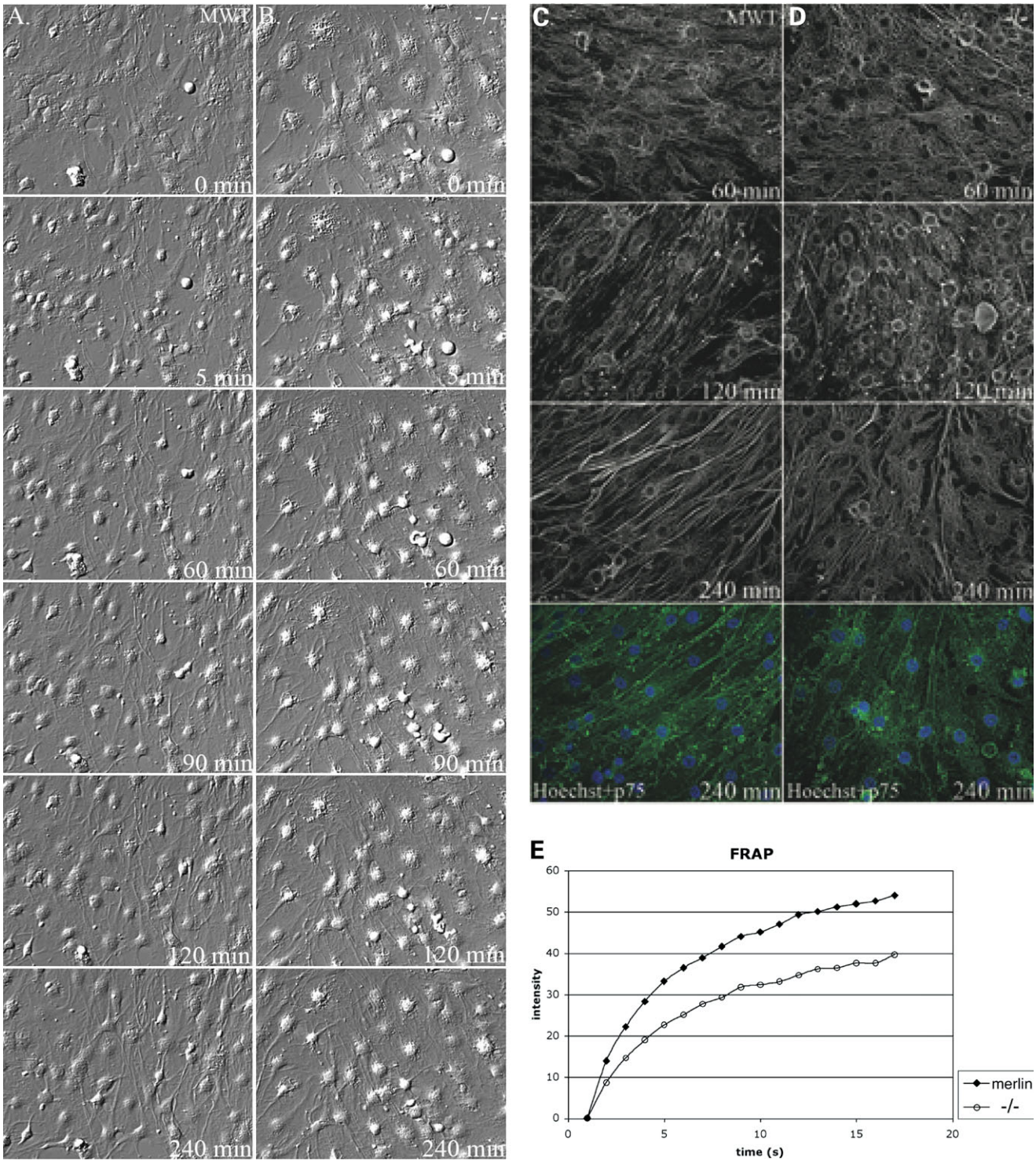

Figure 6. Microtubule recovery is faster in merlin-expressing primary Schwann cells. (**A, B**) Primary mouse Schwann cells lacking merlin (−/−) (**B**) or with adeno-infected merlin add-back (MWT) (**A**) were treated with Nocodazole to depolymerize microtubules. The block was released and cells were either imaged with DIC filter for 4 h once every 30 s (Supplementary videos 1 and 2, 200× magnification) or still images were captured from the indicated time points. Alternatively add-back MWT (**C**) and −/− (**D**) cells were fixed at indicated time points after which cells were stained with β-tubulin and a Schwann cell marker p75 and imaged with fluorescence microscope (magnification 630×) after which the images were deconvoluted. Nuclei were stained with Hoechst (blue). (**E**) For FRAP experiments primary Schwann cells (−/− and add-back) were transfected with EGFP-tubulin and 24 h after transfection the cells were imaged for FRAP with confocal microscope. Pre-bleach images were obtained and the region of interest (equal size region of interest was used with all the cells) was bleached. Post-bleach images were acquired at 2 s intervals. From the data, background was subtracted and normalized similarly for all the samples. Eight cells of each construct (−/− and add-back/MWT) were imaged and the averaged data was used for data analysis. Cells that were expressing merlin had a faster recovery rate of tubulin than the −/− cells ($P < 0.001$).

explain the result. It is possible that the 1–547 mutation leads to an altered folding of the protein and thereby prevents the interaction with tubulin.

An intramolecular association and phosphorylation of S518 in merlin can regulate its binding to microtubules. The binding of several other proteins to microtubules is regulated by phosphorylation. For example a major phosphoprotein in the brain, MAP2, is phosphorylated by PKA and upon phosphorylation dissociates from microtubules (26). Both MAP2 and merlin function as PKA-anchoring proteins (AKAPs) (27,28) and therefore merlin might have a similar function as MAP2, targeting PKA to microtubules. It is of interest that both kinases, PKA and PAK, known to regulate merlin phosphorylation, localize to centrosomes at mitosis and affect microtubule formation, in analogy with merlin (8,9,20,29,30). Previous results have suggested that phosphorylation of merlin results in the conformational opening of the molecule allowing it to interact with other proteins (23). However, in light of our study (and our unpublished observations from other interaction studies) it seems that the regulation is more complex than previously thought. We hypothesize that merlin can be 'open' but non-phosphorylated at S518 since in our results only the open but S518 non-phosphorylated merlin binds tubulin.

To study the role of merlin on microtubule dynamics *in vivo*, we used cells from genetically engineered mouse, in which wild-type *Nf2* gene has been replaced with a $NF2^{flox2/flox2}$ variant. Addition of Cre-recombinase to the cell cultures leads to deletion of exon 2 ($Nf2^{\Delta exon2/\Delta exon2}$ genotype) and to complete loss of merlin (Fig. 5). Overexpression of a Δexon 2 mutant in cultured cells is known to disturb cell adhesion (31). However, in our model, replacement of the wild-type allele with the Nf2Δexon2 leads to a greatly reduced merlin expression, when compared with the wild-type *Nf2* gene as shown in mouse tissues (24). Indeed, Cre-recombinase treated MEF cells from the same mice have previously been used as a model of genetically engineered Nf2 −/− cells (32).

Our data suggest that merlin plays an important role in regulating Schwann cell microtubule cytoskeleton. Loss of merlin in Schwann cells results in a change of the spindle-like morphology and alteration in microtubule organization. Also the ratio of polymerized versus unpolymerized tubulin is affected by merlin, i.e. Schwann cells that lack merlin have more unpolymerized tubulin than cells expressing merlin. The Nf2 −/− cells contain more acetylated tubulin, which is regarded as a marker of older and more stable structures. This might imply that tubulin polymerization/turn-over is not as efficient in the Nf2 −/− cells as in merlin-expressing cells. The results from the Nocodazole-repolymerization experiment confirm these data. Our FRAP data further supports this finding as tubulin turnover appears to be higher in merlin-expressing Schwann cells. Unfortunately, in our experimental FRAP set-up, it was not possible to monitor the dynamics of individual microtubules due to the thickness of the cells and to the high amount of free tubulin dimers. Therefore, by FRAP we have only analyzed tubulin recovery as a tubulin pool and not as individual microtubule polymers. The difference might have been even greater if we were able to study individual microtubule polymers. It also seems that microtubules are a major contributor to the Schwann cell morphology, since Schwann cell morphology resembled that of fibroblasts after depolymerization of microtubules.

Microtubules regulate endocytic pathways (16,33). Recent papers have linked merlin to endocytic events and receptor recycling (10–13). It has been shown that cells use a specific sorting mechanism of fast and slow maturation of the endocytic vesicles. Certain receptors, such as EGFR, are recycled through a dynamic pool of early endosomes that are highly mobile on microtubules and that mature rapidly towards the late endosomes. This rapid movement and maturation is completely dependent on microtubules; if microtubules are disrupted, the dynamic vesicles will non-selectively join all early endosomes and are less-efficiently degraded (34). Two papers have localized merlin to early endosomes (11,13). Thus, merlin may function as a linker at the plasma membrane, helping receptor-containing endocytosed vesicles to attach to microtubules. If cells lack merlin, this receptor recycling might be slower, and the receptors would be cleared from the membrane less efficiently. We propose that merlin plays a dual role at the membrane of Schwann cells, partly by transferring early endocytic vesicles to rapidly growing microtubules with the help of its interaction partner HRS and partly by increasing the microtubule polymerization rate, thus enhancing the vesicle maturation process.

In the past years several tumor suppressor proteins, including p53, APC, VHL and BRCA1 have been shown to bind and regulate microtubules (14). In line with merlin, also APC and VHL show only limited colocalization with microtubules, but yet affect their dynamics *in vivo* (35,36). Here, we show that also merlin binds microtubules, regulates their polymerization and has an important role in the establishment of normal Schwann cell morphology. Schwannoma cells from NF2 patients display altered morphology with long, multiple extensions (37). Based on our study this altered morphology may be associated with a disturbed microtubule cytoskeleton due to the lack of merlin, thus linking the interplay of merlin and tubulin to normal Schwann cell development and possibly to schwannoma formation.

MATERIALS AND METHODS

Cell lines and antibodies

U251 glioma cells were maintained in Dulbecco's Minimum Essential Medium (MEM), supplemented with 10% fetal calf serum (FCS) (PromoCell, Heidelberg, Germany), 1% L-glutamine and 50 μg/ml gentamycin (Invitrogen). Cells were fixed in 3.5% paraformaldehyde, pH 7.5. Primary Schwann cells were isolated and cultured as previously described (38) from NF2 knock-out mice with both alleles of the NF2 exon 2 loxed, thus producing after Cre recombination the $NF2^{\Delta 2/\Delta 2}$ genotype (24). The cells were used either at passage two or three. Anti-merlin polyclonal rabbit antibodies A-19 sc-331 (epitope 2-21), C-18 sc-332 (Santa Cruz Biotechnology, Santa Cruz, CA, USA), 1398 NF2 (39), anti-schwannomin (40) and mouse mAb KF10 (39) were used. TO-PRO 3-iodide probe (Invitrogen, Molecular Probes) was used for DNA staining. Monoclonal anti-α-, -β- and -acetylated-tubulin antibodies (Sigma–Aldrich) were used to detect tubulin. Anti-GST polyclonal

goat antibody (GE Healthcare) was used to detect GST proteins. p75 antibody (41) was used as a Schwann cell marker. Alexa 488-, 568-, 594- and 633-conjugated goat anti-mouse and goat anti-rabbit antibodies (Invitrogen, Molecular Probes) were used as secondary antibodies in immunofluorescence and HRP-conjugated rabbit anti-mouse and swine anti-rabbit and anti-goat (Santa Cruz) secondary antibodies (DAKO A/S, Glostrup, Denmark) in western blot analysis.

Plasmids and protein expression constructs

The following merlin constructs: isoform I (amino acids 1–595), isoform II and isoform I variants S518A, S518D, 1-314, 1-537 and 1-547) in pcDNA3 (Invitrogen) were used for *in vitro* translation. Luciferase cDNA was used as a negative control. For expression of recombinant GST-merlin fusion proteins, the following constructs were used: merlin N-terminus (amino acids 1–100 and 1–309), merlin a-helical domain (amino acids 314–477), C-terminus (amino acids 492–595) and C-terminus with S518A mutation as described previously (9), merlin 1–537 and merlin 1–547.

Adenovirus construct were made using Stratagene's AdEasy system. Full-length merlin was cloned into the adeno vector and the virus was produced according to manufacturer's instructions in 293A cells. The infection titer was optimized to have 100% efficiency and verified by immunofluorescence staining. Schwann cells lacking merlin were infected with adenoviruses 3 days before the experiments were conducted. EGFP-tubulin construct was obtained from Invitrogen, and transfection to primary Schwann cells was done with Lipofectamine PLUS (Invitrogen).

In vitro translation and quantification of labeled proteins

Merlin pcDNA3 plasmids (Invitrogen) were used as a template for a T7-coupled rabbit reticulocyte transcription–translation system (Promega, Madison, WI, USA) in the presence of ^{35}S-methionine. Five microlitres of 50 μl reaction were run in to SDS–PAGE, gel was dried and exposed to film to determine the size and amount of the labeled protein. For quantification the gel was also exposed to PhosphoImager low energy-plate (GE Healthcare), read by TyphoonImager 9400 (GE Healthcare) and analyzed by ImageQuantTL2003 software (GE Healthcare).

GST-fusion protein production

GST-fusion proteins were expressed in *Escherichia coli* DH5α and purified following standard protocol. Fusion protein was eluted from the Glutathione Sepharose beads (GE Healthcare) by 5 mM reduced glutathione in 50 mM Tris–HCl pH 8.0, over night at +4°C. Before some tubulin pull-down assays different amounts of N- and C-terminus were incubated in 50 mM Tris–HCl, 150 mM NaCl (pH 8.0) for 30 min at room temperature. The eluted fusion proteins for the PKA assay were dialyzed against 20 mM Tris–HCl, 10 mM $MgCl_2$, pH 7.4 at +4°C o/n. Wild-type merlin was produced in Sf9 insect cell line. Merlin with an N-terminal GST-tag was cloned into a baculovirus transfer vector pAcG2T (BD Biosciences) and then produced with the BaculoGOLD system (BD Biosciences). Sf9 cells were used to produce recombinant merlin according to user's manual (Invitrogen). Full-length merlin was purified after 1 day of infection following standard GST-purification protocol. The proteins were used immediately after purification.

In vitro phosphorylation

GST-proteins were dialyzed against the reaction buffer and run into SDS–PAGE, protein amounts estimated and equal amounts of each construct were used in the *in vitro* phosphorylation assay. Total volume of the reaction was 40 μl including PKA reaction buffer (20 mM Tris–HCl, 10 mM $MgCl_2$, pH 7.4), 200 mM ATP and purified human or bovine catalytic subunit of PKA (Sigma–Aldrich). Reaction was incubated 30 min at +30°C and was stopped by adding 20 mM PKA inhibitor H89 (Sigma–Aldrich).

Tubulin pull-down assay

Tubulin pull-down was performed with ^{35}S-labeled *in vitro* translated protein, eluted GST-fusion protein or with *in vitro* PKA phosphorylated eluted GST-fusion protein. Equal protein amounts were used in all experiments. Purified bovine tubulin (Cytoskeleton) (70 μg) was added to tubulin polymerization buffer (80 mM PIPES, 0.5 mM MgCl, 1 mM ethylene glycol-bis, 1 mM GTP, pH 6.9, 10% glycerol, 10 mM Taxol) to a final volume of 200 μl and the microtubules were allowed to polymerize at +37°C for 30 min in the presence of different merlin constructs. After this 50 μl were removed and labeled as 'total' fraction and the remaining 150 μl were centrifuged at 11 503 *g* for 30 min at +30°C to collect the polymerized microtubules. Supernatant was removed and the pellet was resuspended in 150 μl of polymerization buffer. Twelve microlitres of each fraction were analyzed on SDS–PAGE.

Western blot

Primary Schwann cells were lysed in ice-cold ELB buffer (150 mM NaCl, 50 mM Hepes pH 7.4, 5 mM EDTA, 0.5% NP40 and complete protease inhibitor cocktail tablet, Roche) or in mild Triton-X buffer (50 mM Tris pH 7.4, 150 mM NaCl, 1 mM EDTA, 1% Triton-X 100, 1 mM PMSF) including protease inhibitors (Complete), cells were incubated on ice for 15 min and centrifuged at full speed in +4°C for 15 min. Alternatively, cells were scraped in ice-cold PBS, centrifuged briefly and the cell pellet was suspended into Urea-buffer (50 mM Tris, 6 M Urea, pH 7.4). The cells were lysed for 15 min and briefly sonicated. The protein amounts were analyzed either by the Bradford assay or by Coomassie staining. Equal amounts of proteins were run into gel transferred into nitrocellulose membrane and blotted with antibodies. As an additional loading control, loading was verified after western blot by staining the filters with Ponceau red. A representative band of the whole filter of approximately 150 kD was chosen as the loading band for Figure 5C.

Immunofluorescence, laser scanning confocal microscopy, live cell imaging and fluorescence recovery after photobleaching

U251 and Schwann cells were fixed in 3.5% PFA for 10 min, washed in PBS and permeabilized for 5 min in 0.1% Triton X-100/PBS and blocked at 5% BSA in PBS. Cells were stained with merlin and tubulin antibodies (diluted 1:100 and 1:200, respectively) followed by secondary antibodies or TO-PRO 3-iodide or DAPI nuclear stain. Double stainings were performed sequentially. Coverslips were mounted in DABCO (Sigma) and Mowiol (Calbiochem) or Vectashield (Vector Laboratories, Burlingame, CA, USA). Cells were examined by confocal microscope: U251 cells with Leica SP2 equipped with Ar and Kr lasers (Leica Microsystems, Heerbrugg, Switzerland) and Schwann cells with Zeiss LSM 510 META (Fig. 1) using the sequential scanning mode. Schwann cell images (Figs 5 and 6D) were acquired by immunofluorescence microscope (Zeiss Axiophot equipped with AxioCam cooled CCD-camera, Carl Zeiss, Esslingen, Germany).

Live cell imaging was performed in pre-warmed microscope chambers at +37°C with 20 mM Hepes as a buffering agent in the medium. Cells were plated on LabTek borosilicate no. 1.5 imaging chambers (Nunc, Naperville, IL, USA) and imaged either with Olympus inverted IX81 microscope (supplemented with 5% CO_2, for the Nocodazole experiment) and CellR program or with confocal Zeiss LSM 510 META microscope. For videos, cells were imaged once every 30 s for 4 h (exposure 122 ms). FRAP analysis was performed with the Zeiss confocal microscope, pre-bleach images were obtained after which lasers were turned to full power and region of interest was bleached 50 times, the same settings were used for all FRAP experiments including the region of interest. Data analysis was performed in Zeiss META and in Microsoft Excel.

Statistical and image analysis

All statistical analyses were performed in Excel with Student's *t*-test using two-tailed distribution and image analysis was performed with Image J 1.36b. Images were processed with Adobe Photoshop, or with Image J 1.36b. Background was subtracted from DIC images with FFT bandpass filter and with Pseudo flat-field filter in Image J. Wide-field immunofluorescence images (Figs 5A, B and 6C, D) were deconvoluted with Huygens Deconvolution software (Scientific Volume Imaging), 30 iterations for each channel.

In vitro tubulin polymerization and other experiments

In vitro tubulin polymerization was performed on UV-permeable 96-well plates. Tubulin was purified from bovine brain as previously described (42) and recombinant merlin was produced in Sf9 insect cells as described in the GST-fusion protein section. Nocodazole 20 μM, Taxol 20 μM (Sigma) and MAP's (purified from bovine brain) were used as controls in the polymerization reaction. The polymerization buffer (80 mM PIPES, 0.5 mM MgCl, 1 mM Ethylene glycol-bis, 1 mM GTP, pH 6.9, 10% glycerol) was mixed with tubulin (25 μM) and merlin constructs (different amounts) were added on ice. At the beginning of the experiment the 96-well plate was transferred to pre-warmed 96-well plate reader that measured the OD at 350 nm every 5 min at +37°C for 60 min. The Nocodazole experiment was performed on primary Schwann cells with or without the re-expression of merlin via adeno-infection. Cells were incubated with 8 μM Nocodazole overnight after which the block was released and the cells were fixed at indicated time points. The cells were stained for tubulin and merlin.

SUPPLEMENTARY MATERIAL

Supplementary Material is available at HMG Online.

ACKNOWLEDGEMENTS

We would like to thank Niclas Setterblad at the Imaging Department of the Institut Universitaire d'Hématologie IFR105 for valuable help in confocal microscopy and FRAP experiments. The imaging department is supported by grants from the Conseil Regional d'Ile-de-France and the Ministère de la Recherche. In addition we would like to thank all the personnel in Dr Giovannini's laboratory for the help with Schwann cell experiments. We also thank M. Hukkanen and M. Liljeström from Molecular Imaging Unit in Biomedicum Helsinki for their help with the image analysis, H. Ahola for her skillful technical assistance and L. Heiska for her comments and critical reading of the manuscript. This study was supported by the grants of Department of Defense DAMD17-00-0550 and W81XWH-05-1-0469, the Finnish Cancer Organizations, Helsinki Graduate School of Biotechnology and Molecular Biology, French embassy in Helsinki, Centre for International Mobility (CIMO), Emil Aaltonen Foundation, Ida Montin Foundation, Maire Taponen Foundation, Svenska kulturfonden and Biomedicum Helsinki Foundation.

Conflict of Interest statement. None declared.

REFERENCES

1. Gutmann, D.H. (1997) Molecular insights into neurofibromatosis 2. *Neurobiol. Dis.*, **3**, 247–261.
2. den Bakker, M.A., Riegman, P.H., Suurmeijer, A.P., Vissers, C.J., Sainio, M., Carpen, O. and Zwarthoff, E.C. (2000) Evidence for a cytoskeleton attachment domain at the N-terminus of the NF2 protein. *J. Neurosci. Res.*, **62**, 764–771.
3. Xu, H.M. and Gutmann, D.H. (1998) Merlin differentially associates with the microtubule and actin cytoskeleton. *J. Neurosci. Res.*, **51**, 403–415.
4. Bretscher, A., Chambers, D., Nguyen, R. and Reczek, D. (2000) ERM-merlin and EBP50 protein families in plasma membrane organization and function. *Annu. Rev. Cell Dev. Biol.*, **16**, 113–143.
5. Gonzalez-Agosti, C., Wiederhold, T., Herndon, M.E., Gusella, J. and Ramesh, V. (1999) Interdomain interaction of merlin isoforms and its influence on intermolecular binding to NHE-RF. *J. Biol. Chem.*, **274**, 34438–34442.
6. Grönholm, M., Sainio, M., Zhao, F., Heiska, L., Vaheri, A. and Carpen, O. (1999) Homotypic and heterotypic interaction of the neurofibromatosis 2 tumor suppressor protein merlin and the ERM protein ezrin. *J. Cell. Sci.*, **112**, 895–904.
7. Nguyen, R., Reczek, D. and Bretscher, A. (2001) Hierarchy of merlin and ezrin N- and C-terminal domain interactions in homo- and heterotypic associations and their relationship to binding of scaffolding proteins EBP50 and E3KARP. *J. Biol. Chem.*, **276**, 7621–7629.

8. Shaw, R.J., Paez, J.G., Curto, M., Yaktine, A., Pruitt, W.M., Saotome, I., O'Bryan, J.P., Gupta, V., Ratner, N., Der, C.J. *et al.* (2001) The Nf2 tumor suppressor, merlin, functions in rac-dependent signaling. *Dev. Cell*, **1**, 63–72.
9. Alfthan, K., Heiska, L., Grönholm, M., Renkema, G.H. and Carpen, O. (2004) Cyclic AMP-dependent protein kinase phosphorylates merlin at serine 518 independently of P21-activated kinase and promotes merlin-ezrin heterodimerization. *J. Biol. Chem.*, **279**, 18559–18566.
10. Fraenzer, J.T., Pan, H., Minimo, L., Jr, Smith, G.M., Knauer, D. and Hung, G. (2003) Overexpression of the *NF2* gene inhibits schwannoma cell proliferation through promoting PDGFR degradation. *Int. J. Oncol.*, **23**, 1493–1500.
11. Scoles, D.R., Huynh, D.P., Chen, M.S., Burke, S.P., Gutmann, D.H. and Pulst, S.M. (2000) The neurofibromatosis 2 tumor suppressor protein interacts with hepatocyte growth factor-regulated tyrosine kinase substrate. *Hum. Mol. Genet.*, **9**, 1567–1574.
12. Lloyd, T.E., Atkinson, R., Wu, M.N., Zhou, Y., Pennetta, G. and Bellen, H.J. (2002) Hrs regulates endosome membrane invagination and tyrosine kinase receptor signaling in *Drosophila*. *Cell*, **108**, 261–269.
13. Maitra, S., Kulikauskas, R.M., Gavilan, H. and Fehon, R.G. (2006) The tumor suppressors merlin and expanded function cooperatively to modulate receptor endocytosis and signaling. *Curr. Biol.*, **16**, 702–709.
14. Fisk, H.A., Mattison, C.P. and Winey, M. (2002) Centrosomes and tumour suppressors. *Curr. Opin. Cell Biol.*, **14**, 700–705.
15. Hergovich, A., Lisztwan, J., Barry, R., Ballschmieter, P. and Krek, W. (2003) Regulation of microtubule stability by the von hippel-lindau tumour suppressor protein pVHL. *Nat. Cell Biol.*, **5**, 64–70.
16. Murray, J.W. and Wolkoff, A.W. (2003) Roles of the cytoskeleton and motor proteins in endocytic sorting. *Adv. Drug Deliv. Rev.*, **55**, 1385–1403.
17. Muranen, T., Grönholm, M., Renkema, G.H. and Carpen, O. (2005) Cell cycle-dependent nucleocytoplasmic shuttling of the neurofibromatosis 2 tumour suppressor merlin. *Oncogene*, **24**, 1150–1158.
18. Stokowski, R.P. and Cox, D.R. (2000) Functional analysis of the neurofibromatosis type 2 protein by means of disease-causing point mutations. *Am. J. Hum. Genet.*, **66**, 873–891.
19. Grönholm, M., Muranen, T., Toby, G.G., Utermark, T., Hanemann, C.O., Golemis, E.A. and Carpen, O. (2006) A functional association between merlin and HEI10, a cell cycle regulator. *Oncogene*, **25**, 4389–4398.
20. Kissil, J.L., Johnson, K.C., Eckman, M.S. and Jacks, T. (2002) Merlin phosphorylation by p21-activated kinase 2 and effects of phosphorylation on merlin localization. *J. Biol. Chem.*, **277**, 10394–10399.
21. Morrison, H., Sherman, L.S., Legg, J., Banine, F., Isacke, C., Haipek, C.A., Gutmann, D.H., Ponta, H. and Herrlich, P. (2001) The NF2 tumor suppressor gene product, merlin, mediates contact inhibition of growth through interactions with CD44. *Genes Dev.*, **15**, 968–980.
22. Xiao, G.H., Beeser, A., Chernoff, J. and Testa, J.R. (2002) p21-activated kinase links Rac/Cdc42 signaling to merlin. *J. Biol. Chem.*, **277**, 883–886.
23. Rong, R., Surace, E.I., Haipek, C.A., Gutmann, D.H. and Ye, K. (2004) Serine 518 phosphorylation modulates merlin intramolecular association and binding to critical effectors important for NF2 growth suppression. *Oncogene*, **23**, 8447–8454.
24. Giovannini, M., Robanus-Maandag, E., van der Valk, M., Niwa-Kawakita, M., Abramowski, V., Goutebroze, L., Woodruff, J.M., Berns, A. and Thomas, G. (2000) Conditional biallelic Nf2 mutation in the mouse promotes manifestations of human neurofibromatosis type 2. *Gene Dev.*, **14**, 1617–1630.
25. Utemark, T., Schubert, S.J. and Hanemann, C.O. (2005) Rearrangements of the intermediate filament GFAP in primary human schwannoma cells. *Neurobiol. Dis.*, **19**, 1–9.
26. Ozer, R.S. and Halpain, S. (2000) Phosphorylation-dependent localization of microtubule-associated protein MAP2c to the actin cytoskeleton. *Mol. Biol. Cell*, **11**, 3573–3587.
27. Rubino, H.M., Dammerman, M., Shafit-Zagardo, B. and Erlichman, J. (1989) Localization and characterization of the binding site for the regulatory subunit of type II cAMP-dependent protein kinase on MAP2. *Neuron*, **3**, 631–638.
28. Grönholm, M., Vossebein, L., Carlson, C.R., Kuja-Panula, J., Teesalu, T., Alfthan, K., Vaheri, A., Rauvala, H., Herberg, F.W., Tasken, K. *et al.* (2003) Merlin links to the cAMP neuronal signaling pathway by anchoring the RIbeta subunit of protein kinase A. *J. Biol. Chem.*, **278**, 41167–41172.
29. Lamb, N.J., Cavadore, J.C., Labbe, J.C., Maurer, R.A. and Fernandez, A. (1991) Inhibition of cAMP-dependent protein kinase plays a key role in the induction of mitosis and nuclear envelope breakdown in mammalian cells. *EMBO J.*, **10**, 1523–1533.
30. Banerjee, M., Worth, D., Prowse, D.M. and Nikolic, M. (2002) Pak1 phosphorylation on t212 affects microtubules in cells undergoing mitosis. *Curr. Biol.*, **12**, 1233–1239.
31. Koga, H., Araki, N., Takeshima, H., Nishi, T., Hirota, T., Kimura, Y., Nakao, M. and Saya, H. (1998) Impairment of cell adhesion by expression of the mutant neurofibromatosis type 2 (NF2) genes which lack exons in the ERM-homology domain. *Oncogene*, **20**, 801–810.
32. Lallemand, D., Curto, M., Saotome, I., Giovannini, M. and McClatchey, A.I. (2003) NF2 deficiency promotes tumorigenesis and metastasis by destabilizing adherens junctions. *Genes Dev.*, **17**, 1090–1100.
33. Petiot, A., Faure, J., Stenmark, H. and Gruenberg, J. (2003) PI3P signaling regulates receptor sorting but not transport in the endosomal pathway. *J. Cell Biol.*, **162**, 971–979.
34. Lakadamyali, M., Rust, M.J. and Zhuang, X. (2006) Ligands for clathrin-mediated endocytosis are differentially sorted into distinct populations of early endosomes. *Cell*, **124**, 997–1009.
35. Kita, K., Wittmann, T., Nathke, I.S. and Waterman-Storer, C.M. (2006) Adenomatous polyposis coli on microtubule plus ends in cell extensions can promote microtubule net growth with or without EB1. *Mol. Biol. Cell*, **17**, 2331–2345.
36. Lolkema, M.P., Mehra, N., Jorna, A.S., van Beest, M., Giles, R.H. and Voest, E.E. (2004) The von Hippel-Lindau tumor suppressor protein influences microtubule dynamics at the cell periphery. *Exp. Cell Res.*, **301**, 139–146.
37. Rosenbaum, C., Kluwe, L., Mautner, V.F., Friedrich, R.E., Muller, H.W. and Hanemann, C.O. (1998) Isolation and characterization of schwann cells from neurofibromatosis type 2 patients. *Neurobiol. Dis.*, **5**, 55–64.
38. Manent, J., Oguievetskaia, K., Bayer, J., Ratner, N. and Giovannini, M. (2003) Magnetic cell sorting for enriching schwann cells from adult mouse peripheral nerves. *J. Neurosci. Methods*, **123**, 167–173.
39. den Bakker, M.A., Riegman, P.H., Hekman, R.A., Boersma, W., Janssen, P.J., van der Kwast, T.H. and Zwarthoff, E.C. (1995) The product of the NF2 tumour suppressor gene localizes near the plasma membrane and is highly expressed in muscle cells. *Oncogene*, **10**, 757–763.
40. Lutchman, M. and Rouleau, G.A. (1995) The neurofibromatosis type 2 gene product, schwannomin, suppresses growth of NIH 3T3 cells. *Cancer Res.*, **55**, 2270–2274.
41. Huber, L.J. and Chao, M.V. (1995) Mesenchymal and neuronal cell expression of the p75 neurotrophin receptor gene occur by different mechanisms. *Dev. Biol.*, **167**, 227–238.
42. Hyman, A.A., Drexel, D., Kellog, D., Salser, S., Sawin, K., Steffen, P., Wordeman, L. and Mitchison, T.J. (1991) Preparation of modified tubulins. *Meth. Enzymol.*, **196**, 478–486.

Protein kinase A mediated phosphorylation of the NF2 tumor suppressor protein merlin at serine 10 affects the actin cytoskeleton organization

Laulajainen M. [1,3]*, Muranen T. [1,3], Carpén O.[1,2], and Grönholm M.[1].

[1] Biomedicum Helsinki, Department of Pathology, 00014 University of Helsinki, Finland.
[2] Department of Pathology, University of Turku and Turku University Central Hospital, 20520 Turku, Finland.

[3] These two authors have contributed equally to this work.

*Corresponding author: Minja Laulajainen
Address: Minja Laulajainen
Biomedicum Helsinki
PL 63
00014 University of Helsinki
Finland

Tel: +358919125651
Fax: +358947171964

E-mail: **Minja.Laulajainen@helsinki.fi**

Running title: PKA phosphorylation of merlin

Keywords: merlin, NF2, PKA, phosphorylation, actin

Abstract

Mutations in the NF2 tumor suppressor gene encoding merlin induce tumors of the nervous system. Merlin localizes to the cell membrane where it links the actin cytoskeleton to membrane proteins. Cell proliferation is regulated by merlin in many cell types, but its tumor suppressor function still remains unclear. Phosphorylation has been suggested to regulate merlin's tumor suppressor activity. The only characterized phosphorlyation site is the C-terminal serine 518, which is phosphorylated both by p21-activated kinases (PAKs) and protein kinase A (PKA). In this work we identify a novel PKA phosphorylation site, serine 10, in the N-terminus of merlin. We show that a non-phosphorylable form of serine 10 (S10A) affects cellular morphology by inducing long extensions. Regulation of this site also affects actin cytoskeleton organization and dynamics in vivo, as merlin S10A reduces the amount of cellular F-actin and merlin S10D stabilizes F-actin filaments. By using a wound-healing assay and live cell imaging we demonstrate that dephosphorylation of serine 10 leads to defects in migration, possibly through altered ability of the cells to form lamellipodia. This study suggests a role for merlin in mediating PKA induced changes of the actin cytoskeleton.

Introduction

Mutations in the NF2 gene predispose to tumors of the nervous system, mainly schwannomas and meningiomas (Baser et al., 2003). The NF2 gene encodes for the tumor suppressor protein merlin (moesin-ezrin-radixin like protein, or schwannomin), which shares overall structural similarity with the highly conserved ERM (ezrin-radixin-moesin) family of proteins (Rouleau et al., 1993; Trofatter et al., 1993). Merlin and the ERM proteins function as linkers between the plasma membrane and cytoskeleton, where they modulate the morphology, growth and migration of the cells (Bretscher et al., 2002). The proteins have an overall homology of 75-80% on the amino acid level, and their structure consists of a large N-terminal FERM domain (amino acids 19-314 in merlin), an α-helical region (amino acids 315-491), and a small globular C-terminus (amino acids 492-595) (Turunen et al., 1998).

Merlin exists as two major isoforms, I and II, as a result of alternative splicing of exon 16 (Rouleau et al., 1993). The two isoforms differ in their C-terminal sequences, but are identical over the first 579 residues. Merlin isoform I is capable of head-to-tail interactions, whereas isoform II is predicted to exist in a constitutively open conformation since it lacks the C-terminal residues implicated in the intramolecular binding (Sherman et al., 1997; Gonzalez-Agosti et al., 1999; Grönholm et al., 1999).

The tumor suppressor mechanism of merlin is still not clear, but it has been suggested that phosphorylation regulates this activity. Shaw et al. (1998) demonstrated that merlin is phosphorylated on several serine and threonine residues, but not on tyrosines, and that the phosphorylation status of merlin varies in response to different growth conditions. Three merlin species with different electrophoretic mobilities have been observed, suggesting that at least three differentially phosphorylated forms of merlin exist. However, only one phosphorylation site has been identified so far. Merlin contains a C-

terminal serine 518 which is phosphorylated both by p21 activated kinase (PAK) and protein kinase A (PKA) (Shaw et al., 2001; Kissil et al., 2002; Xiao et al., 2002; Alfthan et al., 2004). Phosphorylation at this site is predicted to result in a more open conformation incapable of inhibiting cell growth, but instead inducing the activation of Ras signaling pathways leading to cell division (Morrison et al., 2001; Xiao et al., 2002). When serine 518 is dephosphorylated by the myosin phosphatase MYPT-1-PP1δ, the tumor suppressor function of merlin is activated, inhibiting the Ras signaling pathway and leading to growth arrest (Morrison et al., 2001; Jin et al., 2006).

Merlin is able to interact with the ERM proteins, but the heterodimerization requires a conformational change in both proteins (Grönholm et al., 1999). One way to regulate the conformation of merlin is by phosphorylation of serine 518 (Alfthan et al., 2004; Rong et al., 2004), but additional forms of activation may be required. Phosphorylation of S518 also weakens merlin's association with the cytoskeleton (Shaw et al., 2001). Like ERM proteins, merlin interacts with F-actin, however, only through N-terminal sites (Xu and Gutmann, 1998; Brault et al., 2001). Even though the FERM domain of merlin is highly similar to the ERM proteins, the first 18 amino acid in merlin which precede the FERM domain (Brault et al., 2001; Shimizu et al., 2002) are not found in the ERM family (Golovnina et al., 2005). Interestingly, these 18 amino acids have been indicated in the actin binding of merlin (Brault et al., 2001).

We have previously shown that PKA binds to and phosphorylates merlin (Grönholm et al., 2003; Alfthan et al., 2004). PKA is a serine/threonine kinase that regulates the activity of several proteins, including the ERM family member ezrin (Zhou et al., 2003). The cyclic AMP-PKA pathway plays a role in cell division and actin cytoskeleton remodeling (Howe, 2004), and activation of PKA promotes cell growth and cell cycle progression in Schwann cells (Kim et al., 1997). The previously described binding between the α-helical domain of merlin and RIβ, one of the four regulatory subunits of PKA, suggests that merlin might function as a protein kinase A anchoring protein (AKAP) (Grönholm et al., 2003).

Our previous study preliminary identified a PKA site in the N-terminus of merlin in addition to the C-terminal S518. We have now further characterized the N-terminal PKA-catalyzed phosphorylation of merlin, and mapped the phosphorylation site to serine 10. In

addition, we have studied the role of merlin serine 10 in the regulation of actin cytoskeleton.

Results

Merlin contains two PKA phosphorylation sites, serine 10 in the FERM domain and serine 518 in the C-terminal domain Figure 1

Our previous studies suggested that PKA phosphorylates the N-terminal domain of merlin (Alfthan et al., 2004). Metabolic labeling was performed to test whether such phosphorylation can be detected in vivo. 293A HEK cells transfected with wild-type (WT) and S518A (mimicking the unphosphorlyated serine 518) merlin GST-constructs were incubated with ^{32}P labeled orthophosphate together with either forskolin and IBMX to activate PKA, or H89 to inhibit PKA kinase activity. The amount of bound orthophosphate in merlin was compared to the orthophosphate in the empty vector. Forskolin and IBMX treated WT merlin showed pronounced phosphorylation which was reduced but not completely abolished with the PKA inhibitor H89 (Fig.1b). The amount of bound orthophosphate in merlin S518A was lower than in WT, but the construct was still phosphorylated. Treatment of S518A with the PKA inhibitor strongly reduced the amount of orthophosphate in the construct compared to the control lysate.

With deletion constructs, we further mapped the phosphorylated region in vitro to amino acids 1-100 (data not shown), which contains one serine (S10) and two threonines (T28 and T54). These potential kinase recognition motifs were mutated to nonphosphorylatable alanines and an in vitro phosphorylation reaction was performed with recombinant GST-merlin proteins. Incubation of the fusion proteins with [γ-^{33}P] ATP and human recombinant PKA resulted in incorporation of ^{33}P into merlin constructs 1-100, 1-100 T28A, and 1-100 T54A, but not into 1-100 S10A or GST (Fig.1c), indicating that the site phosphorylated by PKA is serine 10.

To verify that serine 10 functions as a substrate residue also in a longer merlin molecule containing more than just the N-terminal part of the protein, we mutated the

phosphorylatable residues in merlin 1-547. WT merlin could not be used since it is degraded when produced as a GST-fusion protein. As shown in Fig.1d, incorporation of ^{33}P was detected both in merlin 1-547 and 1-547 S518A, although phosphorylation of merlin 1-547 S518A was reduced when compared to 1-547. However, when a double mutation (S10A+S518A) was introduced to merlin 1-547 no phosphorylation could be detected. As expected, the merlin C-terminus (amino acids 492-595) was phosphorylated by PKA, but the S518A mutation abolished the phosphorylation. These results indicate that serines 10 and 518 are the only PKA phosphorylation sites present in merlin.

Mutation of serine 10 does not affect serine 518 phosphorylation or ezrin binding

Figure 2

Differentially phosphorylated forms of merlin differ in their electrophoretic mobility. Therefore, previous in vivo phosphorylation studies have been done by investigating the mobility of merlin mutants in SDS-PAGE. WT merlin migrates in the gel as a triplet, with the bands corresponding to hyperphosphorylated, phosphorylated and hypophosphorylated forms of the protein (Shaw et al., 1998; Alfthan et al., 2004). When serine 518 is dephosphorylated, or mutated to alanine (S518A), the slowest migrating, hyperphosphorylated, form of merlin disappears (Alfthan et al., 2004). To determine whether PKA phosphorylation of serine 10 induces similar changes in electrophoretic mobility, we generated mutations mimicking unphosphorylated (S10A or S518A) or phosphorylated (S10D or S518D) forms at both PKA phosphorylation sites. Lysates from 293 HEK cells, transiently transfected with these mutant proteins, were analyzed by immunoblotting. SDS-PAGE analysis revealed that all merlin constructs migrated at expected molecular weights (65-70 kDa). Consistent with earlier studies, WT merlin migrated as a triplet in the gel (Fig.2a). As previously shown, the hyperphosphorylated merlin band was absent in the S518A mutants. However, we observed all three migrating species in S10A, suggesting that phosphorylation of serine 10 does not induce a conformational change that would result in altered electrophoretic mobility. Substitution of serine 10 does also not seem to affect the change caused by serine 518 phosphorylation, since the slowest migrating merlin band was present in constructs with

S10 mutations. Insoluble fractions of the lysates showed similar results and we could not detect any differences in the solubility of the constructs (data not shown), suggesting that S10 does not markedly regulate the association of merlin with detergent-insoluble cytoskeleton.

To further test whether PKA-induced phosphorylation of serine 10 is a prerequisite for serine 518 phosphorylation and to examine the possible link between the two sites, 293 HEK cells were transfected with the mutated merlin constructs and analyzed with an antibody specifically recognizing S518 phosphorylated merlin (pS518 Ab). The expression levels of merlin constructs were verified using merlin mAb KF10 (Fig.2b). Mutation of serine 10 did not reduce the reactivity of pS518 Ab, consistent with the results from the electrophoretic mobility assay. As expected, the pS518 Ab did not detect the S518A construct.

To analyze serine 518 phosphorylation of merlin S10 mutants in cells, COS-7 cells were transfected with the phosphorylation mutants. COS-7 cells were chosen because of their large cell surface, low levels of endogenous merlin expression, and recognizable changes in morphology after merlin transfection (Sainio et al., 1997). Overexpression of WT and S10A merlin induced long thin cellular extensions that were not stained with the pS518 Ab. However, serine 518 phosphorylated merlin was present in shorter thicker protrusions observed in WT, S10A, and S10D transfected cells (Fig.2c). These findings suggest that phosphorylation of serine 10 does not directly affect serine 518 phosphorylation.

We have previously shown that PKA phosphorylation of serine 518 promotes merlin-ezrin heterodimerization (Alfthan et al., 2004). To determine whether serine 10 phosphorylation similarly regulates intermolecular binding with ezrin, we examined the interaction of phosphorylated and unphosphorylated merlin constructs with ezrin in vitro by GST pull-down assays. Equal amounts of merlin constructs were used and the loading was verified by GST-antibody blotting (Fig.2d, lower panel). We observed the previously reported effect of serine 518 phosphorylation on ezrin binding, as PKA treated merlin 1-547 pulled down more full-length ezrin than unphosphorylated merlin 1-547 (Fig.2d, upper panel). In contrast, PKA-mediated phosphorylation of the merlin N-terminus (amino acids 1-314) or 1-547 S518A did not increase merlin-ezrin binding.

Serine 10 affects the morphological changes induced by merlin

Figure 3

Overexpressed WT merlin influences cell morphology (Sainio et al., 1997). To study whether the phenotypic effect of merlin is regulated by modification of serine 10, cultured COS-7 cells and mouse embryonic fibroblasts lacking merlin (Nf2 -/- MEFs) were transiently transfected with WT, S10A, or S10D merlin either in isoform I or isoform II, and examined by immunofluorescence microscopy.

Overexpression of merlin isoform I (WT) affected cell morphology, leading to an increase in the amount of membrane extensions both in COS-7 cells and Nf2 -/- MEFs (Fig.3). Merlin isoform II also induced cell projections, but they were often more abundant and longer than those observed with WT isoform I. Cells expressing merlin S10A produced very long cellular extensions, and these extensions were even more pronounced in S10A isoform II. Interestingly, S10D expression resulted in a morphology with dense filopodia-like structures but only rarely long cellular projections. This data suggest that phosphorylation of serine 10 regulates merlin induced cell morphology.

Serine 10 phosphorylation regulates F-actin organization

Figure 4

Since serine 10 regulates cell morphology and the first 18 amino acids of merlin are involved in actin binding (Brault et al., 2001), we hypothesized that phosphorylation of serine 10 might affect the interplay between merlin and actin. To study the effect of phosphorylation mutants on the organization of actin cytoskeleton, Nf2 -/- MEFs were transfected with merlin WT, S10A, S10D, or S518A. Cells were stained for F-actin and merlin and analyzed by confocal and immunofluorecence microscopy.

Untransfected cells displayed intense F-actin staining in stress fibers, whereas the actin filament staining in WT and S518A merlin transfected cells showed less pronounced fibers and often a dense cytoplasmic actin (Fig.4a). The intensity of cytoplasmic F-actin staining was weaker in cells expressing merlin S10A compared to untransfected cells or

cells expressing other merlin constructs. S10A cells lacked both stress fibers and the actin filament network seen in cells expressing WT merlin, and the F-actin staining was concentrated underneath the cell membrane. These cells were also irregularly shaped and made no lamellipodia. Cells transfected with the S10D mutant displayed stress fibers resembling those of untransfected cells.

The amount of F-actin, visualized by phalloidin fluorescence intensity, was quantified from WT, S10A, and S10D expressing cells and analyzed with Image J software (Fig.4b). The intensity of fluorescent phalloidin in merlin transfected cells was normalized to the intensity of untransfected cells. In cells expressing WT merlin the staining was significantly stronger than in untransfected cells, indicating that these cells contain more filamentous actin. A decrease of F-actin was observed in cells expressing S10A, whereas S10D transfected cells displayed phalloidin intensity most resembling the untransfected cells.

Merlin S10D protects the actin cytoskeleton from Latrunculin B induced depolymerization

Figure 5

Based on our observation that differentially phosphorylated merlin constructs influence cell morphology and actin cytoskeleton organization, we studied actin dynamics in merlin transfected cells. Nf2 -/- MEFs, transfected with merlin WT, S10A, or S10D, were incubated with Latrunculin B (LatB), used to dissociate F-actin. Cells were fixed before or 8 minutes after LatB treatment, stained for merlin and F-actin, and analyzed by immunofluorescence microscopy.

Exposure of the cells to the actin-destabilizing agent caused a change in the subcellular localization of all merlin constructs, which aggregated and relocalized to the cytoplasm (Fig.5). LatB treatment caused actin depolymerization in WT transfected cells, and in S10A cells the actin cytoskeleton was completely disrupted. However, actin filaments in S10D expressing cells depolymerized at a slower rate indicating that this construct stabilizes actin filaments.

Serine 10 phosphorylation regulates cell migration and lamellipodia formation

Figure 6

Rapid actin polymerization at the leading edge of a moving cell results in formation of filopodia and lamellipodia. Since we observed changes in both the morphology and actin organization of merlin transfected cells, we hypothesized that also cell motility may be affected. We did not achieve high infection efficiency in Nf2 -/- MEFs, therefore wound-healing assays were performed with Nf2 -/- Schwann cells, infected with adenovirus constructs and analyzed by phase contrast microscopy. Schwann cells lacking merlin filled the wound in 24 hours whereas the migration of merlin infected cells was slower (Fig.6a). Interestingly, S10A expressing Schwann cells closed the wound even slower than their wild-type counterparts.

The movement of WT and S10A expressing cells was also studied by live cell imaging. Merlin constructs were transfected into Nf2 -/- MEFs together with a GFP vector to allow identification of the merlin containing cells. S10A expressing cells did not display lamellipodia seen in WT transfected cells, but instead the expression promoted the formation of protrusions and extensions (Fig. 6b, supplemental data). Thus, the migration rate of merlin S10A transfected cells may be reduced because of alterations in lamellipodia formation.

Discussion

Post-translational modifications such as phosphorylation regulate the biological activity of merlin. At low cell density, merlin is phosphorylated and growth-permissive, whereas merlin exists in a hypophosphorylated form as a result of serum deprivation, high cell density, or loss of adhesion. The hypophosphorylated form of merlin is growth-inhibitory and represents the functionally active tumor suppressor (Shaw et al., 1998; Morrison et al., 2001). We have previously shown that in addition to PAK, also PKA phosphorylates merlin at serine 518 (Alfthan et al., 2004). We now demonstrate that there is an additional PKA phosphorylation site in merlin, and present evidence showing that this

phosphorylation site plays a role in merlin's ability to control actin cytoskeleton. The identified second PKA phosphorylation site, serine 10, is located in a sequence that is excluded from the FERM domain (Brault et al., 2001; Shimizu et al., 2002), and not conserved in the ERM proteins. However, the residue is conserved in merlin homologues in mouse, rat, and Xenopus, suggesting that the region has important functions.

Merlin contains multiple phosphorylated residues, but the only previously characterized phosphorylation site is serine 518 (Shaw et al., 1998; Shaw et al., 2001; Kissil et al., 2002; Xiao et al., 2002; Alfthan et al., 2004). Phosphorylation of this site participates in the control of cell proliferation, morphology, and motility, all important for the tumor suppressor function of merlin. Serine 518 phosphorylation impairs merlin's ability to self-associate and affects the binding of interacting proteins such as CD44, hepatocyte growth factor-regulated tyrosine kinase substrate (HRS), PKA regulatory subunit RIβ, and tubulin (Grönholm et al., 2003; Rong et al., 2004; Muranen et al., 2007). To analyze if phosphorylation of serine 10 similarly affects the activity of merlin, we created mutants mimicking both phosphorylated and unphosphorylated S10 and examined their ability to mediate functions previously described for merlin. Neither form of serine 10 directly affected the phosphorylation of serine 518, and phosphorylation of serine 10 did not enhance binding to ezrin in contrast to phosphorylation of serine 518. These results suggest that phosphorylation of the two PKA sites have distinct functions and are regulated independently of each other.

Merlin is localized underneath the plasma membrane especially at areas of membrane remodeling (Gonzalez-Agosti et al., 1996; Sainio et al., 1997). Phosphorylation of serine 518 promotes the appearance of multiple cell extensions in different cell types (Surace et al., 2004; Thaxton et al., 2007). Serine 518 phosphorylated merlin relocalizes to larger membrane protrusions in LLC-PK1 cells and is present at the most peripheral regions of lamellipodia, microspikes, and radial membrane protrusions in Schwann cells (Kissil et al., 2002; Thaxton et al., 2007). Our data suggests that merlin's phosphorylation state, not only at serine 518 but also at serine 10, influences cell morphology. Merlin S10A induced the appearance of long cellular extensions. These structures lacked serine 518 phosphorylated merlin, which instead was present in cellular protrusions. In contrast, S10D merlin promoted the formation of multiple short filopodia-like protrusions where

serine 518 phosphorylation was apparent. This suggests that merlin, in its dephosphorylated form, induces long cellular extensions, whereas the phosphorylated form localizes to areas of membrane ruffling and filopodia. Only a subset of merlin molecules at specific membrane structures are hyperphosphorylated suggesting that the phosphorylation status of merlin is tightly regulated possibly through the presence of active kinases at these restricted areas of membrane remodeling. Interestingly, we detected a more prominent cell-extension effect with merlin isoform II containing the S10 mutations, indicating that phosphorylation of serine 10 in an open merlin molecule is more efficient in promoting changes in cell morphology. This effect might be mediated through actin, since deformation of the cell membrane require reorganization of actin filaments and merlin isoform II has been shown to bind actin stronger than isoform I (James et al., 2001).

Cytoskeletal alterations may be linked to changes in cell growth and ultimately tumor formation as cellular transformation is often associated with disorganization of the cell cytoskeleton. Nf2 deficient schwannoma cells exhibit cytoskeletal abnormalities manifested by membrane ruffling, large surface areas, and F-actin instability (Pelton et al., 1998). It has previously been shown that the merlin FERM domain and isoform II have the ability to stabilize actin filaments and reduce depolymerization rates (James et al., 2001), whereas PAK phosphorylation of serine 518 weakens merlin's association with the cytoskeleton (Shaw et al., 2001). Serine 10 appears to be involved in regulating some of the cytoskeletal changes observed, as both the F-actin organization and the amount and depolymerization of F-actin was affected by S10 mutations. Interestingly, a drastic decrease of F-actin was detected in S10A expressing cells, suggesting that dephosphorylation of serine 10 reduces actin filament formation, while S10D mutant merlin stabilizes the filaments. Thus, serine 10 is important for actin filament dynamics affecting the stability of F-actin filaments in vivo. We could not, however, detect any difference in actin binding of S10A or S10D compared to WT in a co-sedimentation assay, nor in the depolymerization rate of actin (data not shown). Thus, we hypothesize that the observed effect of merlin on actin cytoskeleton is indirect through merlin interaction partners regulating actin cytoskeleton such as the ERM proteins.

Cell movement is induced by protrusion of a leading edge, movement of the cell body, and finally by retraction of the cell. Nf2 deficient primary fibroblasts migrate faster than wild-type cells containing merlin in wound-healing assays (Shaw et al., 2001), which we also observed in our studies with Nf2 deficient Schwann cells. However, S10A merlin expressing Schwann cells migrated even slower than the WT infected cells showing that regulation of serine 10 is important for cell motility. S10D cells migrated with the same rate as S10A cells (data not shown) indicating that regulation of the phosphorylation state at serine 10 is important. S10A transfected cells also displayed altered lamellipodia formation. The lamellipodium is critical for cell motility since it localizes protein complexes needed for actin polymerization (Small et al., 2002). Thus, as proper formation of lamellipodia is impaired in S10A merlin expressing cells, their ability to migrate may be altered.

It has been proposed that the very N-terminal sequence of merlin may function as a common protein-binding motif (Golovnina et al., 2005). However, so far it has only been shown to contain sequences important for actin binding (Brault et al., 2001). Interestingly, Bai et al. (2007) recently showed that the first 50 amino acids of merlin contain regulatory residues that affect the interplay between merlin, ezrin, actin, and CD44. Our results suggest that phosphorylation of serine 10 could be involved in regulating these complex formations.

The results described in this study indicate that phosphorylation of serine 10 is an important factor in the functional regulation of merlin. We propose that PKA-dependent phosphorylation of serine 10 participates in cytoskeletal organization.

Materials and methods

Plasmids and antibodies

For eukaryotic expression human merlin isoform I (WT, amino acids 1-595) and isoform II (amino acids 1-590) were cloned in pcDNA3 vector (Invitrogen, Carlsbad, CA, USA). For expression of recombinant GST-fusion proteins, the following constructs were used: merlin 1-100, merlin N-terminus (amino acids 1-314), merlin 1-547, merlin C-terminus

(amino acids 492-595), and full-length ezrin, all in pGEX4T1 vector (Amersham Biosciences, Buckinghamshire, UK). S10A, S10D, S518A, and S518D mutations of merlin in pcDNA3 and pGEX4TI vectors were made by site-directed mutagenesis using the QuikChange Kit (Stratagene, La Jolla, CA, USA). WT or S518A merlin in pDEST27 vector (Invitrogen) containing an N-terminal GST-tag was used for metabolic labeling. All constructs were verified by sequencing. GFP-α-actinin used in live cell imaging has been described before (Hotulainen and Lappalainen, 2006).

Anti-merlin pAb A-19 sc-331 (Santa Cruz Biotechnology, Santa Cruz, CA, USA) and mAb KF10 (den Bakker et al., 1995) were used to detect merlin. S518 phosphorylated merlin was detected with pS518 pAb (Biodesign, Saco, ME, USA). 3C12 mAb (Böhling et al., 1996) was used for ezrin detection, Alexa-568 conjugated phalloidin (Invitrogen-Molecular Probes) to detect F-actin, and anti-GST polyclonal goat antibody (GE Healthcare, Budapest, Hungary) to detect GST-proteins. Alexa-488-, Alexa-568- and Alexa-594-conjugated goat anti-mouse and goat anti-rabbit antibodies (Invitrogen-Molecular Probes) were used as secondary antibodies in immunofluorescence and HRP-conjugated rabbit anti-mouse and swine anti-rabbit (both from DAKO A/S, Glostrup, Denmark) and swine anti-goat (Santa Cruz Biotechnology) secondary antibodies in western blot analysis.

Cell culture, transfections, and immunoblotting

293 HEK cells were maintained in RPMI 1640 medium supplemented with 10% fetal calf serum (FCS) (PromoCell, Heidelberg, Germany). COS-7 cells, merlin -/- mouse embryonic fibroblasts (Nf2 -/- MEFs), and 293A HEK cells were all grown in Dulbecco's minimum essential medium (DMEM) with 10% FCS. Primary Nf2 knock-out Schwann cells (Giovannini et al., 2000) were isolated and cultured as previously described (Manent et al., 2003). The cells were immortalized and used before passage 20.

Cells were transfected using Fu-GENE6 reagent (Roche, Basel, Switzerland) and incubated for 48 h before analysis. Cells grown on glass coverslips were fixed in 3.5% paraformaldehyde (pH 7.5) for immunofluorescence. For western blotting, cells were rinsed with PBS and lysed in ELB buffer (50 mM HEPES, pH 7.4, 150 mM NaCl, 5 mM EDTA) containing 0.5% Nonidet P-40 (NP-40), 1.5 µM okadaic acid (Calbiochem, San

Diego, CA, USA), HALT phosphatase inhibitors (Pierce, Rockford, IL, USA), and Complete protease inhibitors (Roche). Lysed cells were centrifuged at 20 000 g for 30 min at +4°C. Protein concentrations were determined by Bio-Rad Protein Assay (Bio-Rad, Hercules, CA, USA). Equal amounts of proteins were run in 8-12% SDS-PAGE, transferred to nitrocellulose filters, and analyzed by immunoblotting. Proteins were visualized by enhanced chemiluminescence.

Metabolic labeling

72 h prior to metabolic labeling, 293A HEK cells were plated on 60 mm cell culture dishes and transfected with merlin cDNA 24 h later. 48 h after transfection cells were changed into serum- and phosphate free DMEM (Gibco-Invitrogen), and 1 mCi/ml of ^{32}P labeled orthophoshate (Amersham Biosciences) was added for 2 h. Cells were treated with 50 µM IBMX and 25 µM forskolin or 40 µM H89 (all from Sigma-Aldrich, St. Louis, MO, USA) for 30 min or 2 h respectively. After washing with TBS, the cells were lysed in ELB-buffer with 1% NP-40, phosphatase inhibitors (HALT, 1.5 µM Calyculin A (Calbiochem), Cocktail Set IV (Calbiochem), 1.5 µM okadaic acid), and protease inhibitors, and centrifuged at 14 000 g for 30 min at +4˚C. Samples were diluted to a final concentration of 0.5% NP-40, 100 µl of Glutathione Sepharose (Amersham Biosciences) was added to the lysates to pull-down merlin, and the samples were incubated o/n at +4˚C. After washing the beads twice with ELB-buffer containing inhibitors, Laemmli reducing buffer was added and samples were run in 8% SDS-PAGE. Gels were silver stained following standard protocol, dried and exposed on a PhosphoImager plate, read by TyphoonImager 9400 and analyzed by ImageQuant TL2003 software (all by GE Healthcare). The amount of phosphorous label was normalized to the merlin amount of the same construct and the background radioactivity (empty GST plasmid) was subtracted.

In Vitro Phosphorylation

GST-fusion proteins were expressed in E. coli DH5α and purified. Glutathione-Sepharose beads to which 5 mg of fusion protein was conjugated were washed twice in PKA buffer (20 mM Tris-HCl, 10 mM MgCl2, pH 7.4). The phosphorylation reaction was carried out in a 30 µl buffer volume including 10 µCi of [γ-^{33}P] ATP (PerkinElmer, Waltham, MA,

USA) and 2 ng of purified human recombinant PKA (Sigma-Aldrich) for 30 min at +30°C. The reaction was stopped by washing the beads in PKA buffer and subsequently adding 30 µl of Laemmli reducing buffer. 15 µl of the boiled sample was resolved by 12% SDS-PAGE. The gel was fixed and stained by Coomassie Blue followed by exposion on PhosphoImager plate and detection with Typhoon as previously described.

Merlin-Ezrin pull-down

GST-merlin and ezrin fusion proteins were bacterially expressed and purified. Full-length ezrin was cleaved from GST by washing the beads in thrombin buffer (50 mM TrisCl pH 7.5, 150 mM NaCl, 2.5 mM $CaCl_2$), after which 3 U of thrombin (Sigma-Aldrich) per 500 µg of protein was added to the samples followed by incubation o/n in +4˚C. Glutathione-Sepharose beads carrying 5 mg of merlin fusion proteins were washed twice in PKA buffer (20 mM Tris-HCl, 10 mM $MgCl_2$, pH 7.4) and phosphorylated by human recombinant PKA. The phosphorylation reaction was done as described above except that 200 µM of cold ATP (Sigma-Aldrich) was used. The reaction was stopped by washing the beads in binding buffer (50 mM HEPES pH 7.4, 150 mM NaCl, protease inhibitors). Four µg of thrombin cleaved ezrin was incubated with phosphorylated or unphosphorylated merlin 1-314, 1-547, or 1-547 S518A under rotation for 2 h at +4˚C. Beads were washed twice with binding buffer and bound proteins were resolved in 30 µl of reducing Laemmli buffer. 15 µl of boiled samples were run in 12% SDS-PAGE. Proteins were detected with ezrin and GST-antibodies.

Actin stainings and quantification

Nf2 -/- MEFs, transfected with WT, S10A, S10D, or S518A were stained with merlin pAb A-19 and phalloidin. Images were taken with Leica SP2 confocal microscope, equipped with Ar and Kr lasers (Leica Microsystems, Heerbrugg, Switzerland). For quantification of actin, cells were imaged with immunofluorecence microscopy (Zeiss Axiophot equipped with AxioCam cooled CCD camera, Carl Zeiss, Esslingen, Germany) using a fixed exposure of 900 ms for phalloidin. The intensity of the actin staining was analyzed by Image J (v10.2) software. Total fluorescence from twenty merlin transfected cells and untransfected cells from the same slides were analyzed separately, and the

staining intensities were normalized to the untransfected cells. The experiment was repeated three times with similar results.

Latrunculin B assay

Nf2 -/- MEFs were fixed (zero timepoint) or treated with 2.5 μM Latrunculin B (Sigma-Aldrich) for 8 min 48 h after transfection. Fixed cells were stained for merlin and phalloidin and analyzed with a fluorescence microscope.

Wound-healing assay

For wounding assays, Nf2 -/- Schwann cells (P18) were plated on laminin coated 24-well plates and infected with adenovirus constructs containing merlin WT, S10A, or empty virus as previously described (Muranen et al., 2007). Plates were wounded 24 hours after infection with a Pasteur pipet producing a 1 mm wide gap, and the wound-healing was monitored every 12 hours. After 72 hours, cells were fixed and stained with merlin A-19 pAb to control infection efficiency. The experiment was repeated four times with similar results.

Live cell imaging

Nf2 -/- MEFs, grown on LabTek glass chamber slides (Nunc, Naperville, IL, USA), were co-transfected with GFP-α-actinin and merlin 24-48 h prior to imaging. Cells were imaged with an inverted Olympus IX81 microscope and CellR program at +37˚C, 5% CO_2. Images were taken once every 30 seconds for 5 h. GFP-expression images were taken before and after the experiment, and the cells were stained for merlin to verify expression. Imaging was done from seven cells of both constructs with similar results.

Acknowledgements

We would like to thank Dr. Giovannini for the Nf2 -/- MEFs and Schwann cells. We also thank H. Ahola for her skillful technical assistance. This study was supported by the

grants of Department of Defense W81XWH-05-1-0469, the Finnish Cancer Organizations, the Medical Research Fund of Turku University Central Hospital District, Helsinki Graduate School of Biotechnology and Molecular Biology, Biomedicum Helsinki Foundation, Medicinska Understödsföreningen Liv och Hälsa, Emil Aaltonen Foundation, Oskar Öflund Foundation, and Svenska kulturfonden.

Supplementary information is available at Oncogene's website.

References

Alfthan K, Heiska L, Grönholm M, Renkema GH, Carpén O. (2004). Cyclic AMP-dependent protein kinase phosphorylates merlin at serine 518 independently of p21-activated kinase and promotes merlin-ezrin heterodimerization. J. Biol. Chem. **279:**18559-18566.

Bai Y, Liu YJ, Wang H, Xu Y, Stamenkovic I, Yu Q. (2007). Inhibition of the hyaluronan-CD44 interaction by merlin contributes to the tumor-suppressor activity of merlin. Oncogene **26:**836-850.

Baser ME, R Evans DG, Gutmann DH. (2003). Neurofibromatosis 2. Curr. Opin. Neurol. **16:**27-33.

Brault E, Gautreau A, Lamarine M, Callebaut I, Thomas G, Goutebroze L. (2001). Normal membrane localization and actin association of the NF2 tumor suppressor protein are dependent on folding of its N-terminal domain. J. Cell. Sci. **114:**1901-1912.

Bretscher A, Edwards K, Fehon RG. (2002). ERM proteins and merlin: Integrators at the cell cortex. Nat. Rev. Mol. Cell Biol. **3:**586-599.

Böhling T, Turunen O, Jääskelainen J, Carpén O, Sainio M, Wahlström T et al. (1996). Ezrin expression in stromal cells of capillary hemangioblastoma. an immunohistochemical survey of brain tumors. Am. J. Pathol. **148:**367-373.

den Bakker MA, Tascilar M, Riegman PH, Hekman AC, Boersma W, Janssen PJ et al. (1995). Neurofibromatosis type 2 protein co-localizes with elements of the cytoskeleton. Am. J. Pathol. **147:**1339-1349.

Giovannini M, Robanus-Maandag E, van der Valk M, Niwa-Kawakita M, Abramowski V, Goutebroze L et al. (2000). Conditional biallelic Nf2 mutation in the mouse promotes manifestations of human neurofibromatosis type 2. Genes Dev. **14:**1617-1630.

Golovnina K, Blinov A, Akhmametyeva EM, Omelyanchuk LV, Chang LS. (2005). Evolution and origin of merlin, the product of the neurofibromatosis type 2 (NF2) tumor-suppressor gene. BMC Evol. Biol. **5:**69.

Gonzalez-Agosti C, Wiederhold T, Herndon ME, Gusella J, Ramesh V. (1999). Interdomain interaction of merlin isoforms and its influence on intermolecular binding to NHE-RF. J. Biol. Chem. **274:**34438-34442.

Gonzalez-Agosti C, Xu L, Pinney D, Beauchamp R, Hobbs W, Gusella J et al. (1996). The merlin tumor suppressor localizes preferentially in membrane ruffles. Oncogene **13:**1239-1247.

Grönholm M, Sainio M, Zhao F, Heiska L, Vaheri A, Carpén O. (1999). Homotypic and heterotypic interaction of the neurofibromatosis 2 tumor suppressor protein merlin and the ERM protein ezrin. J. Cell. Sci. **112:**895-904.

Grönholm M, Vossebein L, Carlson CR, Kuja-Panula J, Teesalu T, Alfthan K et al. (2003). Merlin links to the cAMP neuronal signaling pathway by anchoring the RIbeta subunit of protein kinase A. J. Biol. Chem. **278:**41167-41172.

Hotulainen P, Lappalainen P. (2006). Stress fibers are generated by two distinct actin assembly mechanisms in motile cells. J. Cell Biol. **173:**383-394.

Howe AK. (2004). Regulation of actin-based cell migration by cAMP/PKA. Biochim. Biophys. Acta **1692:**159-174.

James MF, Manchanda N, Gonzalez-Agosti C, Hartwig JH, Ramesh V. (2001). The neurofibromatosis 2 protein product merlin selectively binds F-actin but not G-actin, and stabilizes the filaments through a lateral association. Biochem. J. **356:**377-386.

Jin H, Sperka T, Herrlich P, Morrison H. (2006). Tumorigenic transformation by CPI-17 through inhibition of a merlin phosphatase. Nature **442:**576-579.

Kim HA, DeClue JE, Ratner N. (1997). cAMP-dependent protein kinase A is required for schwann cell growth: Interactions between the cAMP and neuregulin/tyrosine kinase pathways. J. Neurosci. Res. **49:**236-247.

Kissil JL, Johnson KC, Eckman MS, Jacks T. (2002). Merlin phosphorylation by p21-activated kinase 2 and effects of phosphorylation on merlin localization. J. Biol. Chem.

277:10394-10399.

Manent J, Oguievetskaia K, Bayer J, Ratner N, Giovannini M. (2003). Magnetic cell sorting for enriching schwann cells from adult mouse peripheral nerves. J. Neurosci. Methods **123:**167-173.

Morrison H, Sherman LS, Legg J, Banine F, Isacke C, Haipek CA et al. (2001). The NF2 tumor suppressor gene product, merlin, mediates contact inhibition of growth through interactions with CD44. Genes Dev. **15:**968-980.

Muranen T, Grönholm M, Lampin A, Lallemand D, Zhao F, Giovannini M et al. (2007). The tumor suppressor merlin interacts with microtubules and modulates schwann cell microtubule cytoskeleton. Hum. Mol. Genet. **16:**1742-1751.

Pelton PD, Sherman LS, Rizvi TA, Marchionni MA, Wood P, Friedman RA et al. (1998). Ruffling membrane, stress fiber, cell spreading and proliferation abnormalities in human schwannoma cells. Oncogene **17:**2195-2209.

Rong R, Surace EI, Haipek CA, Gutmann DH, Ye K. (2004). Serine 518 phosphorylation modulates merlin intramolecular association and binding to critical effectors important for NF2 growth suppression. Oncogene **23:**8447-8454.

Rouleau GA, Merel P, Lutchman M, Sanson M, Zucman J, Marineau C et al. (1993). Alteration in a new gene encoding a putative membrane-organizing protein causes neuro-fibromatosis type 2. Nature **363:**515-521.

Sainio M, Zhao F, Heiska L, Turunen O, den Bakker M, Zwarthoff E et al. (1997). Neurofibromatosis 2 tumor suppressor protein colocalizes with ezrin and CD44 and associates with actin-containing cytoskeleton. J. Cell. Sci. **110:**2249-2260.

Shaw RJ, McClatchey AI, Jacks T. (1998). Regulation of the neurofibromatosis type 2 tumor suppressor protein, merlin, by adhesion and growth arrest stimuli. J. Biol. Chem. **273:**7757-7764.

Shaw RJ, Paez JG, Curto M, Yaktine A, Pruitt WM, Saotome I et al. (2001). The Nf2 tumor suppressor, merlin, functions in rac-dependent signaling. Dev. Cell. **1:**63-72.

Sherman L, Xu HM, Geist RT, Saporito-Irwin S, Howells N, Ponta H et al. (1997). Interdomain binding mediates tumor growth suppression by the NF2 gene product. Oncogene **15:**2505-2509.

Shimizu T, Seto A, Maita N, Hamada K, Tsukita S, Tsukita S et al. (2002). Structural basis for neurofibromatosis type 2. crystal structure of the merlin FERM domain. J. Biol. Chem. **277:**10332-10336.

Small JV, Stradal T, Vignal E, Rottner K. (2002). The lamellipodium: Where motility begins. Trends Cell Biol. **12:**112-120.

Surace EI, Haipek CA, Gutmann DH. (2004). Effect of merlin phosphorylation on neurofibromatosis 2 (NF2) gene function. Oncogene **23:**580-587.

Thaxton C, Lopera J, Bott M, Baldwin ME, Kalidas P, Fernandez-Valle C. (2007). Phosphorylation of the NF2 tumor suppressor in schwann cells is mediated by Cdc42-pak

and requires paxillin binding. Mol. Cell. Neurosci. **34:**231-242.

Trofatter JA, MacCollin MM, Rutter JL, Murrell JR, Duyao MP, Parry DM et al. (1993). A novel moesin-, ezrin-, radixin-like gene is a candidate for the neurofibromatosis 2 tumor suppressor. Cell **75:**826.

Turunen O, Sainio M, Jääskelainen J, Carpén O, Vaheri A. (1998). Structure-function relationships in the ezrin family and the effect of tumor-associated point mutations in neurofibromatosis 2 protein. Biochim. Biophys. Acta **1387:**1-16.

Xiao GH, Beeser A, Chernoff J, Testa JR. (2002). p21-activated kinase links Rac/Cdc42 signaling to merlin. J. Biol. Chem. **277:**883-886.

Xu HM, Gutmann DH. (1998). Merlin differentially associates with the microtubule and actin cytoskeleton. J. Neurosci. Res. **51:**403-415.

Zhou R, Cao X, Watson C, Miao Y, Guo Z, Forte JG et al. (2003). Characterization of protein kinase A-mediated phosphorylation of ezrin in gastric parietal cell activation. J. Biol. Chem. **278:**35651-35659.

Titles and legends to figures

Figure 1. Merlin contains two PKA phosphorylation sites, serine 10 and serine 518. a) Schematic overview of merlin's structural domains. Numbers indicate amino acids. b) In vivo phosphorylation of merlin. Cells transfected with GST-merlin and treated with either forskolin and IBMX or H89 were metabolically labeled with [^{32}P] orthophosphate. Merlin was pulled down, run on SDS-PAGE, silver stained (lower panel) and exposed (upper panel). Chart shows quantification of the orthophosphate signal. S518A is still

phosphorylated in forskolin/IBMX-treated cells. c) GST-merlin fusion proteins were phosphorylated in vitro using [γ-^{33}P] ATP and human recombinant PKA. Proteins were separated on SDS-PAGE and exposed (upper panel). The Coomassie-staining shows loading of the constructs (lower panel). Merlin 1-100 is phosphorylated by PKA and S10A mutation abolishes the phosphorylation. d) Merlin 1-547 and merlin 492-595 constructs with serine 10 and/or serine 518 substituted with alanine were used to confirm the PKA phosphorylation of merlin. The double mutant (1-547 S10A+S518A) is not phosphorylated by PKA.

Figure 2. Electrophoretic mobility, ezrin binding, and cellular localization of merlin mutants.

a) 293 HEK cells were transfected with merlin constructs and soluble fractions of cell lysates were immunoblotted. Wild-type (WT) merlin migrates as a triplet of hyperphosphorylated, phosphorylated, and hypophosphorylated forms. Mutation of serine 10 does not affect the electrophoretic mobility of merlin. Merlin was detected with KF10 mAb. b) Western blot analysis of lysates from transfected 293 HEK cells. WT, S10A, and S10D merlin are recognized with the pS518 pAb, whereas S518A is not detected (upper panel). Expression levels of constructs are shown with merlin KF10 mAb (lower panel). c) COS-7 cells transfected with WT, S10A, S10D, and S518A merlin were stained with antibodies detecting merlin (KF10 mAb, red) and merlin phosphorylated at S518 (pS518 pAb, green). Long cell extensions in WT and S10A expressing cells are not stained with pS518 pAb (arrow). Serine 518 phosphorylated merlin is present in shorter protrusions observed in WT, S10A, and S10D transfected cells (arrowhead). pS518 Ab does not detect merlin S518A mutant. d) Nonphosphorylated (-) or PKA phosphorylated (+) GST-merlin was incubated with purified full-length ezrin. Proteins were run in SDS-PAGE and detected with ezrin 3C12 mAb (upper panel) and merlin with GST pAb (lower panel). Phosphorylation of merlin 1-547 enhances ezrin binding whereas no difference in binding affinity is detected with phosphorylated merlin 1-314 or 1-547 S518A.

Figure 3. Phenotypic effect of serine 10 mutations.

COS-7 cells and Nf2 -/- MEFs were transfected with WT, S10A, or S10D mutant merlin isoform I (WT) or isoform II and stained with merlin KF10 mAb (COS-7) or merlin pAb A-19 (Nf2 -/- MEFs). WT and S10A merlin expressing cells have long extensions (arrows) not seen in cells expressing S10D. S10D expression induces dense filopodia-like structures (arrowheads) not seen in WT, isoform II or S10A transfected cells.

Figure 4. Altered F-actin organization in cells expressing merlin mutants.

Nf2 -/- MEFs transfected with WT, S10A, S10D, or S518A were stained with merlin pAb A-19 (green) and phalloidin (red) and analyzed with a confocal microscope. a) Single confocal sections at the plane close to ventral surface are shown. Right panel shows a higher magnification of the marked area. b) Intensity of phalloidin staining in WT, S10A, and S10D expressing cells analyzed with Image J software after normalization against control cells. WT cells show increased and S10A cells display decreased phalloidin staining intensity.

Figure 5. Actin depolymerization in merlin expressing cells.

Nf2 -/- MEFs, transfected with merlin WT, S10A, or S10D were fixed before (left panel) or 8 minutes after (right panel) Latrunculin B (LatB) treatment. Cells were stained with merlin pAb A-19 and phalloidin, arrowheads indicate merlin transfected cells. LatB treatment induces actin depolymerization in WT and S10A cells, whereas S10D cells are more resistant to the LatB effect.

Figure 6. Mutation of S10 leads to defects in cell migration and lamellipodia formation.

a) Nf2 -/- Schwann cells infected with adenovirus constructs expressing either merlin WT, S10A, or empty vector were wounded and examined by phase contrast microscopy. Schwann cells lacking merlin filled the wound in 24 hours, whereas cells expressing WT and S10A merlin were slower in their migration. Grey lines show cell monolayer edges. b) Nf2-/- MEFs were co-transfected with GFP-α-actinin and merlin WT or S10A. Live cells expressing merlin were chosen by their GFP-expression and imaged for 5 h with a DIC filter (videos are provided as supplemental material). Still images from the videos

are shown (second and fourth panel) together with the GFP-expression (first panel) and merlin staining (third panel). WT expressing cells form lamellipodia (arrow) which are also seen in untransfected cells. Arrowhead in S10A mark filopodia.

Supplementary Video 1. Live Nf2 -/- MEFs expressing WT merlin were identified by GFP-expression. Cells were imaged for five hours with images taken every 30 seconds.

Supplementary Video 2.

Live Nf2 -/- MEFs expressing S10A merlin were identified by GFP-expression. Cells were imaged for five hours with images taken every 30 seconds.

Figure1.

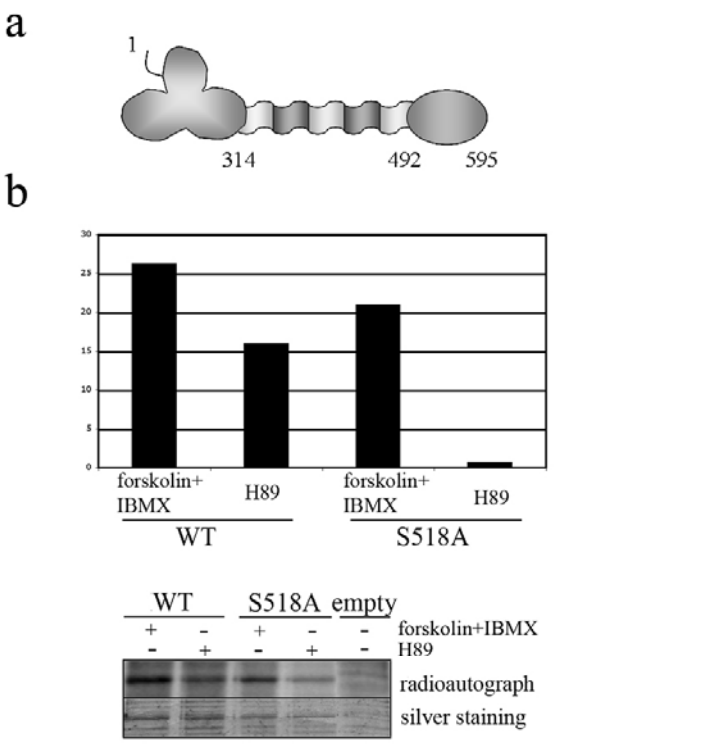
a
1
314
492
595
b
forskolin+ IBMX
H89
forskolin+ IBMX
H89
WT
S518A
WT
S518A
empty
forskolin+IBMX
H89
radioautograph
silver staining
c
1-100
S10A
T28A
T54A
1-100
GST
radioautograph
coomassie
d
1-547
1-547 S518A
1-547 S10A+ S518A
492-595
492-595 S518A
GST
radioautograph
coomassie

Figure 2.

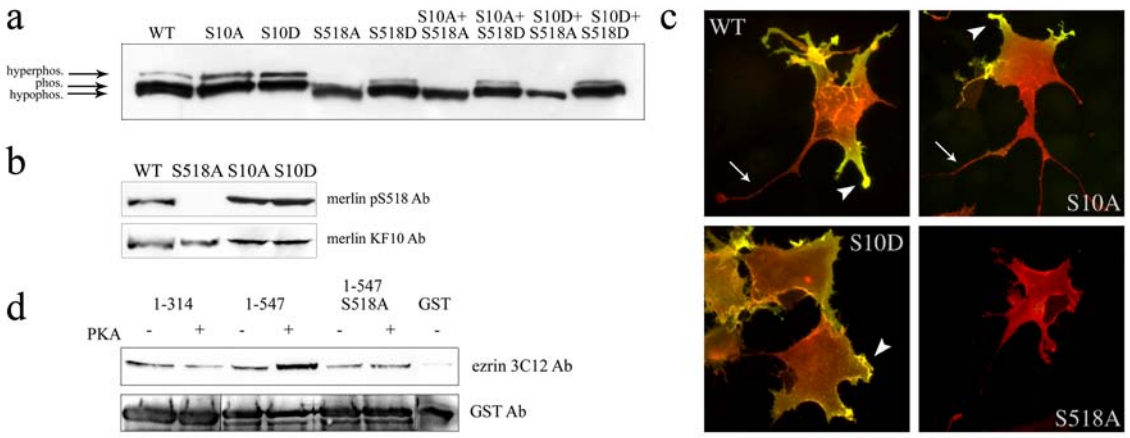
a
WT
S10A
S10D
S518A
S518D
S10A+ S518A
S10A+ S518D
S10D+ S518A
S10D+ S518D
hyperphos.
phos.
hypophos.
b
WT S518A S10A S10D
merlin pS518 Ab
merlin KF10 Ab
c
WT
S10A
S10D
S518A
d
1-314
1-547
1-547 S518A
GST
PKA
ezrin 3C12 Ab
GST Ab

Figure 3.

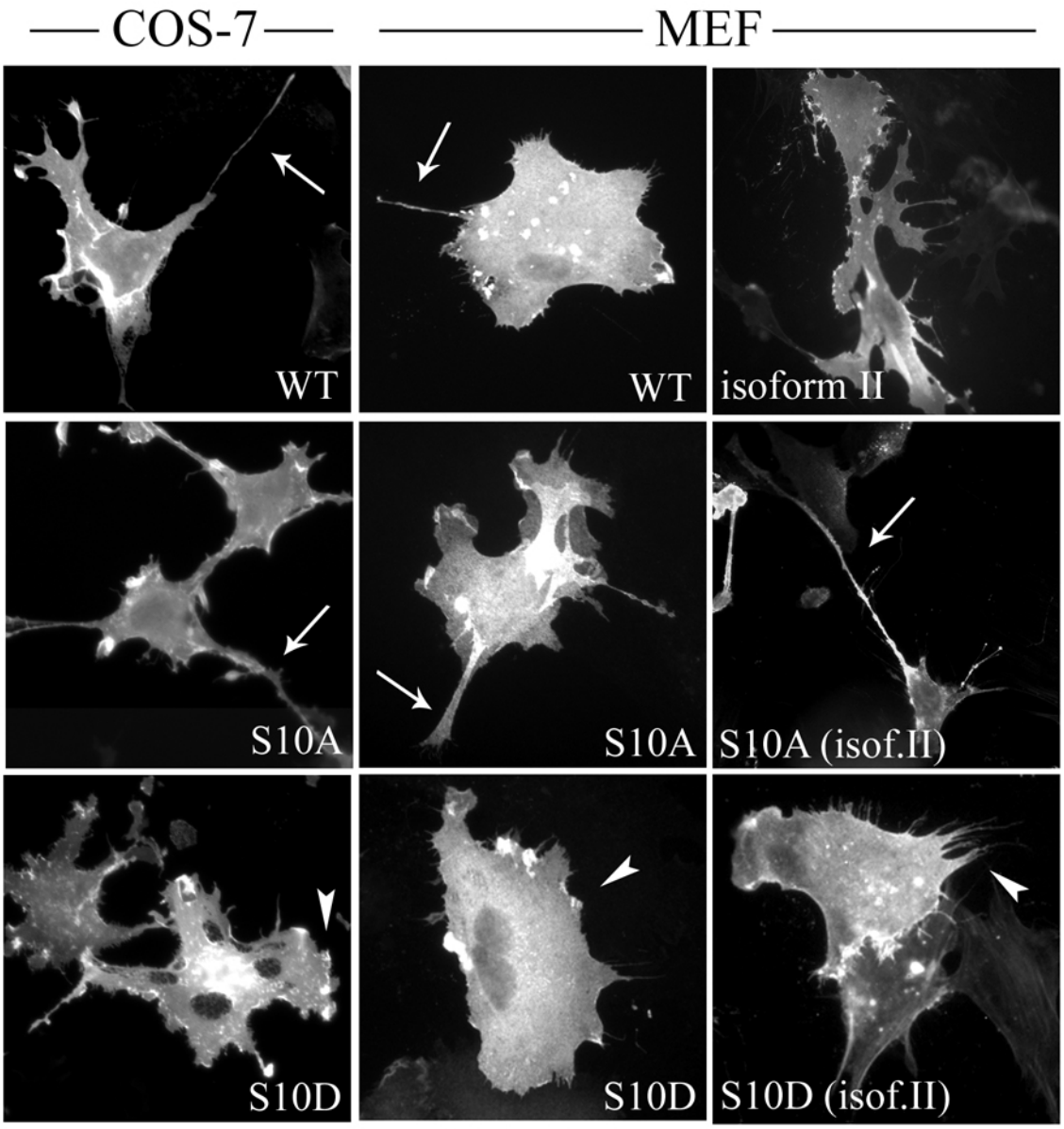
COS-7
MEF
WT
WT
isoform II
S10A
S10A
S10A (isof.II)
S10D
S10D
S10D (isof.II)

Figure 4.

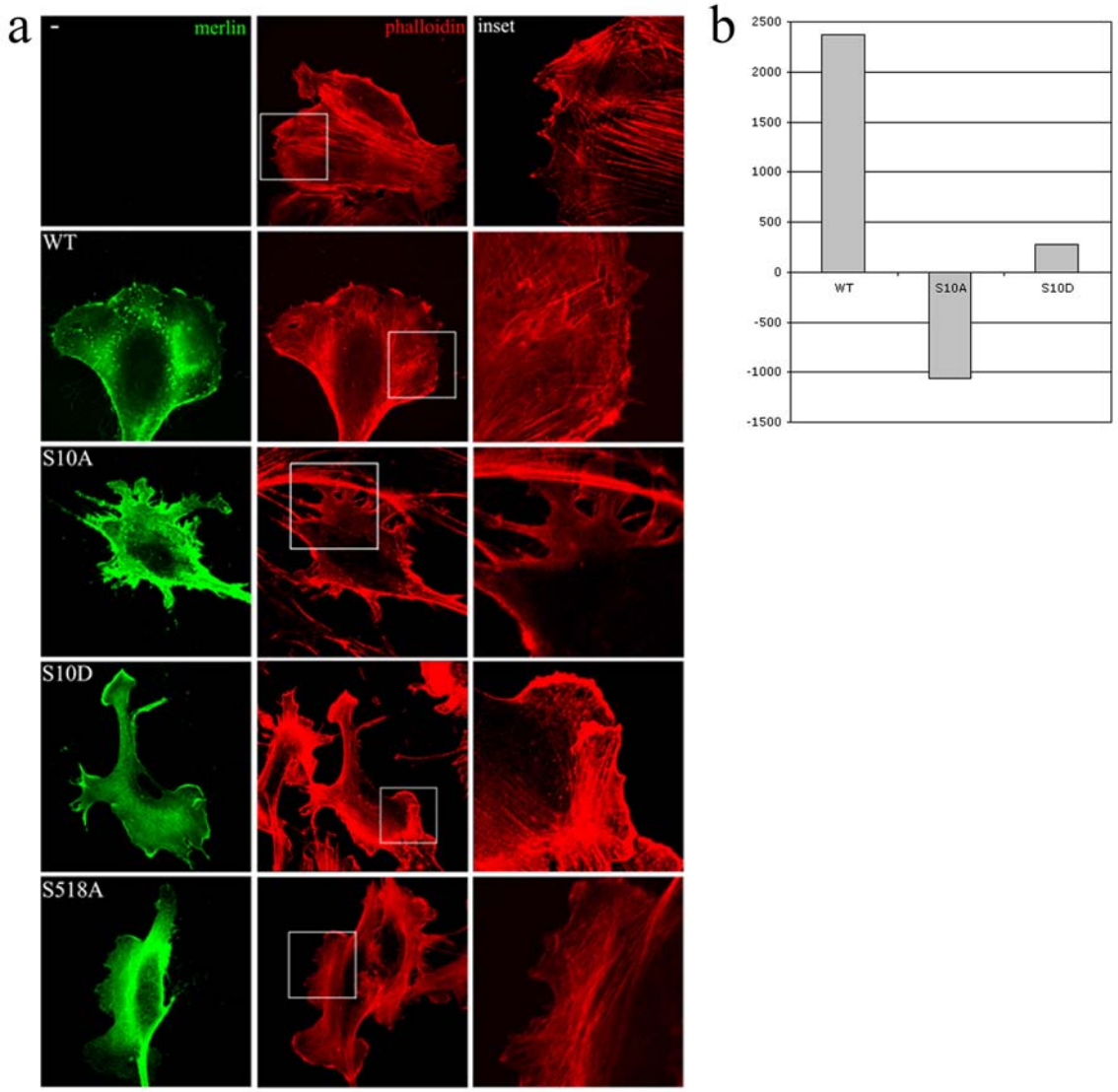
a
-
merlin
phalloidin
inset
WT
S10A
S10D
S518A
b
2500
2000
1500
1000
500
0
-500
-1000
-1500
WT
S10A
S10D

Figure 5.

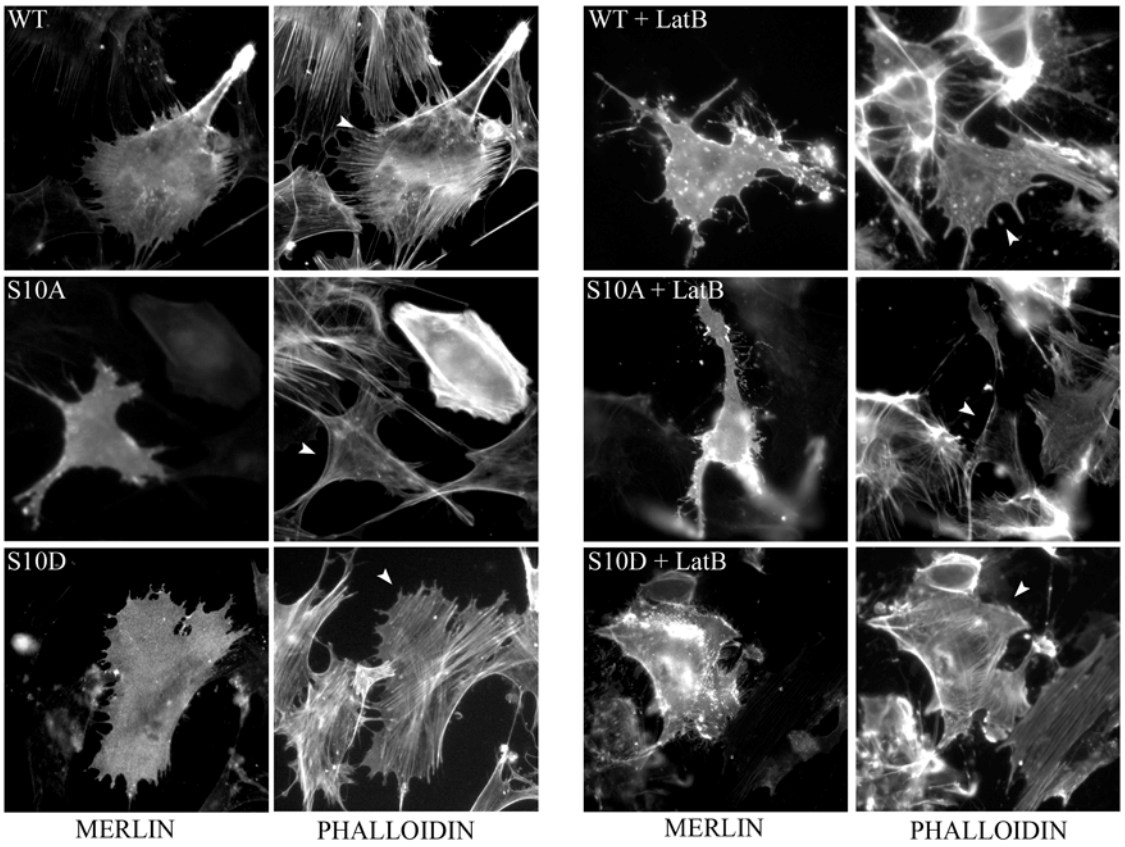
WT
S10A
S10D
WT + LatB
S10A + LatB
S10D + LatB
MERLIN
PHALLOIDIN
MERLIN
PHALLOIDIN

Figure 6.

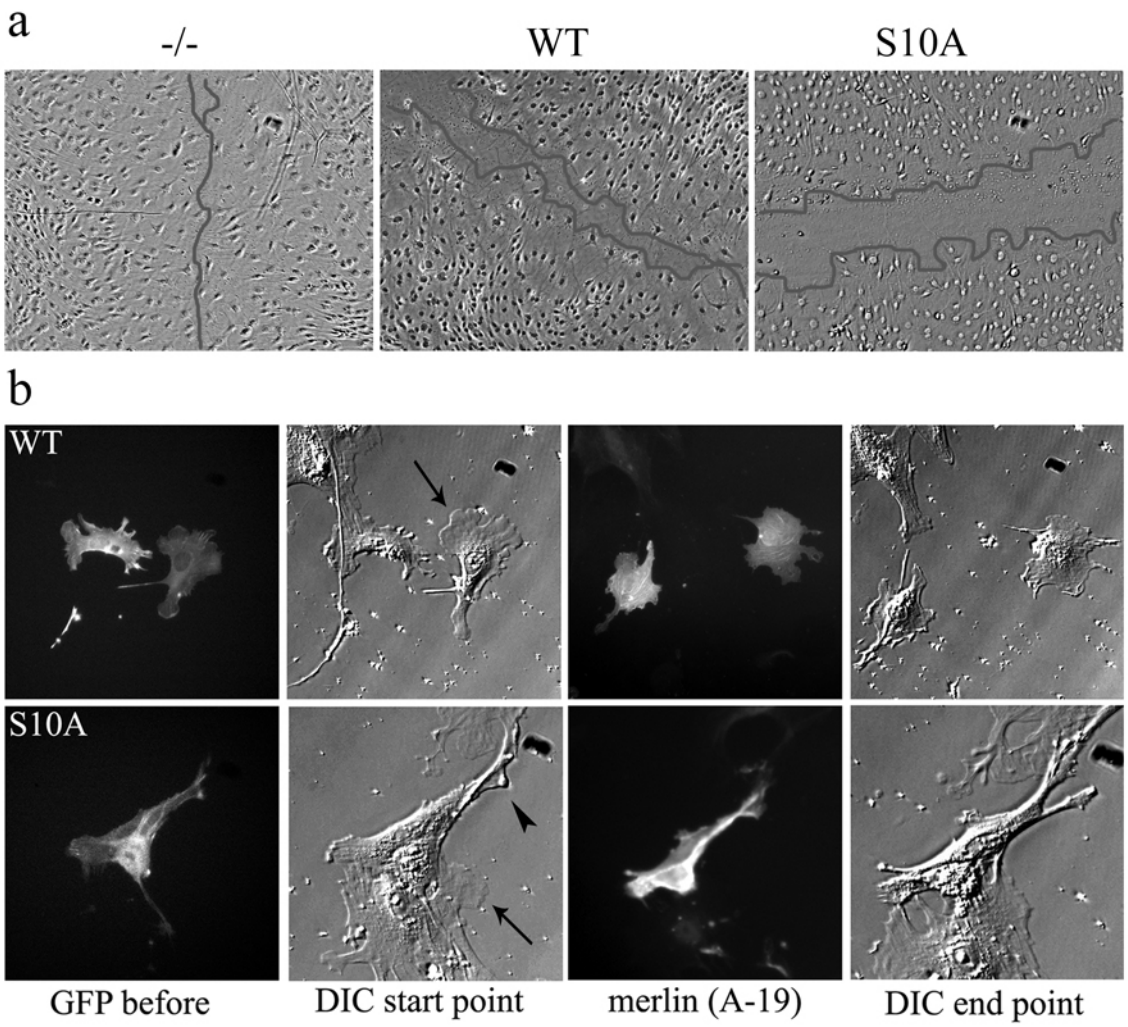
a
-/-
WT
S10A
b
WT
S10A
GFP before
DIC start point
merlin (A-19)
DIC end point

Ezrin is key regulator of Src-induced malignant phenotype in three-dimensional environment

Heiska Leena‡, Zhao Fang‡, Saotome Itsiko#, McClatchley Andrea I#, and Carpén Olli‡¶§

‡Biomedicum Helsinki, Department of Pathology, Neuroscience Program, University of Helsinki and Helsinki University Hospital, FIN-00014 Helsinki, Finland; #MGH Cancer Center and Harvard Medical School of Pathology, Charlestown, MA; and ¶Department of Pathology, University of Turku and Turku University Hospital, FIN-20520 Turku, Finland

Running title:
Key words:

§ Corresponding author:
Olli Carpén
Department of Pathology
Kiinamyllynkatu 10
20520 Turku, Finland
Tel.: 358-2-3337217
Fax: 358-2-3337459
E-mail: ocarpen@utu.fi

SUMMARY

The oncogenic tyrosine kinase Src is activated in various cancers. Src activation promotes invasive and metastatic behaviour and may therefore play a role at later stages of cancer development. Src has numerous substrates and it activates a myriad of signaling pathways. It is not clear, however, which of these alterations promote malignant phenotype. One of Src substrates is ezrin, a multifunctional protein that organises actin cytoskeleton and regulates signal transduction. Ezrin is essential in experimental metastatic osteosarcoma and increased ezrin expression correlates with metastatic behaviour and poor outcome of diverse cancers. To study, whether Src and ezrin act in concert in tumorigenesis, we reconstituted genetically ezrin-deficient cell lines with wild-type or phosphorylation deficient ezrin together with constitutively active Src. In two-dimensional cultures, Src induced malignant features independent of whether the cells expressed wild-type or mutant ezrin or were ezrin deficient. However, only cells expressing wild type ezrin and active Src grew efficiently in soft agar. Furthermore, expression of ezrin significantly promoted Src-induced growth and invasion in Matrigel, a three-dimensional extracellular matrix from mouse tumor. Wild-type and mutant ezrin expressing cells had identical morphology on culture plates but showed marked differences in three dimensional matrix, where only wild-type ezrin was targeted to specific regions on the plasma membrane. We conclude that the pathways activated by Src depend on the type of environment and that ezrin is a crucial element of Src-induced malignant features of cells growing in three dimensional matrices.

INTRODUCTION

The nonreceptor tyrosine kinase Src is the first identified proto-oncogene (reviewed in {{1037 Martin,G.S. 2001;}}). Src-dependent oncogenic mechanisms affect a wide variety of cellular functions and signaling pathways, for example pathways leading to cell survival, migration and invasion. Increased expression or activation of Src has been shown in many types of human primary cancers and especially in metastastic tumors {{891 Irby,R.B. 2000;893 Frame,M.C. 2002;892 Summy,J.M. 2003;}} and hence, Src inhibitors are extensively investigated for cancer therapy {{1044 Summy,J.M. 2006;}}. Increased Src activity is thought not to be essential for early tumorigenic events. Rather, Src appears to provide a selective advantage to tumor cells during metastatic processes by facilitating invasion and spreading to distant organs {{1044 Yeatman,T.J. 2004;}}.

One of Src kinase substrates is ezrin, a linker protein that connects cell membrane and actin cytoskeleton (reviewed in {{425 Bretscher,A. 2002;615 Tsukita,S. 1999;}}). Ezrin belongs to the ERM (ezrin-radixin-moesin) proteins, which fold as inactive molecules through an N- to C-terminal association. Ezrin is activated via binding to PIP_2 and phosphorylation of a conserved threonine residue {{277 Fievet,B.T. 2004;}}. Ezrin is implicated in signal transduction networks both as a regulator and an effector; it interacts with various members of protein kinase A, Rho and phosphatidylinositol-3 kinase signaling pathways. Ezrin is the only ERM protein shown to be directly phosphorylated on tyrosine by the Src family kinases Lck and Src {{387 Autero,M. 2003;897 Heiska,L. 2005;901 Srivastava,J. 2005;}}. The Src-induced phosphorylation of ezrin tyrosine 477 leads to binding of a Kelch-repeat family protein KBTBD2 (Kelch-repeat and BTB/POZ domain binding 2) {{897

Heiska,L. 2005;}}. On the other hand, Src binds ezrin through its SH2 domain {{37 Bretscher,A. 2000;901 Srivastava,J. 2005;}}. Src and ezrin act cooperatively in deregulation of cell-cell contacts and scattering of carcinoma cells {{832 Elliott,B.E. 2004;}}. However, the cellular effects of ezrin's Src-dependent phosphorylation are largely unknown.

Ezrin has been indicated in human tumorigenesis and especially metastatic processes {{182 McClatchey,A.I. 2003;275 Curto,M. 2004;}}. Upregulation of ezrin correlates to invasive characteristics of malignant cell lines {{644 Akisawa,N. 1999;604 Ohtani,K. 1999;}} as well as to malignancy, metastasic behavior and poor clinical outcome of diverse cancers {{28 Geiger,K.D. 2000;95 Makitie,T. 2001; 458 Ohtani,K. 2002;1039 Ilmonen,S. 2005;1042 Weng,W.H. 2005;1040 Kobel,M. 2006;1041 Kobel,M. 2006;}}. Ezrin was discovered in a subtractive hybridization screen for metastasis-associated genes of rat pancreatic and mammary carcinomas {{132 Nestl,A. 2001;}}. By a microarray approach, Khanna et al. identified ezrin as an essential protein for experimental metastasic osteosarcoma and a marker of poor outcome in spontaneous canine osteosarcomas and in pediatric osteosarcomas {{123 Khanna,C. 2001;151 Khanna,C. 2004;}}. The ezrin-dependent osteosarcoma metastasis was later linked to mammalian target of rapamycin (mTOR) pathway downstream of Akt {{1043 Wan,X. 2005;}}. Furthermore, microarray-based profiling of highly and poorly metastatic rhabdomyosarcoma lines and a subsequent analysis of the corresponding human patient samples showed that ezrin expression is a key prometastatic regulator {{150 Yu,Y.L. 2004;1007 Yu,Y. 2006;}}. Ezrin was required for breast cancer metastasis in a mouse model, and Src kinase and PI3K were the effectors of ezrin in the metastatic process {{832 Elliott,B.E. 2004;}}.

Src is thought to induce malignant phenotype by altering various signaling pathways. However, until now, there is no single down-stream element that would unite the characteristic phenotypic changes, *i.e.* adhesion-independent survival, increased invasiveness and ability to grow, pre-eminently in three dimensional matrices. Since increased ezrin expression and Src activity correlate with malignant behavior *in vivo* and since ezrin is substrate for Src {{897 Heiska,L. 2005;}}, we investigated whether ezrin and Src act in concert in induction of metastatic characteristics. We utilized genetically engineered ezrin deficient mouse embryonic fibroblasts and reintroduced wild-type (WT) ezrin or an unphosphorytable mutant form to them in combination with constitutively active Src. Our results show that ezrin is a major regulator of Src-induced anchorage-independency, growth and cell invasion and that a form of ezrin that cannot be phosphorylated by Src does not promote these activities. Moreover, the interplay between ezrin and Src is only evident in cells grown in three-dimensional environment.

MATERIALS AND METHODS

Cell lines

Embryonic fibroblasts derived from ezrin -/- mouse {{887 Saotome,I. 2004;}} were spontaneously immortalized by serial dilution and maintained in D-MEM medium including 10% fetal calf serum (FCS) and antibiotics. Two independently immortalized MEF lines were established and all experiments performed with the two different sets of cells. For establishing the stable ezrin add-back

lines, the wild-type (WT) and the mutant versions of the full-length ezrin cDNA were introduced to pBABEpuro vector {{899 Morgenstern,J.P. 1990;}}. 293 Eco Phoenix retrovirus packaging cell line was transfected with the different constructs, the virus containing supernatant collected and used in the transduction of the MEFs according to a standard protocol {{898 Miller,A.D. 1993;}}.The expression vector containing cell populations were selected with 2.5 mg/ml of puromycin (Sigma) in the medium. To express constitutively active Src, the cells were further introduced with a retroviral construct pLXSH-SrcY527F {{776 Cary,L.A. 2002;}}, kindly provided by Dr. J. A. Cooper (Fred Hutchinson Cancer Research Center, Seattle, WA), and selected with 0.25 mg/ml of hygromycin B (Calbiochem). The amino acid numbering of ezrin is according to Krieg et al. {{777 Krieg,J. 1992;}}.

Antibodies

Phosphotyrosine was detected with the monoclonal anti-phosphotyrosine antibody (mAb) clone PT-66 (Sigma-Aldrich). The polyclonal rabbit antibody against human ezrin (Ez9) has been described {{4 Alfthan,K. 2004;}}. Mouse IgG1 (Dako Cytomation, Glostrup, Denmark) or rabbit preimmune serum were used as controls. Rabbit phosphospecific antibodies against active (pY418)Src and against phosphorylated (pT558)moesin were from BioSource International (Camarillo, CA) and Santa Cruz Biotechnology (Santa Cruz, CA), respectively. Rat monoclonal anti-moesin antibody M22 was a kind gift of Dr. Sa. Tsukita (Kyoto University, Kyoto, Japan), and mouse anti-cortactin mAb was from Upstate (Lake Placid, NY).

Immunoprecipitation of ezrin

The cells were lysed in cold RIPA buffer (50 mM TrisHCl, 150 mM NaCl, 1% NP-40, 0.5% deoxycholate, 0.1% SDS, 1 mM orthovanadate, proatease inhibitor mix, pH 7.4) and centrifuged at 16 000 x g for 10 min. Ezrin was immunoprecipitated from the supernatants with the Ez9 antibody followed by incubation with the protein G Sepharose beads (Amersham Pharmacia). The beads were washed four times in RIPA buffer and suspended to Laemmli buffer. The immunoprecipitate was resolved on SDS-PAGE, blotted on nitrocellulose and analyzed by immunoblotting with appropriate antibodies using ECL-detection (Amersham Pharmacia).

Cell proliferation assay

On day 0, 5 x 10^3 cells/well were plated on a 24 well cell culture plate in quadruple. On the day of analysis, the wells were washed with PBS and incubated with 200 µl of 40 mg/ml MTT ([3-(4,5-dimethylthiazol-2-yl)-2,5-diphenyltetrazolium-bromide], Sigma) in PBS for 3 hours, after which the liquid was discarded and the converted dye suspended into 200 µl of DMSO. 100 µl aliquots were analyzed with a microtiter plate reader at 550 nm.

Cell adhesion analysis

The cells were serum starved overnight, detached with trypsin, washed twice in excess PBS and plated 2 x 10^5 cells per well in medium without serum on 96 well cell culture plates coated with fibronectin (10 µg/ml). The cells were monitored by light microscopy during attachment. To quantify the attached

cells, the wells were washed with PBS after different time periods, the attached cells stained with crystal violet, and the bound dye measured after extraction with 0.1 % Triton X-100 with a microtiter plate reader at 595 nm.

Fluorescence microscopy, confocal microscopy and 3-D reconstruction

Cells were grown on glass coverslips, fixed in 3,5 % formaldyhyde, permeabilized in 0,1 % Triton X-100 in PBS, incubated with the primary antibody for 30 min at 37˚C, washed and incubated with the secondary antibody similarly. The secondary antibody was rhodamine conjugated donkey anti-rabbit or anti-mouse $F(ab')_2$ (Jackson Immunoresearch). For labeling of F-actin, rhodamine conjugated phalloidin (Molecular Probes) was used. To stain the cells inside Matrigel (growth-factor reduced Matrigel, BD BioSciences, Bedford, MA), a modification of the method described by Debnath et al. {{1032 Debnath,J. 2003;}} was used. Briefly, eight-well glass chamber slide was coated with a layer of Matrigel (50 µl per well). A mixture of 5 x 10^3 cells, Matrigel (1/3 of the total volume) and culture medium was added on the solidified bottom layer in a volume of 100 µl per well. The solidified mixture was overlaid with cell culture medium and the slide incubated for 24 – 48 h. The wells were fixed in 3.5 % paraformaldehyde, permeabilized in 0.5 % Triton X-100 for 10 min, and rinsed three times with 130 mM NaCl, 7 mM Na_2HPO_4, 3.5 mM NaH_2PO_4, 100 mM glycine. The wells were blocked in 10 % normal swine serum diluted into IF buffer (130 mM NaCl, 7 mM Na_2HPO_4, 3.5 mM NaH_2PO_4, 0.1 % bovine serum albumine, 0.2 % Triton X-100, 0.05 % Tween-20) for 2 h. The primary antibody was incubated overnight in the blocking solution. The wells were washed three times 15 min with the IF buffer, incubated with the secondary antibody diluted in the blocking buffer, followed by washes with the IF buffer. The slide was mounted with Mowoil (Calbiochem) mixed 1:3 with 1,4-diazabicyclo[2.2.2. octane] (Sigma). All the steps were done at room temperature. The slides were visualized under epifluorescence microscope and Leica SP2 confocal microscope. Serial sections for 3D reconstruction were taken by confocal microscope using half thickness of the objective lens's z-resolution as step size. The 3D reconstruction was performed by Leica LCS 3D software package.

Spheroid formation and cell scattering experiments

The spheroids were formed by a method described by Bizik {{1067 Eleveld-Trancikova,D. 2002;}}. Briefly, 5 x 10^3 cells were made to form spheroids by plating them on U-bottomed microtiter wells, which were precast with a thin film of 1 % agar. The cells were incubated for 24 – 48 hours. The formed spheroids were carefully removed and transferred on a 24 well plate, which was precast with a solution containing 1 mg/ml type I collagen (BD Biosciences), 10 % fetal calf serum and 50 mM $NaHCO_3$. The spheroids were overlaid with culture medium and observed by light microscope.

Cell culture in Soft agar and insuspension

5 x 10^4 cells were plated in triplicate in 0.3 % agar containing DMEM and 10 % fetal calf serum on a layer of precast 0.6 % agar. The number and size of the resulting colonies was determined by microscopic visualization after 14 – 21 days. For growth in suspension, 5 x 10^5 cells were seeded on bacterial 35 mm plates in medium containing 0.5 % methyl cellulose (Sigma). The clusters of > 10

cells from two different plates of each subclone were counted under a light microscope after 7 - 10 days.

Invasion assay

Invasion was measured using growth factor reduced Matrigel invasion chamber (BD Biosciences, Bedford, MA) according to manufacturer's protocol. The inserts were rehydrated with 0.5 ml cell culture medium, 5 x 10^4 cells were seeded to the chamber in medium containing 1 % fetal calf serum, and the plate wells were filled with 0.75 ml medium containing 10 % fetal calf serum. After 36 hours, the non-invading cells were removed with a cotton swap, the membrane fixed in 3,5 % paraformaldehyde and the invaded cells stained with crystal violet. The cells were counted using 20 x magnification from 5 different fields.

Cell culture inside Matrigel

96 well microtiter cell culture plates were precast with 50 µl of Matrigel diluted 1:3 in culture medium. The layer was overlaid with 100 µl of a mixture containing 5 x 10^3 cells, Matrigel (1/3 of the volume) and medium. After the gel had solidified, the wells were overlaid with medium and incubated for 14 days. The Matrigel plug was fixed in 100 µl of 3.5 % paraformaldehyde, indubated on ice until liquified, and the cells counted using hemocytometer.

RESULTS

Characterization of MEF cell lines

To study the role of ezrin in Src-induced cellular functions in a model without intervening endogenous ezrin, we utilized MEF cells from the ezrin knock-out mouse {{887 Saotome,I. 2004;}}. In two previous publications, the target residues of Src kinase on ezrin have been mapped as Y145 and Y477 {{901 Srivastava,J. 2005;897 Heiska,L. 2005;}}. Therefore, the ezrin -/- MEF cells were stably introduced with the WT, the Y145F mutant, or the Y477F mutant full-length ezrin expression constructs or with the plasmid vector alone. Ezrin expression in addback cells was verified by immunoblotting (Fig. 1A). The ezrin -/- MEFs introduced with the plasmid vector as a control did not show any ezrin expression. The endogenous levels of a related ERM protein, moesin were equal in the parent MEFs or in the subclones (Fig. 1B). This indicates that the presence or absence of ezrin is not compensated by upregulation of other ERM proteins. Similarly, the level of phosphorylated threonine 558 of moesin was unchanged as detected with an anti-p(558T)moesin antibody (Fig. 1C). In longer exposures, the anti-(pT558)moesin antibody faintly cross-reacted with a band corresponding to the molecular size of ezrin in the ezrin-containing subclones (data not shown); this reactivity was equal between the clones harboring the WT or the mutant forms of ezrin. The result indicates that the presence or absence of the WT or the mutated forms of ezrin does not affect threonine phosphorylation and conformational activation of the ERM proteins.

To express active Src kinase, the cells were further introduced with a constitutively active Src (Y527F) expression construct. The expression of active Src was verified by immunoblotting of the cell lysates

with an anti-(pY418)Src antibody, which recognizes Src only when its autoactivating Y418 residue is phosphorylated (Fig. 1D). The cells expressing Y527FSrc showed prominent overall tyrosine phosphorylation compared to the cells which were not expressing active Src, as detected with an anti-(pY)antibody (data not shown). Introduction of active Src construct lead to upregulation of ezrin in the MEF addback clones (compare lane 2 in fig. 1A with lanes 4-6), in line with previous fingerprint analysis of Src-regulated changes in gene expression (Malek et al. 2002).

To study, whether ezrin serves as a Src substrate in this model and to identify the substrate tyrosine, we immunoprecipitated ezrin from the various sublines. The anti-(pY)antibody did not react with the WT ezrin in the absence of active Src (Fig. 1E). On the contrary, in the presence of Src kinase activity both the WT and the Y145F mutant ezrin were phosphorylated on tyrosine, whereas mutation of Y477 abolished the reactivity. The results verify that ezrin is a substrate for Src-induced tyrosine phosphorylation and Y477 is the main target in the MEF subclones. Therefore, in the following experiments the cells expressing empty vector, WT ezrin or the Y477F mutant ezrin were included.

Ezrin is not required for Src-induced alterations in cells grown on two-dimensional surfaces

Next we examined the localization of ezrin in the different sublones grown on coverslips. In the ezrin -/- MEF addback cells, both the WT (Fig. 2A) and the Y477F form of ezrin (not shown) localized to short microvilli-like extensions at the cell membrane. The staining was specific, as the vector control cells were not stained by the anti-ezrin antibody (Fig. 2D). Introduction of active Src changed the cellular morphology from the normal fibroblast-like to more a polygonal and refracted appearance; *i.e.* the shape characteristic for transformed cells. No differences were seen between the localization of WT and the mutant form of ezrin. Both forms were partly concentrated to the plasma membrane and partly located diffusely in the cytoplasm (Fig. 2B, C). Brightly stained spots of ezrin were seen at cellular protrusions or in filopodial structures. Occasionally the staining in the cytoplasm showed a fine reticular pattern. The actin cytoskeleton was prominently altered after introduction of active Src. The pronounced stress fibers (Fig. 2E) disappeared, and actin was concentrated heavily on podosomal or rosette-like structures regardless of the ezrin protein status in the cells (Fig. 2F; not all subclones are shown). The active form of Src also located on the podosome-like structures described originally in Rous sarcoma virus-transformed fibroblasts {{1033 Tarone,G. 1985;}} (Fig. 2G). The localization of active Src was similar in the subclones containing WT or the Y477F mutant ezrin (Fig. 2H). The typical podosomal structures further contained cortactin, a well-known Src substrate (not shown). In ezrin-containing subclones these structures occasionally contained ezrin, whether the mutant or the WT form (data not shown). The results confirm earlier studies of the effects of Src kinase activity to the cell cytoskeleton and show that ezrin is not required for podosome formation in fibroblasts. Furthermore, the results indicate that the role of ezrin tyrosine phosphorylation by Src is not in targeting of either ezrin or Src in two-dimensional cell cultures.

To further address the role of ezrin tyrosine phosphorylation, we set up standard assays for functions implicated in Src activation. First, we measured the proliferation capacity of the different subclones

grown on cell culture plates (Fig. 3A). The absence or presence of the WT or mutated ezrin did not affect the adhesion dependent growth of the clones. On the contrary, the presence of active Src clearly enhanced the proliferation of all clones compared to the parental clones which were not introduced with the Src expression construct (the clone harboring WT ezrin is shown in the figure).

Next we studied the effects on cell adhesion or migration. The cellular adhesion was judged both visually and quantitatively by plating serum-starved cells on fibronectin coated dishes for different time periods. No ezrin-dependent differences in attachment or in the kinetics of adherence were seen, when the morphology and appearance of the attaching cells was monitored by microscopical examination (not shown). Adhesion was further studied by quantitative measurements. The presence of active Src increased the rate of adherence in all subclones (Fig. 3B). In the classical wound healing experiments the subclones containing different ezrin constructs or the plasmid control did not show any differences in migration (data not shown). The cells containing constitutively active Src were highly motile and easily detached from the substrate in this assay.

A tyrosine phosphorylable form of ezrin is required for Src-induced malignant behavior of cells in three-dimensional matrix

In earlier studies ezrin has been implicated in migration of cancer cells in three-dimensional matrices or in tubulogenesis of kidney cells in collagen matrix {{202 Sahai,E. 2003;733 Crepaldi,T. 1997;638 Gautreau,A. 1999;}}. We set up assays involving 3D matrices in order to evaluate possible differences of the subclones and the significance of the Src-induced phosphorylation. First we studied the localization of ezrin in cells expressing different forms of ezrin in combination with active Src and growing inside a 3D matrix. In cells WT ezrin cells seeded in Matrigel (Fig. 4A), ezrin was concentrated in large submembraneous patches or polarized on one side of the cell. Instead, the Y477F mutant ezrin was located diffusely inside the cell and did not concentrate to the surface or localize to cell extensions. Active Src was concentrated the same way, as visualized with anti-(pY418)Src antibody (Fig. 4B) in cells harboring either the WT or the Y477 mutant ezrin. This indicates that targeting of Src is not dependent on ezrin phosphorylation, but in three-dimensional matrix ezrin targeting is dependent on Src kinase. In contrast, the focal adhesion scaffold protein paxillin, also a substrate of tyrosine phosphorylation via Src and the focal adhesion kinase FAK, was localised in a significantly more diffuse manner also in cells containing WT ezrin. To analyze other components in the WT ezrin containing patches, we double stained cells with fluorescent phalloidin or anti-cortactin antibody (Fig. 4C). The results showed that ezrin concentrates contained also aggregates of filamentous actin. Cortactin, a well characterized actin-binding Src substrate, was partially colocalized to the concentrated ezrin areas, but not exclusively. In Y477F cells the staining patterns of cortactin and ezrin differed more notably.

To study the migration and scattering of cells, cell spheroids were formed and seeded on a collagen gel. The morphology of the scattering cells was distinct; the cells harboring WT ezrin showed a rounded morphology (Fig. 4D, left). As earlier publications have implicated Rho kinase in the ezrin-dependent

amoeboid mode of cancer cell motility {{202 Sahai,E. 2003;}}, we treated the WT cells with the Rho kinase inhibitor Y-27632. The treated cells stayed longer as a compact spheroid, and the scattered cells showed an extended morphology (Fig 4D, middle). If the spheroids were treated with the Src kinase family selective inhibitor PP2, the sheroids on collagen were disrupted, and the individual cells were not viable (Fig 4D, right) indicating that Src kinase activity was required for the maintenance of the spheroids and for the viability of the cells in these conditions. The cells harboring the Y477F mutant ezrin showed an extended morphology resembling the Rho inhibitor treated WT cells (Fig. 4D, lower left). These results imply that the Src induced phosphorylation of ezrin is specifically involved in the growth and migration patterns of cells in three-dimensional environments.

We also studied the ability of the subclones to grow in soft agar (Fig. 5). The cells expressing WT ezrin but lacking active Src did not were not able to form colonies in soft agar. The cells containing active Src and the plasmid control induced few cell colonies, whereas the cells harboring both active Src and WT ezrin induced large, multicellular colonies visible already after some days. In 2-3 weeks, the number of colonies formed by WT ezrin expressing cells was four fold as compared to cells expressing active Src alone (Fig. 5B). If the cells expressed Y477F, growth in soft agar was greatly diminished. Moreover, if the medium in soft agar contained PP2, a Src family kinase selective inhibitor, the growth of the clone containing both WT ezrin and active Src was abolished. The results show that efficient growth of MEF cells in soft agar requires both Src kinase activity and ezrin with an intact Y477 residue.

As Src activation is required for resistance to anoikis (REF esim Windham 2002, Frisch 1994, Hisano 2003, Wei 2004), we studied the subclones when grown in suspension with methyl cellulose (Fig. 6A). Again, coexpression of WT ezrin and active Src promoted cell growth several fold better than Src alone. Furthermore, Y477F ezrin did not provide any growth-promoting effect. The result indicates that the presence of WT ezrin is beneficial in situations of impaired anchorage or anoikis. As ezrin has been shown to be involved in the migration of cancer cells {{202 Sahai,E. 2003;}}, the ability of the subclones to invade three-dimensional matrices was analyzed by counting the cells capable to transverse a layer of Matrigel cast on one side of a porous membrane (Fig. 6B). The results show that the presence of the WT but not Y477F ezrin facilitated the migration of the cells through the matrix in a Src kinase dependent manner. To analyze the ability of the cells to grow inside a 3D matrix, we quantified the cells growing inside Matrigel after 7 days (Fig. 6C). The cells harboring WT ezrin showed increased cell numbers compared to the other subclones. In summary, the results of these experiments indicate that the presence of WT but not Y477F form of ezrin promotes Src-dependent functions that are related to the cell's ability to migrate, invade and proliferate in a three-dimensional environment such as mammalian tissue.

DISCUSSION

Oncogenic processes and formation of metastases require complex alterations in cell behavior. Cells must proliferate, survive apoptosis, lose contact inhibition and polarity, become independent of

adhesion and gain ability to invade. Src kinase is the first characterized oncogene and linked especially with metastatic processes. We have used a study model of MEFs expressing active form of Src to delineate ezrin's role in malignant behavior. While our results do not show any ezrin dependent effects on morphology, proliferation or adhesion of the cells in the usual two-dimensional cell culture conditions, the picture becomes different when the cells are subjected to growth in a three-dimensional environment. Specifically therein, the presence of WT ezrin promotes functions related to malignancy, whereas introduction of the Y477F mutated ezrin does not give cells any advantage in comparison to the parental cells lacking ezrin protein.

Src is implied in many important pathways in tumor biology. Elevated or activated Src is particularly associated with later events in oncogenesis and with advanced metastatic cancers (reviewed in {{1044 Yeatman,T.J. 2004;}}. Src activity is an independent indicator of poor clinical prognosis in all stages of human colon carcinoma {{1052 Aligayer,H. 2002;}}, but increased Src levels and activating mutations are detected as colon tumors progress {{1048 Talamonti,M.S. 1993;1047 Cartwright,C.A. 1994;1045 Mao,W. 1997;1046 Irby,R.B. 1999;}}. Src activity is not required for proliferation or growth of tumors, whereas altered adhesion, invasion and the presence of micrometastases are strictly Src-dependent {{1049 Jones,R.J. 2002;1051 Boyd,D.D. 2004;1038 Boyer,B. 2002;}}. Inhibition of Src leads to decreased incidence of metastases in breast cancer and pancreatic adenocarcinoma {{1056 Rucci,N. 2006;1057 Trevino,J.G. 2006;}} as well as decreased invasion of prostate carcinoma and glioma cells {{1054 Slack,J.K. 2001;1055 Angers-Loustau,A. 2004;}}.

Several studies provide compelling evidence for ezrin's role as a prometastatic factor. Two distinct mouse tumor models show that ezrin is necessary for the metastatic capacity of osteosarcoma and rhabdomyosarcoma {{123 Khanna,C. 2001;151 Khanna,C. 2004;150 Yu,Y.L. 2004;}}. Ezrin inhibition significantly reduces osteosarcoma lung metastases in mice, and high ezrin expression in primary tumors is associated with significantly shortened DFI in dogs and human pediatric patients. In addition to mesenchymally derived cancers, ezrin has been identified in a screen which was searching for metastasis-associated genes in colorectal and mammary cancer {{132 Nestl,A. 2001;}}. Significant correlations between ezrin overexpression and increased malignancy or infiltrative growth are seen in uveal and cutaneous melanoma, astrocytoma, endometrioid and ovarian carcinoma and soft tissue sarcoma {{95 Makitie,T. 2001;1039 Ilmonen,S. 2005;28 Geiger,K.D. 2000;1041 Kobel,M. 2006;1040 Kobel,M. 2006;928 Weng,W.H. 2005;}}. Invading tumor cells of lung adenocarcinoma are strongly positive for ezrin, but not for moesin or radixin {{31 Tokunou,M. 2000;}}. In a mouse model of breast carcinoma inhibition of ezrin significantly reduces metastases to lung {{900 Elliott,B.E. 2005;}}.

Src affects various signal pathways and has several substrates. Ezrin is a known Src family kinase target {{387 Autero,M. 2003;897 Heiska,L. 2005;901 Srivastava,J. 2005;}}. Although the litterature on Src substrates is extensive, none of the target proteins has previously been shown to confer specific advantage in a three dimensional environment only. For many years it has been appreciated that two-dimensional culturing of cells is a highly unnatural model with cells attached only at their ventral

surface on an abnormally rigid structure. Three-dimensional culture systems can serve as a design which corresponds more closely to *in vivo* environments and provides a system to mimic *eg.* dissemination of cancer cells. The differences between two-dimensional and three-dimensional culture affect many cellular functions. For instance, adhesion structures are different both in composition and in structure (ref. Cukierman 2001; roskelley Bissell 1995); similarly, the migration of cells rely on different mechanisms (ref. Friedl). Moreover, gene expression profiles and signal transduction of cells grown in two- vs. three-dimensional culture differ (Birgesdotter, Cukierman). The differences are relevant to our understanding of cells in their physiological environment and especially in complex phenomena like oncogenesis and tumor dissemination.

Our findings have substantial implications for future studies, as they point out to a specific regulation of cells which is confined to growth in three-dimensional conditions mimicking the circumstances in tissues. Not surprisingly, the cell lysates of the MEF subclones growing in normal cell culture conditions did not show differences when probed with antibodies recognizing active forms of the ezrin-linked signalling molecules (Akt, MAPK, mTOR/p70S6/4EBP1; data not shown). However, as the Src-dependent phosphorylation of ezrin plays a role only in 3D conditions, the biochemical dissection of the pathways involved has to be done from extractions *in situ*. Sensitive methods using microarray or proteomic approach will be of interest for the evaluation of Src-induced pathways linking ezrin to tumorigenesis.

The pathways downstream ezrin in a three-dimensional environment are currently under investigation. Several signal transduction networks are connected to ezrin, e.g. the cell survival pathway PI3K, which can lead to oncogenesis by disruption of the apoptotic control of cell proliferation. In osteosarcoma metastasis the Akt, MAPK and mTOR/S6K1/4EBP1-pathway pathways are important in ezrin-mediated early metastatic survival {{151 Khanna,C. 2004; 1043 Wan,X. 2005;}}. Interestingly, ezrin also interacts with hamartin, the gene product of the TSC1 tumour suppressor gene, which is a negative regulator of the mTOR pathway {{63 Lamb,R.F. 2000;}}. Src is one of the regulators of PI3K/Akt and mTOR signaling networks, providing one possible link to ezrin-mediated malignant behavior.

Contrary to MEF cells, ezrin Y145 has been reported as a Src target in porcine epithelial kidney cells. The Y145F mutation delays epithelial cell spreading on fibronectin by inhibiting events leading to FAK activation {{901 Srivastava,J. 2005;}}. Overexpression of ezrin and active Src leads to increased scattering and disrupted cell-cell contacts in mammary carcinoma cells {{832 Elliott,B.E. 2004;}}. Our experiments suggest that the presence of ezrin and active Src promotes malignant behavior more widely than only in epithelial cells, although the exact molecular mechanisms may vary in different tissues and cell types.

Ezrin is also participating to Rho family signaling pathways by interacting with Rho GTPase regulating factors and as a target for Rho-dependent threonine phosphorylation (reviewed in {{425 Bretscher,A. 2002;}}). Intriguingly, ezrin is required for the amoeboid mode of cancer cell invasion in a 3D

Matrigel matrix; inhibition of ezrin or Rho/ROCK signaling blocks the amoeboid motility, whereas proteolytic activity or matrix metalloproteinases are not needed {{202 Sahai,E. 2003;}}. The location of ezrin in the cells which use the amoeboid-type of invasion is highly concentrated to the direction of the movement, analogous to our results with the MEF cells growing inside Matrigel matrix. Moreover, the scattering ezrin WT MEF cells from spheroids on collagen have similar rounded morphology as in amoeboid motility; inhibition of Rho kinase activity or expression of Y477F mutated ezrin alter cell morphology from rounded to extended, analogous to a switch from amoeboid to mesenchymal invasion. However, many compensating pathways are exploited when one mechanism of invasion is blocked and adaptive mechanisms occur {{1066 Wolf,K. 2003;}}. A link between ezrin and matrix metalloproteinase expression and activity has been reported {{118 Wick,W. 2001;}}. Obviously more experiments are needed to clarify the role of ezrin for the invasion of cancer cells.

We show that ezrin promotes Src-dependent functions which are related to cell's ability to survive anoikis, invade and proliferate, indicating one possible mechanism giving selective advantage in tumorigenesis and metastatic processes. As the vast majority of the human deaths in cancer is specifically due to metastases, most clinical benefit would be obtained by overcoming dissemination and initial steps of metastatic progression. Currently, several Src-kinase inhibitors are in clinical trials {{1064 Summy,J.M. 2006;}}. However, more research is still needed to identify specific and relevant targets for cancer treatment and prevention of metastases.

FIGURE LEGENDS

Fig. 1. Characterization of the ezrin -/- MEF cells and their addback subclones. A. Cell lysates were separated by SDS-PAGE and immunoblotted with a polyclonal anti-ezrin antibody. WT = ezrin wild-type; ctr = vector control (pBABEpuro); Y145F = ezrin Y145F mutant; Y477F = ezrin Y477F mutant; Src CA = constitutively active Src. B. The same cell lysates were probed with an anti-moesin antibody. C. The lysates were probed with an antibody recognizing phosphorylated T588moesin. D. The lysates were probed with an antibody recognizing active Src (phosphorylated on Y418). E. Ezrin was immunoprecipitated from cell lysates and tyrosine phosphorylation was detected with an anti-phosphotyrosine antibody (left panel). The same filter was stripped and subsequently probed with the anti-ezrin antibody (right panel). WCL = whole cell lysate; pre-imm = preimmune control immunoprecipitation. The arrows indicate the positions for the specific bands in each subfigure.

Fig. 2. Immunofluorescence analysis of the ezrin -/- MEF addback cells grown on coverslips. Upper panel: Immunofluorescence staining of ezrin; (A) cells harboring WT ezrin but lacking active Src; (B) cells harboring WT ezrin and active Src; (C) cells harboring the Y477F mutant ezrin and active Src; (D) cells harboring the vector control and active Src. Lower panel: The localisation of F-actin detected by phalloidin in cells containing ezrin but lacking active Src (E); and in cells introduced with ezrin and active Src (F). The localization of active Src in the cells harboring WT ezrin (G) or Y477F mutant ezrin (H).

Fig. 3. Proliferation or adhesion of the ezrin -/- MEF addback cells is not dependent on the Src-induced ezrin phosphorylation. A. Cell growth was analyzed at different time points using the MTT-assay as described in Materials and Methods. Circle: cells harboring WT ezrin but lacking active Src; square: cells harboring the vector control and active Src; triangle: cells harboring WT ezrin and active Src; diamond: cells harboring the ezrin Y477F mutant and active Src. B. Cells were serum-starved overnight and plated on fibronectin coated dishes for 40 min. The attached cells were stained with crystal violet and the amount of bound dye measured by absorbance at 595 nm.

Fig. 4. MEF addback cells expressing WT ezrin and Y477F mutant demonstrate phenotypic differences in three-dimensional matrices. A. Cells grown in Matrigel were stained for ezrin and analyzed by confocal microscopy. The cells containing WT ezrin and growing inside three-dimensional matrix display locally concentrated ezrin, whereas the Y477F mutant ezrin is diffusely distributed. B. Cells grown in Matrigel were stained with an antibody against the active form of Src (anti-pY418Src) or an antibody against paxillin. Active Src is concentrated locally in the cells containing either WT ezrin or the Y477F mutant ezrin (left and middle). On the contrary, paxillin is localized diffusely (right). C. Cells grown in Matrigel were double stained with an antibody against ezrin and fluorescent phalloidin or an antibody against cortactin. The ezrin containing patches contain also filamentous actin (left). Cortactin was partially colocalized with the WT ezrin concentrated regions (middle), but did not colocalize with the Y477F ezrin mutant (right). D. Scattering WT and Y477F ezrin expressing cells display different morphology on collagen matrix. The cells were seeded on a collagen matrix as spheroids of 5000 cells. The scattering of the cells inside collagen was detected after 24 h. The scattering WT cells have rounded, amoeboid morphology (left). If 10 µmol of the Rho kinase inhibitor Y-27632 is present, the scattering cells display extended morphology (middle); if 5 µmol of the Src kinase family selective inhibitor PP2 is present (right), the spheroid is disrupted and the cells are not viable. The scattering Y477F ezrin expressing cells have elongated cell morphology (lower left).

Fig. 5. WT but not Y477F ezrin promotes Src-induced growth in soft agar. A. Photographs of the MEF -/- addback cells growing in soft agar. B. Quantification of the colonies growing in soft agar in the absence or presence of 5 µmol PP2, a Src-family selective inhibitor.

Fig. 6A. WT but not Y477F ezrin promotes Src-induced growth in suspension and invasion and growth in three-dimensional matrix. A. Cells were grown in 0.5 % methyl cellulose on bacterial plates. After 7 days, the number of colonies larger than 10 cells were counted by microscopic examination. B. Cells were seeded on a layer of Matrigel on a porous filter. The cells invading through the layer and migrating to the other side of the membrane were visualized by crystal violet staining and counted after 36 hours. C. Cells were seeded inside a layer of Matrigel. After 14 days, the matrices were fixed, the gel liquidified on ice and the cells were counted. The graphs in each subfigure are representatives of at least three different experiments with similar results.

ACKNOWLEDGMENTS

We thank J.A. Cooper for the pLXSH-SrcY527F plasmid; Sa. Tsukita for the anti-moesin antibody; and H. Ahola for technical assistance. Finnish Cancer Organizations, US Department of Defense grant W81XWH-05-1-0469.

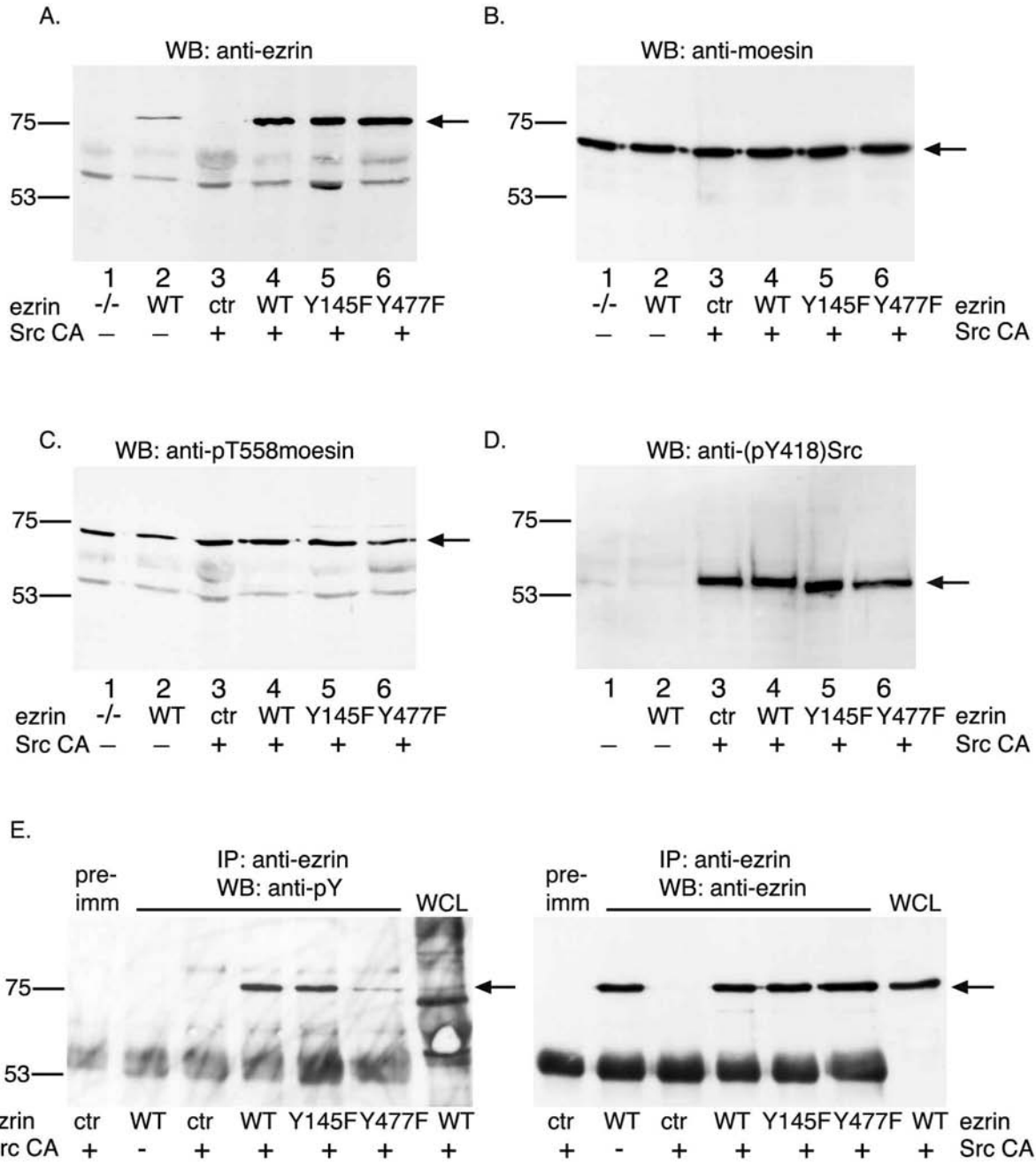
A.
WB: anti-ezrin
75
53
1 2 3 4 5 6
ezrin -/- WT ctr WT Y145F Y477F
Src CA – – + + + +
B.
WB: anti-moesin
75
53
1 2 3 4 5 6
-/- WT ctr WT Y145F Y477F ezrin
– – + + + + Src CA
C.
WB: anti-pT558moesin
75
53
1 2 3 4 5 6
ezrin -/- WT ctr WT Y145F Y477F
Src CA – – + + + +
D.
WB: anti-(pY418)Src
75
53
1 2 3 4 5 6
WT ctr WT Y145F Y477F ezrin
– – + + + + Src CA
E.
pre-imm
IP: anti-ezrin
WB: anti-pY
WCL
75
53
ezrin ctr WT ctr WT Y145F Y477F WT
Src CA + - + + + + +
pre-imm
IP: anti-ezrin
WB: anti-ezrin
WCL
ctr WT ctr WT Y145F Y477F WT ezrin
+ - + + + + + Src CA

Figure 1

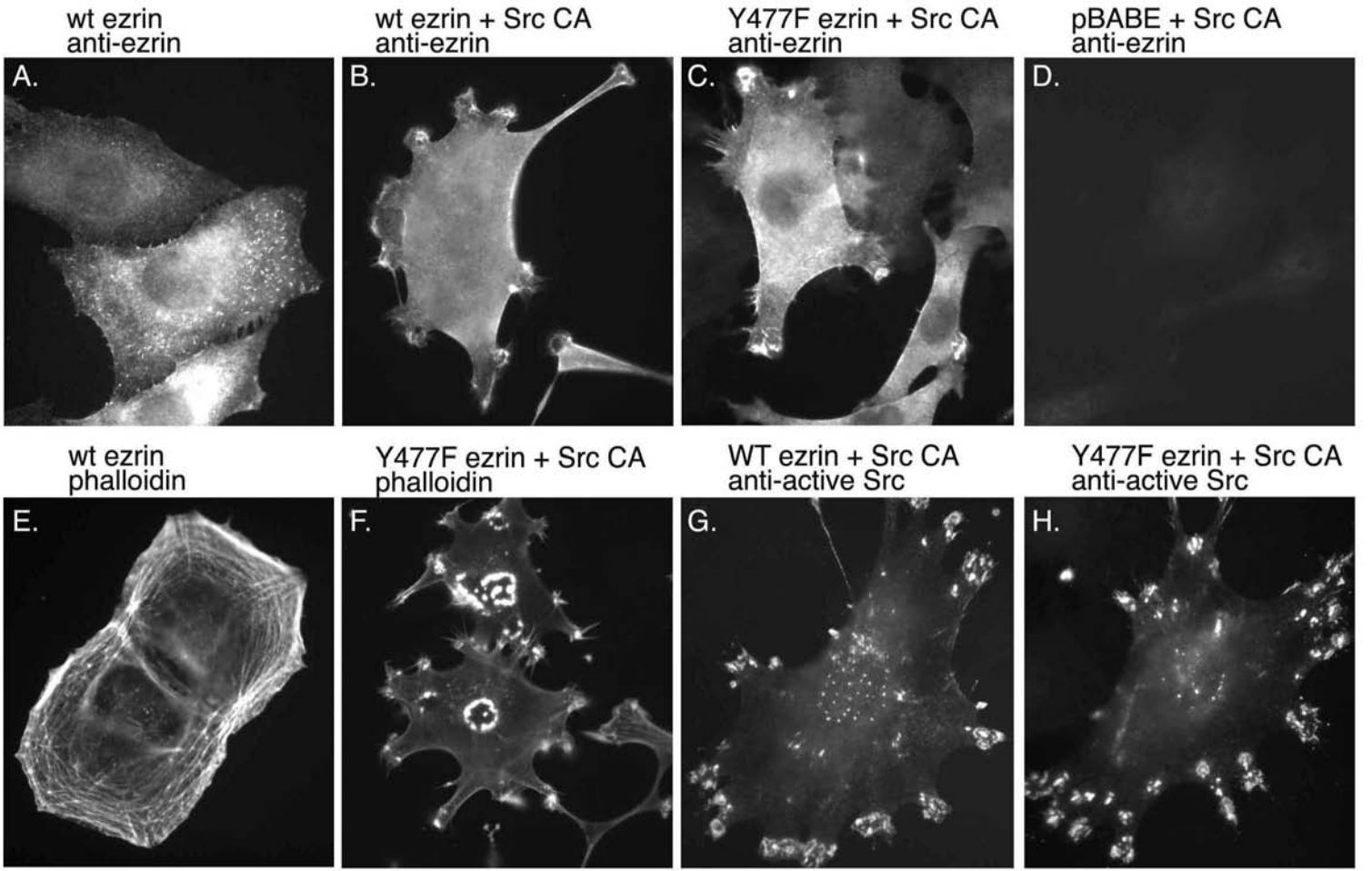
wt ezrin
anti-ezrin
A.
wt ezrin + Src CA
anti-ezrin
B.
Y477F ezrin + Src CA
anti-ezrin
C.
pBABE + Src CA
anti-ezrin
D.
wt ezrin
phalloidin
E.
Y477F ezrin + Src CA
phalloidin
F.
WT ezrin + Src CA
anti-active Src
G.
Y477F ezrin + Src CA
anti-active Src
H.

Figure 2

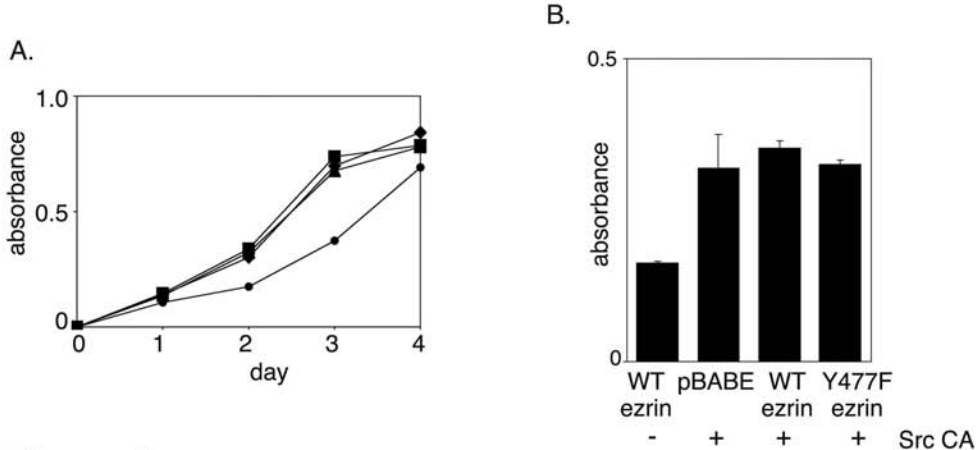
A.
1.0
0.5
0
absorbance
0
1
2
3
4
day
B.
0.5
0
absorbance
WT ezrin
pBABE
WT ezrin
Y477F ezrin
-
+
+
+
Src CA

Figure 3

A

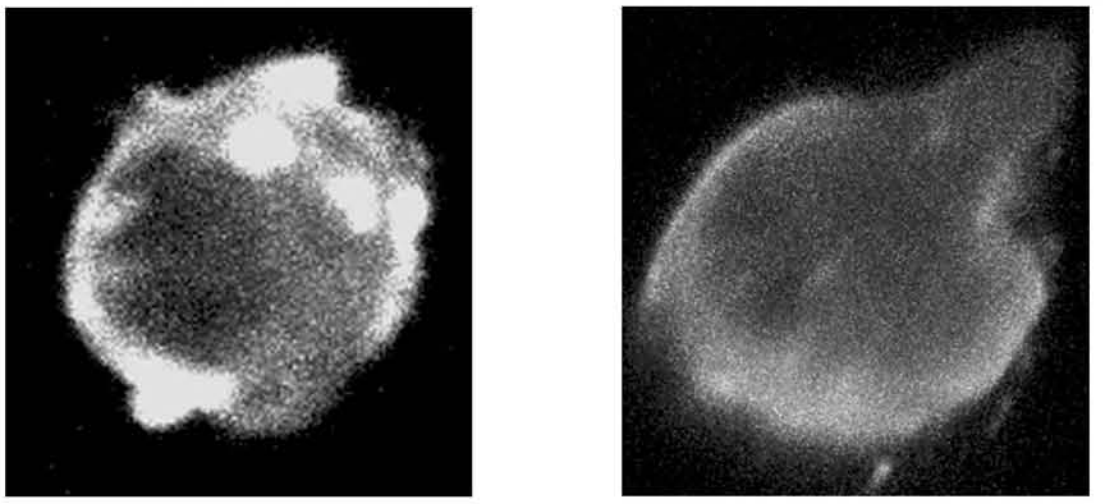

B

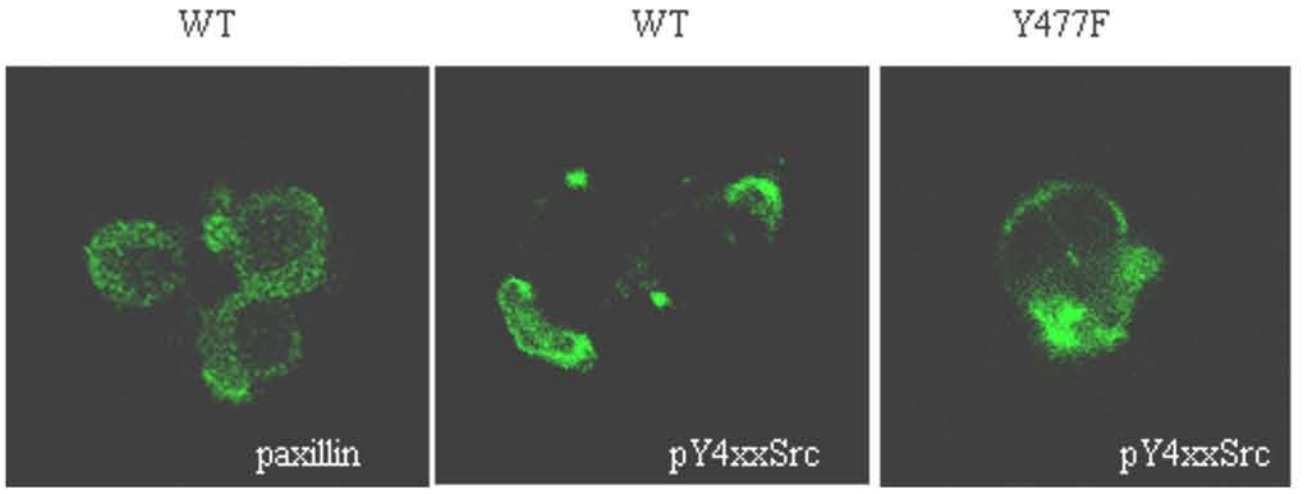

C

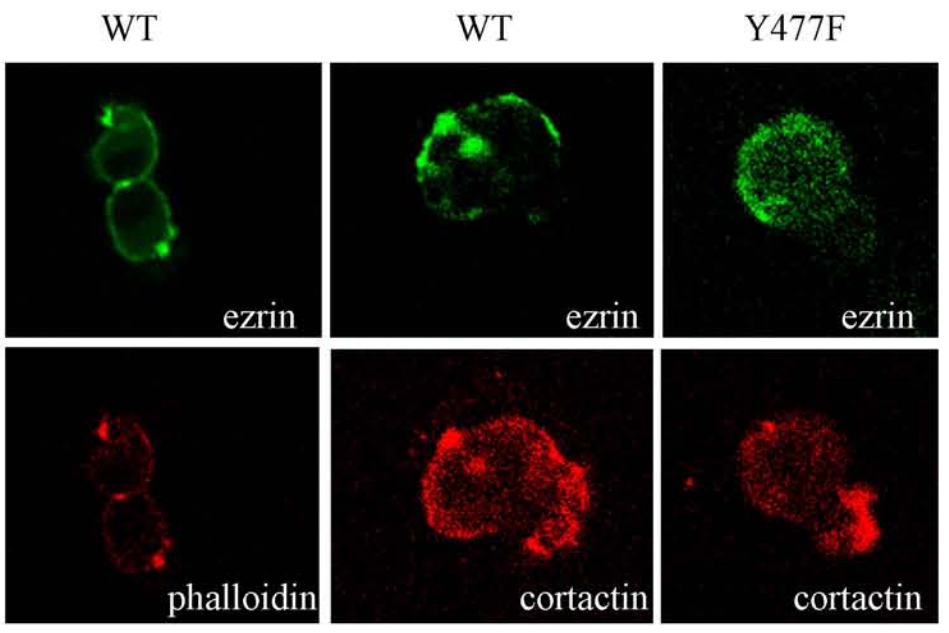

D

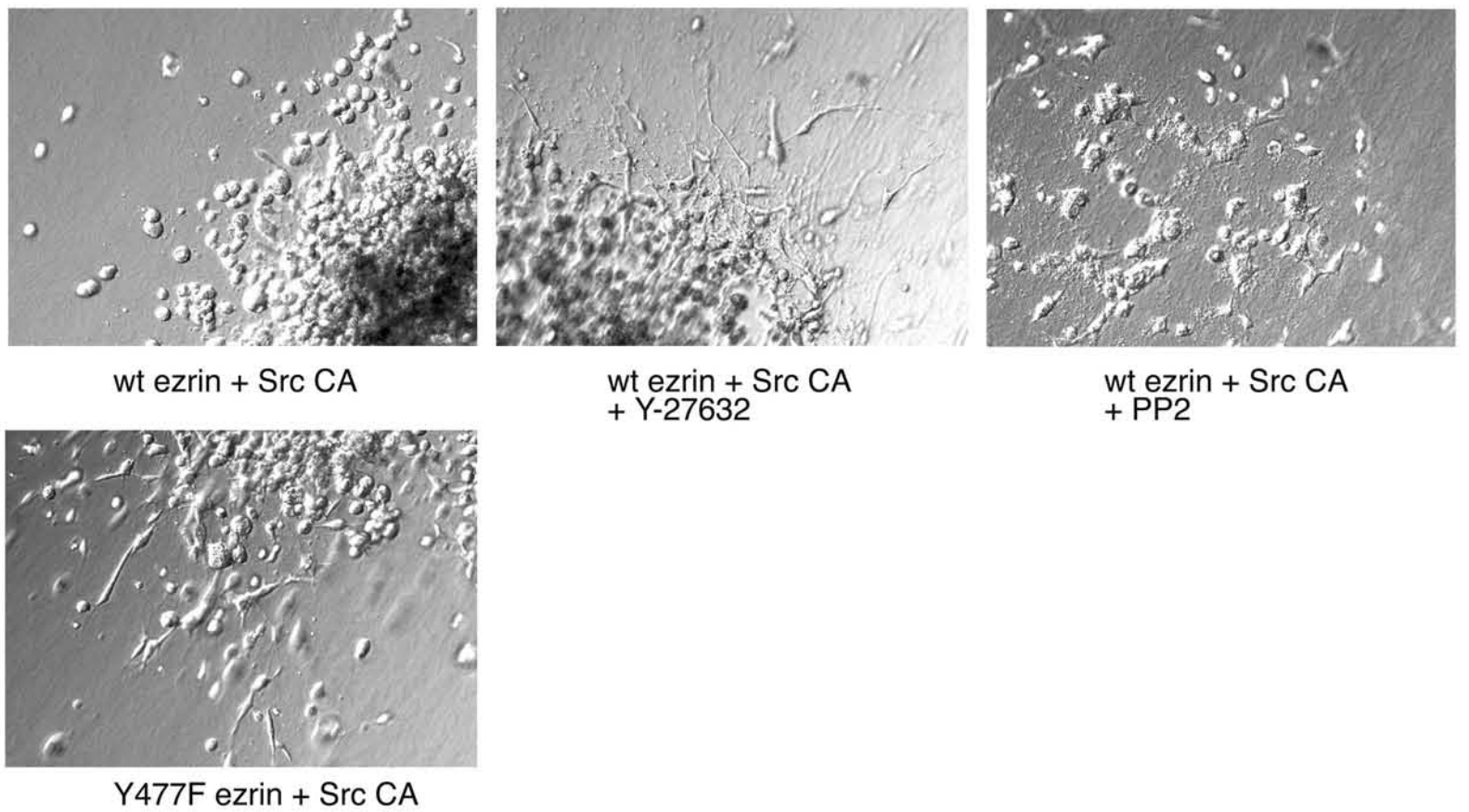

Figure 4

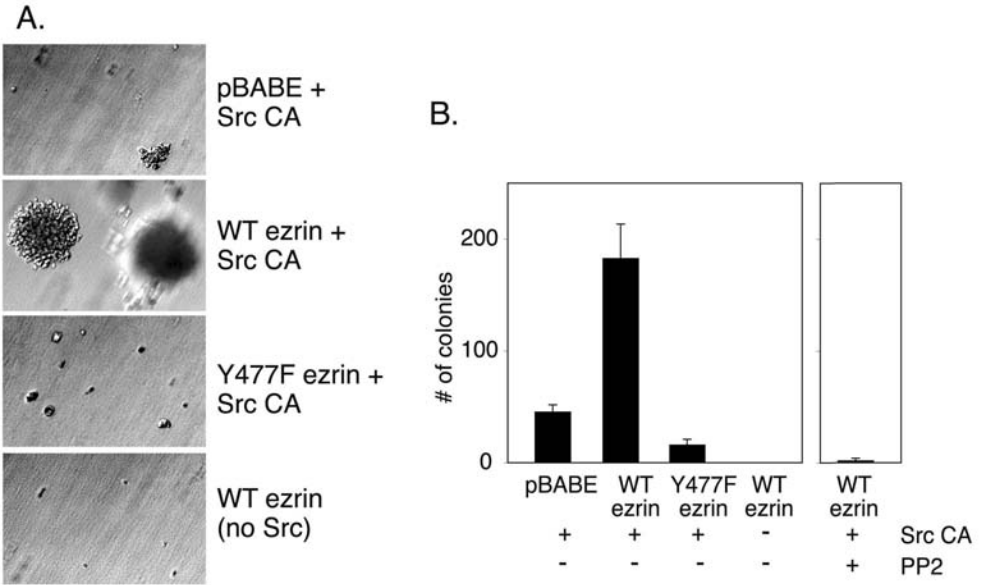
A.
pBABE +
Src CA
WT ezrin +
Src CA
Y477F ezrin +
Src CA
WT ezrin
(no Src)
B.
# of colonies
200
100
0
pBABE
WT
ezrin
Y477F
ezrin
WT
ezrin
WT
ezrin
+ + + - + Src CA
- - - - + PP2

Figure 5

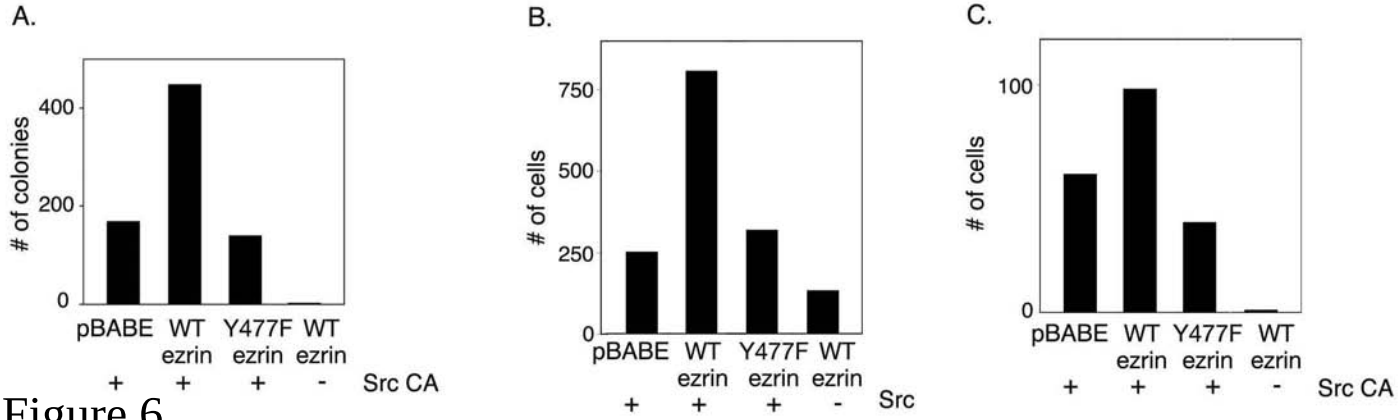
A.
# of colonies
400
200
0
pBABE
WT ezrin
Y477F ezrin
WT ezrin
+
+
+
-
Src CA
B.
# of cells
750
500
250
0
pBABE
WT ezrin
Y477F ezrin
WT ezrin
+
+
+
-
Src
C.
# of cells
100
0
pBABE
WT ezrin
Y477F ezrin
WT ezrin
+
+
+
-
Src CA

Figure 6